NJ-2016-002-3

Design and Fabrication of Orthotropic Deck Details

FINAL REPORT
Vol. III
February 2016

Submitted by

Sougata Roy, Ph.D.
Former Principal Research Scientist
ATLSS Center
Lehigh University

Soham Mukherjee
Former Research
Assistant
ATLSS Center
Lehigh University

NJDOT Research Project Manager
Ms. Priscilla Ukpah

In cooperation with

New Jersey
Department of Transportation
Bureau of Research

DISCLAIMER

TECHNICAL REPORT
STANDARD TITLE PAGE

1. Report No. NJ-2016-002-3	2.Government Accession No.	3. Recipient's Catalog No.

4. Design and Fabrication of Orthotropic Deck Details
FINAL REPORT
Vol. III of VII Volumes

5. Report Date
February 2016

6. Performing Organization Code

7. Author(s)
Roy, Sougata Ph.D. and Soham Mukherjee

8. Performing Organization Report No.

9. Performing Organization Name and Address
Advanced Technology for Large Structural
Systems (ATLSS) Engineering Research Center,
Lehigh University
117 ATLSS Drive
Bethlehem, PA 18015

10. Work Unit No.

11. Contract or Grant No.

12. Sponsoring Agency Name and Address

New Jersey Department of Transportation
PO 600
Trenton, NJ 08625

13. Type of Report and Period Covered

14. Sponsoring Agency Code

15. Supplementary Notes
Volume 3 has 116 pages. All seven volumes total 804 pages.

16. Abstract

The objectives of the research were to verify the design and fabrication of the orthotropic deck details proposed for the lift bridge, for infinite fatigue life. Multi-level 3D finite element analyses (FEA) of the proposed deck were performed to determine the critical stresses at the connections, the corresponding load position, and the deck specimen. To develop cost-effective connection details, three variations of rib-to-floor beam and rib-to-deck plate connection details, including the influence of different fabrication parameters, were explored in full-scale small size mockups. Subsequently, the infinite life fatigue performance of the connection details were evaluated by laboratory testing of a full-scale prototype. The fatigue testing was conducted under simulated rear tandem axle loading of the AASHTO fatigue truck with adequate boundary condition. The prototype testing was runout after 8 million cycles, verifying the infinite life fatigue performance of the deck design.

17. Key Words
Lift Span, Orthotropic Deck, Rounded Bottom Ribs, Infinite Fatigue Life, Full-Scale Prototype, Fatigue Testing, AASHTO, Run-Out, Cost-Effective, Fabrication.

18. Distribution Statement

19. Security Classif (of this report) Unclassified	20. Security Classif. (of this page) Unclassified	21. No of Pages 116	22. Price

Form DOT F 1700.7 (8-69)

ACKNOWLEDGEMENTS

The authors wish to acknowledge the efforts of the New Jersey Department of Transportation (NJDOT) including the Project Manager Ms. Priscilla Ukpah and Ms. Camille Crichton-Sumners, Manager of the Bureau of Research. The authors thank the Research Selection and Implementation Panel members that included the following NJDOT employees: Ms. Xiaohua Hannah Cheng, Mr. Eddy Germain, Mr. Fred Lovett, Mr. Mahesh Patel, Mr. David Lambert, Mr. Nat Kasbekar, Mr. Eric Kraehenbuehl, Mr. Jayant Dalal, Mr. Vijaykumar Thaker, Ms. Kiranben Patel and Mr. Javier Estradal. These individuals offered valuable comments and suggestions on the research project resulting in an improved product.

Editing of the final report was performed by Dr. Richard Sause, Director of the ATLSS Center.

The research was performed with the assistance of Mr. Xudong Zhao, Mr. Philipp Keller, Mr. Frank Artmont, Mr. Yeun Chul Park and Mr. Juan Tzoc, and the support staff of ATLSS Engineering Research Center and Fritz Engineering Laboratory for their help with successful execution of the project.

The authors would also like to specially thank Mr. Ronnie Medlock, Vice President of Technical Services of High Steel Structures for valuable input on fabrication of this deck and to Dr. John W. Fisher for sharing his vast experience regarding orthotropic decks.

CONTENTS (VOLUME I)

CONTENTS (VOLUME II)

CONTENTS (VOLUME III)

CONTENTS (VOLUME IV)

CONTENTS (VOLUME V)

CONTENTS (VOLUME VI)

CONTENTS (VOLUME VII)

LIST OF FIGURES (VOLUME III)

LIST OF TABLES (VOLUME III)

6. DESIGN OF FULL-SIZE SPECIMEN AND TEST SETUP

The activities undertaken in Tasks 5 and 6 of the research project related to design of full-size specimen and test setup are reported in this chapter. The full-size specimen and the test setup was designed based on the FEA of the global model and the submodel. FEA of the global model identified the most fatigue critical location and the corresponding disposition of the tandem axle. The solid submodel with all the weld details modelled, provided the fatigue critical stresses at the welded connections. The specimen consisted of a deck plate, three floor beams, five ribs and a part of the box girder web. The specimen was tested in a novel test setup with adequate fixtures such that the critical stress state of the full-bridge deck could be reproduced in the specimen. Two above-deck actuators simulating AASHTO tandem axle loading and an under-deck actuator simulating the global displacement boundary condition, were used for loading the specimen.

6.1 Determination of Size of the Full-size Specimen

6.1.1 Longitudinal Extent of the Specimen

Global model and submodel analyses showed that the deformation of the deck was highly localized under the load patches and was limited within three floor beams in the longitudinal direction, FB 14 about which the loads were symmetrically placed and FB 13 and FB 15 on either side FB 14. FB 14 will be referred as the inner FB and the two other floor beams will be referred as the outer FB in the subsequent texts and figures. Figure 237 and Figure 238 show the variation of in-plane bending moment and shear force respectively, in inner FB and one of the outer FB. The moment in the outer FB was much less as compared to the inner FB. As observed from FEA, a diagonal tension field formed from the bottom flange of the floor beam to the top corner, due to transfer of load from floor beam to box girder as shear and was responsible for stress concentration at the rib-to-floor beam connection. Thus, shear force in the floor beam web was the primary factor and Figure 238 clearly shows that the shear force in the outer FB was negligible. Figures 239 and 240 compares the deformed configuration of inner FB and outer FB. The inner FB essentially deflected like a propped cantilever in between the BG-1 and BG-2 with support settlement at BG-1 while the outer FB essentially deflected like a rigid body with support settlement. The deflection in inner FB was also much higher than outer FB. As it can be seen, the deformation was mostly localized around inner FB and inclusion of three floor beams in the longitudinal direction of the specimen was the best choice. Hence, three floor beams was included in the longitudinal direction of the full-size specimen.

6.1.2 Transverse Extent of the Specimen

After conducting multiple FE trials, two alternatives were decided for the full-size specimen. Refer to Appendix N, which is contained in Volume VII of this report, for details of the FE trials.

Option 1 and 2 for the Specimen

Fourth and fifth trial FE models were the two alternatives for the full-size specimen. The fourth trial FE model and the fifth trial FE model will be referred as Option 1 and Option 2 respectively in the subsequent text and figures. The 3D views of the models are shown in Figures 241 and 242. Figure 243 shows principal stress comparison with the submodel analysis. The principal stress contour in the inner floor beam web matched well for both the options with the submodel analysis results. This can also be seen from Figures 244 and 245 which show a good correlation of the in-plane bending moment and shear in the inner floor beam web of the options with the global model analysis results However, it was envisaged that installation of Option 2 in the lab would require more space than Option 2, which is shown in Figures 246 and 247. It was also realized that the steel consumption of fabricating Option 2 would be more than that of Option 1. So, Option 1 was selected for subsequent refinement to design the full-size specimen.

Modified Option 1

Option 1 was modified keeping the transverse width of the deck as 15 ft. The deck plate was trimmed further and was cut 3ft. 6 in. short of the specimen end. The deck plate was extended 6 in. beyond the centerline of the box girder. The depth of the box girder was adjusted such that the total depth of the girder including the deck was 4 ft. 4 in. The depth of the floor beams were increased from 3 ft. to 3 ft. 4 in. The depth of the floor beams was variable as per the design drawings for the full-bridge deck and the average depth of the floor beam in the part of the deck under consideration was about 3 ft. 4 in. To accommodate this, the depth of the floor beam was increased. The sectional elevation at the inner floor beam section is shown in Figure 248. Figure 249 shows principal stress comparison with the submodel analysis. The principal stress contour in the inner FB web matched well with the submodel analysis results.

6.2 Determination of Design Lift-up

The upward vertical displacement or the design lift-up at the box girder flange at the centerline of the inner FB was determined both graphically and analytically. The procedures for determining the design lift-up are discussed in the following.

6.2.1 Determination of Design Lift-up Graphically

The steps for graphical determination of the design lift-up are shown in Figures 250 and 251. Figure 250 shows the deflected shape of the inner and outer FBs as determined from FEA of the global model. The centerline of the box girder web is identified by point B and the other end of the specimen model is identified by point A. For making the peripheral plane (consisting of the longitudinal edges of the specimen and the two outer floor beams) horizontal, the chord joining points A and B was made horizontal by giving a rigid body rotation to it. The deflected shape of the inner FB was corrected for the same rigid body rotation and the resulting deflected shape of the inner FB after correction is shown in Figure 250. This was done to have the end of the outer floor beams at the same elevation during laboratory testing. It was envisaged that during testing condition, the tangent to the deflected shape of the inner FB at the opposite end of the box girder would horizontal. So the deflected shape of the inner FB was rotated further to make the tangent horizontal and resulting deflected shape is shown in Figure 251. The distance between the tangent and tip of the inner FB at the centerline of box girder was the design lift-up, and it was measured graphically to be about 0.1 in.

6.2.2 Determination of Design Lift-up Analytically

The design lift-up was also determined analytically by taking reaction forces at the end of the inner FB obtained from global model analysis and calculating the resulting displacement by statics. Figure 252 shows the reaction forces at the ends of the inner FB obtained from the global model analysis. The inner floor beam was acted upon a by vertical reaction and a moment at the centerline of the box girder web. The portion of the wheel loads coming to the inner floor beam is identified as P. Value of P was determined by vertical force equilibrium and was about 26 kip. Then the resulting deflection at the centerline of box girder web was calculated under combined action of reaction force, reaction moment and P. The resulting displacement was calculated to be about 0.1 inch upward, which verifies the graphical calculation. Hence, an upward displacement of 0.1 inch was applied at the flange of the simulated box girder web aligned with centerline of the inner FB during FEA of the specimen model and laboratory testing.

6.3 Description of the Full-size Specimen

The 3D view of the full-size specimen is shown in Figure 253. The specimen consisted of a deck plate with 3 floor beams, 5 ribs and a part of box girder web provided with bottom flange. The floor beam at the midspan is identified as the “inner FB” and two other floor beams are identified as “outer FB”. The simulated box girder web, along with the bottom flange is identified as the edge girder. The ribs are numbered sequentially, starting from the edge girder side with the rib adjacent to the edge girder identified as “Rib 1”. The specimen was oriented along the east-west direction of the laboratory, and the north direction is shown in the figure. The extent of the specimen in the submodel is shown in Figure 254.

The plan view of the full-size specimen is shown in Figure 255. The specimen was 27 ft. 6 in. (8.4 m) long and 12 ft. (3.7 m) wide. The floor beams were extended 3 ft. 6 in. (1.1 m) beyond the deck plate on the north side through floor beam extensions. The floor beam extensions were spliced to the floor beams using bolts. The specimen was fabricated in two panels 15 ft. 9 in. (4.8 m) and 11 ft. 9 in. (3.6 m) in lengths, and were spliced in the laboratory. The details of the splice connection is given in section 8.3. The dimensions of the prototype deck elements were according to the design drawings of the Wittpenn Bridge. The sectional elevation of the specimen is shown in Figure 256.

The thickness of the deck plate was ¾ in. (19 mm). The ribs were of closed trapezoidal shape with rounded bottom (U-shaped) having an overall depth of 1ft. 2 in. (356 mm). The ribs were $^{5}/_{16}$ in. (8 mm) thick and had a rounding radius of 4 in. to the inner surface of the rib wall. The ribs were spaced at 2ft. 4 in. (711 mm) center-to-center. The floor beams were of inverted T-section having ½ in. thick web and a 12 in. x ¾ in. thick bottom flange. The floor beams have an overall depth of 3 ft. 4 in. (1 m). The floor beams were spaced at 11 ft. 9 in. (3.6 m) center-to-center. The overall depth of edge girder was 4 ft. 4 in. (1.3 m) and was provided with a 12 in. x ¾ in. bottom flange. The deck plate was extended 6 in. beyond the centerline of the edge girder towards the south side. The edge girder web was stiffened with $^5/_8$ in. thick transverse stiffeners aligned with the centerline of the floor beams. Longitudinal stiffeners matching the width of the bottom flange of the floor beam were also provided at the web of the edge girder. The transverse stiffeners were run continuous. The specimen drawings are provided as Appendix C, which is contained in Volume VII of this report.

6.4 Analytical Studies of the Specimen Model

6.4.1 Details of the Specimen Model

The detail description of the specimen is given before in section 6.3. The deck was proposed to be fabricated in two panels to simulate the transverse field splice condition. Accordingly, the splice connection between the two deck panels was simulated in the specimen model. The bolted splice connections at the ribs and the edge girder were modelled as tie constraints with hard contact definition between the mating surfaces. However, the CJP weld at the deck plate was not modelled. All other welded connections in the specimen were modelled as $^5/_{16}$ (8 mm) fillet welds with idealized zero notch radius at the weld toes and complete penetration at the weld root. The elements of the prototype deck were modelled as an integral unit.

6.4.2 Material Properties

Widely accepted linear elastic material properties of steel were used for analysis. The modulus of elasticity and Poisson's ratio of steel were assumed as 29000 ksi and 0.3 respectively.

6.4.3 Element Type and Meshing

The specimen was meshed with 3D continuum solid hexahedral elements, incorporating twenty node, quadratic, reduced integration and isoparametric formulation. In ABAQUS, this element is identified as C3D20R. For correct assessment of stresses at the welded connections, finer meshing was required. In addition, the quality of the meshing was important to obtain accurate solution. As recommended by ABAQUS, elements with aspect ratio greater than 10 or with face angle as less than 10° or with the large face angle greater than 160° were avoided as much as possible. The specimen model was meshed with an average minimum mesh size of 1 in. and an average aspect ratio of about 6. The average maximum and minimum corner angles were 82° and 98° respectively. The quality of mesh was in accordance with the standards set by ABAQUS. Each node of the element had three displacement degrees of freedom. The specimen model consisted of 492,295 elements and 2,710,612 nodes, generating 8,191,836 solution variables or nodal degrees of freedom.

6.4.4 Loading

The specimen was analyzed for the most critical disposition of the tandem axle as determined from global model analysis and consistent with the laboratory testing. The load position in plan and elevation are shown in Figures 257 and 258 respectively. The specimen model was analyzed for load position L1T29, to produce the most critical stress state at the rib-to-floor beam connection adjacent to the box girder. The Rib 10-to-FB 14 connection adjacent to the box girder was identified as the most fatigue critical location in the global model analysis. In the specimen model, the welded connection between Rib 1 and inner FB adjacent to the edge girder is equivalent to the Rib 10-to-FB 14 connection in the global model. The load from each wheel pair of the tandem axle was uniformly distributed over a rectangular load patch of 10 in. long and 20 in. wide as specified by AASHTO LRFD Bridge Design Specifications. These load patches are identified as LP in Figure 257. Each pair of load patches in the transverse direction represented one axle of the tandem rear axle. Although a transverse gap of 1 in. exists in the middle of each wheel pairs, it was ignored in the idealized rectangular wheel contact for simplicity in modelling. As seen from Figure 257, the tandem axles were symmetrically placed 2 ft. on either side of inner FB simulating symmetric longitudinal disposition of tandem axles (longitudinal load position L1). In the transverse direction (Figure 258), the wheel pairs adjacent to the edge girder was placed centrally between ribs 1 and 2, simulating transverse load position T29. The spacing between the tandem axles in the longitudinal direction and the spacing between the load patches in the transverse direction were consistent with the latest provisions of the AASHTO LRFD Bridge Design Specifications. The total load applied on the deck was 82.8 kip, which is three times the AAHTO fatigue design load (0.75×HS20 + 15% impact) as specified by AASHTO for Fatigue I limit state design of orthotropic decks. This resulted in a total load of 41.4 kip per axle or 20.7 kip per wheel pair or load patch. The load was applied as a uniformly distributed pressure load of 0.1035 ksi per load patch. The loading in the specimen model were consistent with loading in the static and fatigue tests of the prototype deck and the location of load patches were consistent with the location of the load pads on the prototype deck during laboratory testing.

6.4.5 Boundary Condition

The boundary conditions applied to the specimen model are shown in an underside view of the model in Figure 259. The north end of the floor beams were assigned fixed boundary conditions where all the nodes on the surface were restrained against displacement in all three directions. To the south, the bottom flange of the edge girder aligned with the centerline of the two outer floor beams was restrained against displacement in all the three directions.

The bottom flange of the edge girder aligned with the centerline of the inner FB was given displacement boundary condition as determined from the global model and submodel analyses. Displacement degrees of freedom in the horizontal plane were restrained, but an upward displacement of 0.1 inch was applied at that location. This upward displacement or design lift-up was determined from the global and submodel analyses as discussed in section 6.2. In the laboratory testing, the under-deck actuator giving the design lift-up was floor mounted and the top and bottom clevises of the actuator was arrange to allow in-plane rotation of the inner floor beam. To account for this, the top and bottom clevises of the under-deck actuator were modelled as solid blocks and the hydraulic jack was modelled by a “slot and cordon” connector element. The connector element was given a vertical displacement boundary condition of 0.1 in. and rotational degree of freedom about y-axis of the element or in-plane rotation of the inner FB. The bottom surface of the bottom clevis of the simulated actuator was restrained against displacement in all three directions to simulate the condition of under-deck actuator being fixed to the lab floor through the actuator support. The bolted connection between the bottom flange of the edge girder and the top clevis of the actuator was modelled as tie constraint in the specimen model. The arrangement of the under-deck actuator in the specimen model is shown in Figure 260.

6.4.6 Analysis Results

Behavior of the Deck Plate and the Ribs

The contours of the maximum principal stress on deformed configuration of the deck are shown in Figures 261 and 262. Two way deformation of the deck was observed with high stresses and deformation of the deck plate locally under the load pads. The response of the deck plate and the ribs was evaluated by investigating the variation of normal stresses along two longitudinal sections, one through the centerline of the south side load pads in between ribs 1 and 2 and the other section through the centerline of Rib 4. Variation of normal stress along a transverse section through the east load pads was also investigated to study the transverse deformation of the deck. The transverse section was selected on the east side, because the deck showed lesser stress values on the west side due to the presence of transverse deck splice.

Figures 263 and 264 show the variation of normal stress in the longitudinal direction on the top and bottom surfaces of the deck plate along a section centrally between ribs 1 and 2. It can be seen that the stresses peaked under the load pads and decreased sharply away from it. The stresses on the top and bottom surfaces of the deck were opposite in sign under the load pads, indicating local flexural deformation of the deck under load pads. As expected, the stresses on the top surface of the deck plate under the load pads were compressive and on the bottom surface were tensile. The tensile stresses were slightly higher than the compressive stress indicating the presence of some membrane stress in the deck plate.

The variation of normal stress on the top surface of the deck plate and on the soffit of rib 4 at a section through the centerline of rib 4 is shown in Figures 265 and 266 respectively. Centerline of rib 4 was chosen for the section because the entire rib 4 was covered by the north side load pads. The stresses in the deck plate were similar to that at the section through the south side load pads, peaking under the load pads and decreasing sharply away from them. Stresses at the bottom of ribs were tensile except the inner floor beam where it was compressive. The rib deflected in sagging curvature in between the floor beams, but deflected in hogging curvature over the inner floor beam. Rib 4 essentially showed response like a continuous beam supported by the floor beams and subjected to concentrated load.

The variation of transverse stresses on the top and the bottom surfaces of the deck plate, and the outer and inner faces of the rib wall along a section aligned with the centerline of the east load pads are shown in Figure 267, along with the deformed configuration of the deck at that section. Tensile stresses are plotted on the top surface of the deck plate and the outer face of the rib wall. Tensile stresses were considered as +ve. As is evident, the deck plate deformed like a continuous beam supported over the ribs, where it deflected in sagging curvature in between the ribs and in hogging curvature over the rib-to-deck plate connections. So the stresses on the top surface of the deck plate were compressive and on the bottom surface were tensile in between the ribs. Opposite trend was observed when the deck plate deflected in hogging curvature over the connections as is expected for continuous beam showing opposite trend over the supports. The stresses in the deck plate peaked under the load pads as it underwent maximum transverse deformation under the load pads, and the stresses were insignificant away from the load pads. It can also be seen that the stresses at the inner and the outer faces of the rib wall was localized under the load pads, confirming that the response of the orthotropic deck is localized under the wheel loads. Ribs 1 and 2 which were under the north side load pads and rib 4 which was under the south side load pads, underwent maximum deformation as the stresses on their walls were much higher as compared to other ribs. The ribs under the load pads distorted due to the framing action between the rib and the deck plate. The distortion introduced linearly distributed stresses in the rib walls. The stresses were of opposite sense on the inner and the outer faces where the rib walls underwent flexural deformation. However, the magnitude of the these stresses on the inner and the outer faces of the rib walls under the wheel loads were different due to the presence of axial stresses in the ribs. The stresses on the top and the bottom surfaces of the deck plate are also compared in Figure 268 which clearly indicates flexural deformation of the deck plate as continuous beam supported by the ribs. The stresses on the top and bottom surfaces of the deck plate were almost of similar magnitude, indicating pure bending in the transverse direction with insignificant membrane stress.

It should be noted that the stresses at the bottom surface of the deck plate and the outer surface of the rib wall near the rib-to-deck plate connection were compressive. However, due to the presence of high tensile residual stresses at the weld toe, the connection could experience a total tensile stress cycle under the action of nominal compressive stresses under the wheel loads and hence can develop fatigue cracking from the weld toe as it was observed in existing bridges in service. Hence, this connection being fatigue critical, was extensively instrumented at a section under the load pads during the laboratory testing to measure the stress ranges at those connection that the deck will see when put to service. The instrumentation at the rib-to-deck plate connections is discussed later in section 8.4, contained in Volume IV.

Behavior of Floor Beams

Global model and submodel analyses showed that the stresses in FB 14 i.e. the floor beam around which the loads were positioned, was significantly more than the other floor beams. Accordingly, the behavior of the floor beams in specimen model analysis has been presented here in terms of the response of the inner FB which is essentially represents FB 14 of global model.

The deformed configuration of the inner floor beam is shown in Figure 269 overlaid on the undeformed configuration. The bottom flange of the edge girder aligned with the centerline of the inner floor beam was given upward displacement of 0.1 in. Consequently, the inner FB deformed as a propped cantilever with support displacement (vertically upward) at the edge girder side.

The maximum principal stress contour on the inner FB web is shown in Figure 270. Since the inner floor beam was integral with the edge girder, the wheel loads were transferred to the box girder through the floor beam by shear. The transfer of wheel loads as shear to the box girder resulted in a diagonal tension field from the bottom (tension) flange to the top corner formed by the floor beam web and the edge girder web. The shear induced tensile stress in the floor beam web was interrupted by the cutouts, and the stress field deviated around the cutout. As a result, high stress concentration developed in the web at the rib-to-floor beam connection of the of the floor beam where the tension fields were approximately tangential to the cutout. The rib-to-floor beam connection (rib 1 adjacent to the edge girder) also contributed to the increase in stress due to the presence of weld toe notch. As such, the high stress concentration was observed at the Rib 1-to-inner FB connection (Figure 270) in specimen model analysis similar to the global model analysis, and hence this connection was identified as most fatigue critical corresponding to the most critical disposition of the tandem axle. Stresses were tensile at the connection towards the edge girder side and compressive on the other side. The maximum tensile principal stress in the inner FB web was about 11.7 ksi which.

Fatigue cracking at the weld toe is primarily attributed to crack growth from micro discontinuities subjected to the stress range normal to the weld toe. The variation of stress normal to the weld toe at the Rib 1-to-inner floor beam weld toe on inner FB web is shown in Figure 271. The magnitude of the maximum normal stress in the tension side was about 5.7 ksi and in the compression side was about 7.4 ksi. Both the maxima occurred at about 50° from the rib soffit, and hence the Rib 1-to-inner floor beam weld toe at 50° from the rib soffit was critical for fatigue cracking from the weld toe and thus was extensively instrumented at that location (see section 8.3).

Experimental studies of the mockup specimens showed a failure mode where crack growth was observed from the weld root subjected the maximum principal stress field in the floor beam web. The variation of maximum principal stress at the rib 1-to-inner floor beam weld root is shown in Figure 272. The magnitude of the maximum principal stresses at the weld root were about 8.3 ksi and 12.4 ksi at the tension and compression sides respectively. Both the maxima occurred at about 50° from the rib soffit.

Out-of-plane bending of the inner floor beam was expected due to the presence of access holes on the rib soffit at the transverse splice location, which affected the flexural and torsional stiffness of the ribs. Figure 273 shows the variation of the stress normal to the weld toe on the east and west faces inner FB at Rib 1, along a path normal to the weld toe on the floor beam web. As is evident from the figure, significant out-of-plane stress was observed at the weld toe, which gradually decreased away from the weld toe and became primarily in-plane.

6.4.7 Comparison of Specimen Model Analysis with Global and Submodel Analyses

The specimen model was a slight modification of the modified Option 1 FE where only the design lift-up was changed from 0.07 in. to 0.1 in. Accurate determination of the lift-up made the results very close to the global and submodel analyses. Figure 274 compares the shear force in the specimen model with the global model analysis, and it shows a very good correlation with the global model analysis. This was also verified by comparing the principal stress contour in the inner FB web with submodel and is shown in Figure 275. The principal stress contour matched very well with the submodel analysis results.

6.5 Design of the Test Setup

The test setup for laboratory testing was devised based on the FEA, such that the critical stress state of the full-bridge deck could be reproduced in the specimen. The north elevation of the test setup is shown in Figure 276. The floor beam extensions were fixed to the north wall using wall fixtures to simulate the fixed boundary conditions. To the south, the specimen was supported at the bottom flange of the edge girder on two support columns aligned with the centerline of two outer floor beams, which simulated the pinned boundary conditions. The details of setup and the fixtures is given in Section 8, contained in Volume IV. The AASHTO fatigue loading was simulated by two above-deck actuators installed in the critical load position as determined from FEA. The two actuators were placed symmetrically 2 ft. on either side of the inner FB. In the transverse direction (Figure 277, the south load pads were placed centrally between ribs 1 and 2. An under-deck actuator was installed supporting the edge girder flange at the centerline of the inner floor beam for giving the global displacement boundary condition. The details of the loading and the loading protocol is discussed in Section 8.7, of Volume IV.

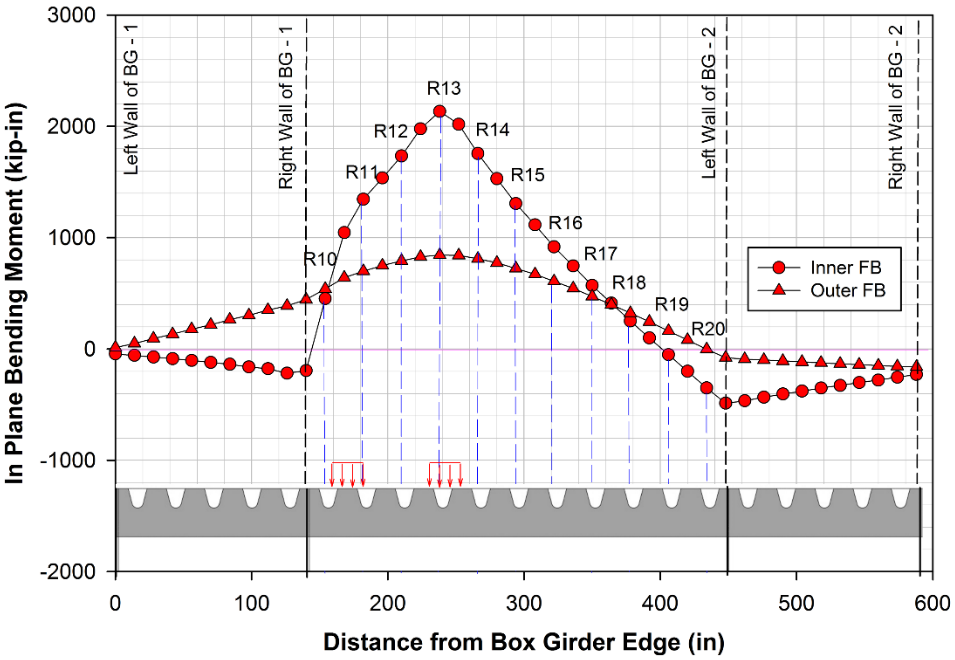

Figure 237. Variation of in-plane bending moment in floor beams

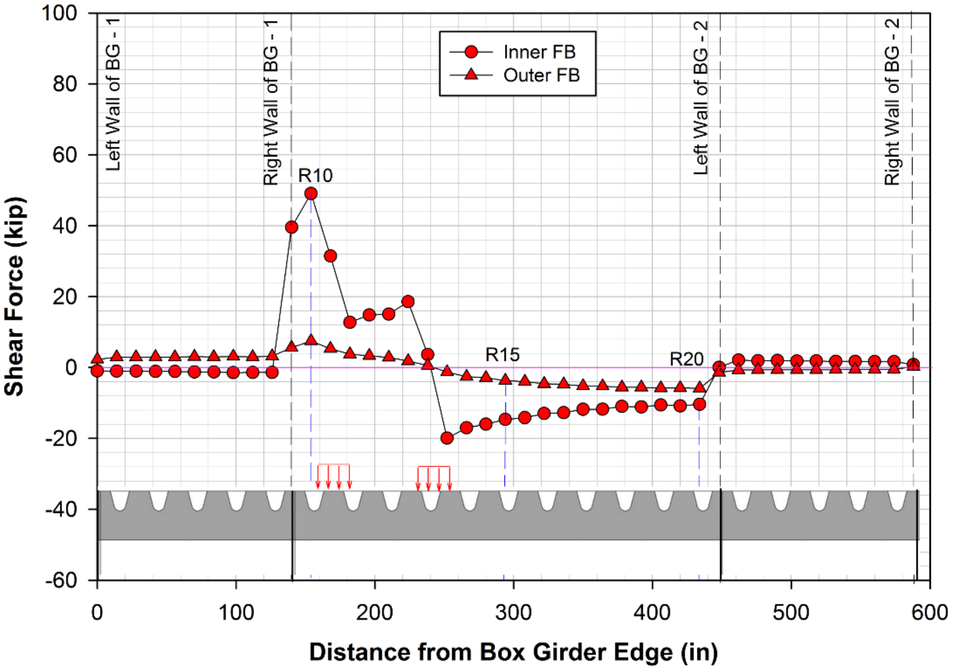

Figure 238. Variation of shear in floor beams

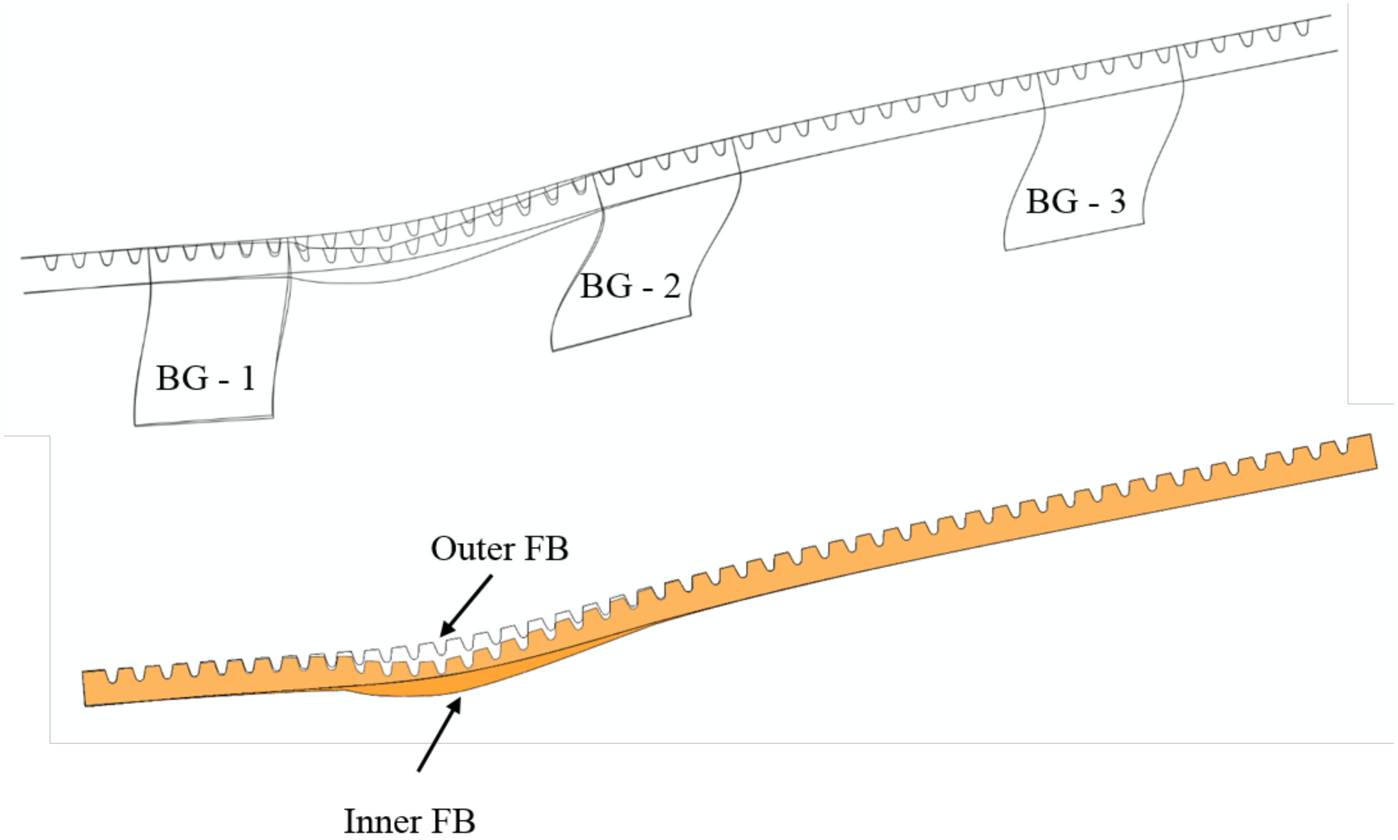

Figure 239. Comparison of deformed configuration of inner and outer floor beams

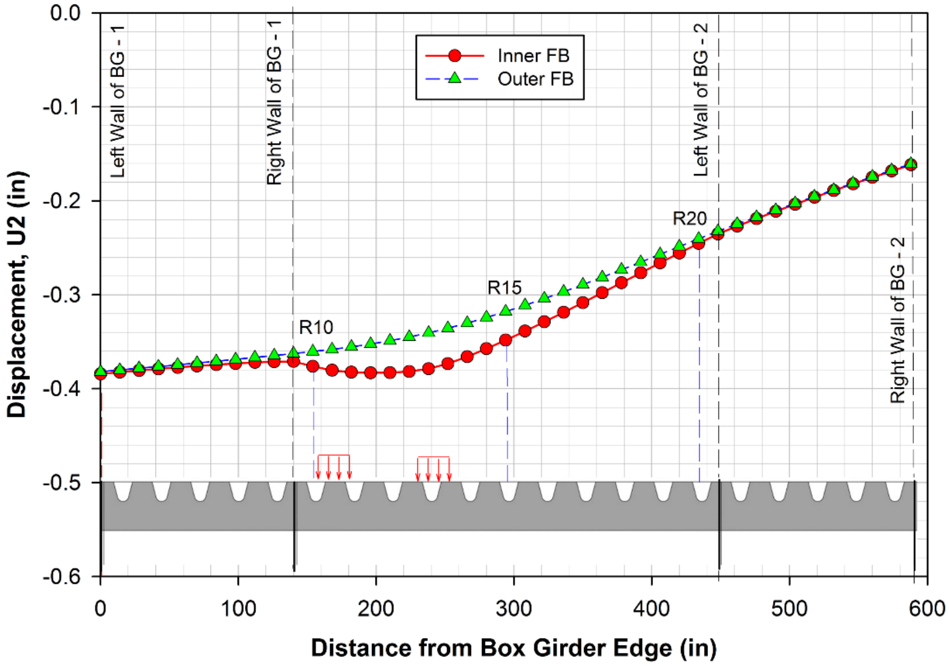

Figure 240. Comparison of deflection of inner and outer floor beam

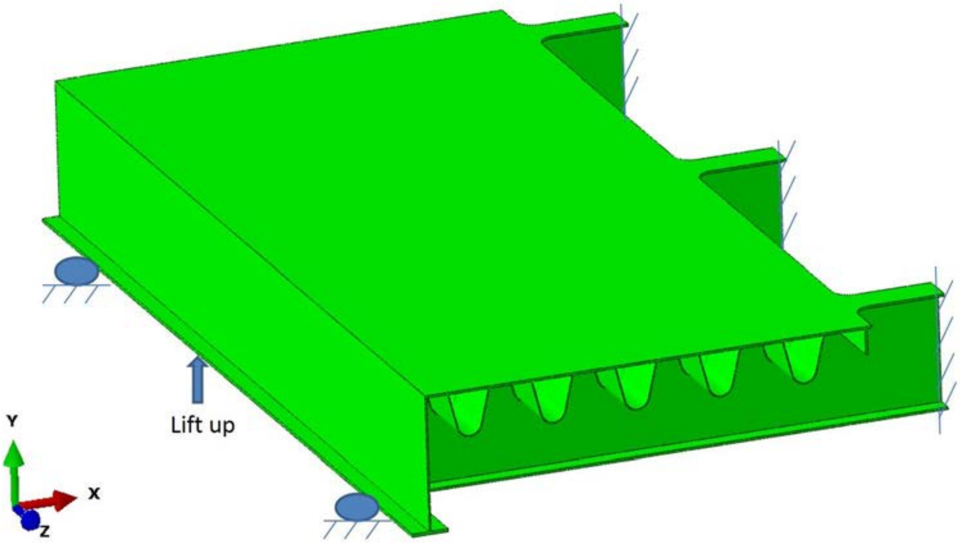

Figure 241. 3D view of Option 1 (fourth trial FE model)

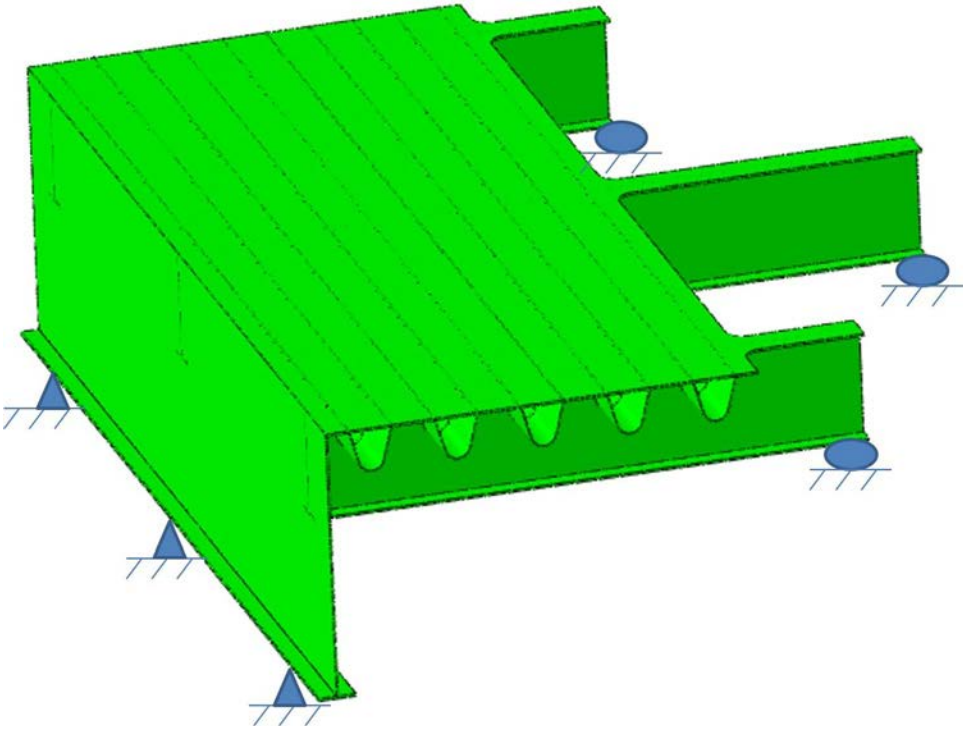

Figure 242. 3D view of Option 2 (fifth trial FE model)

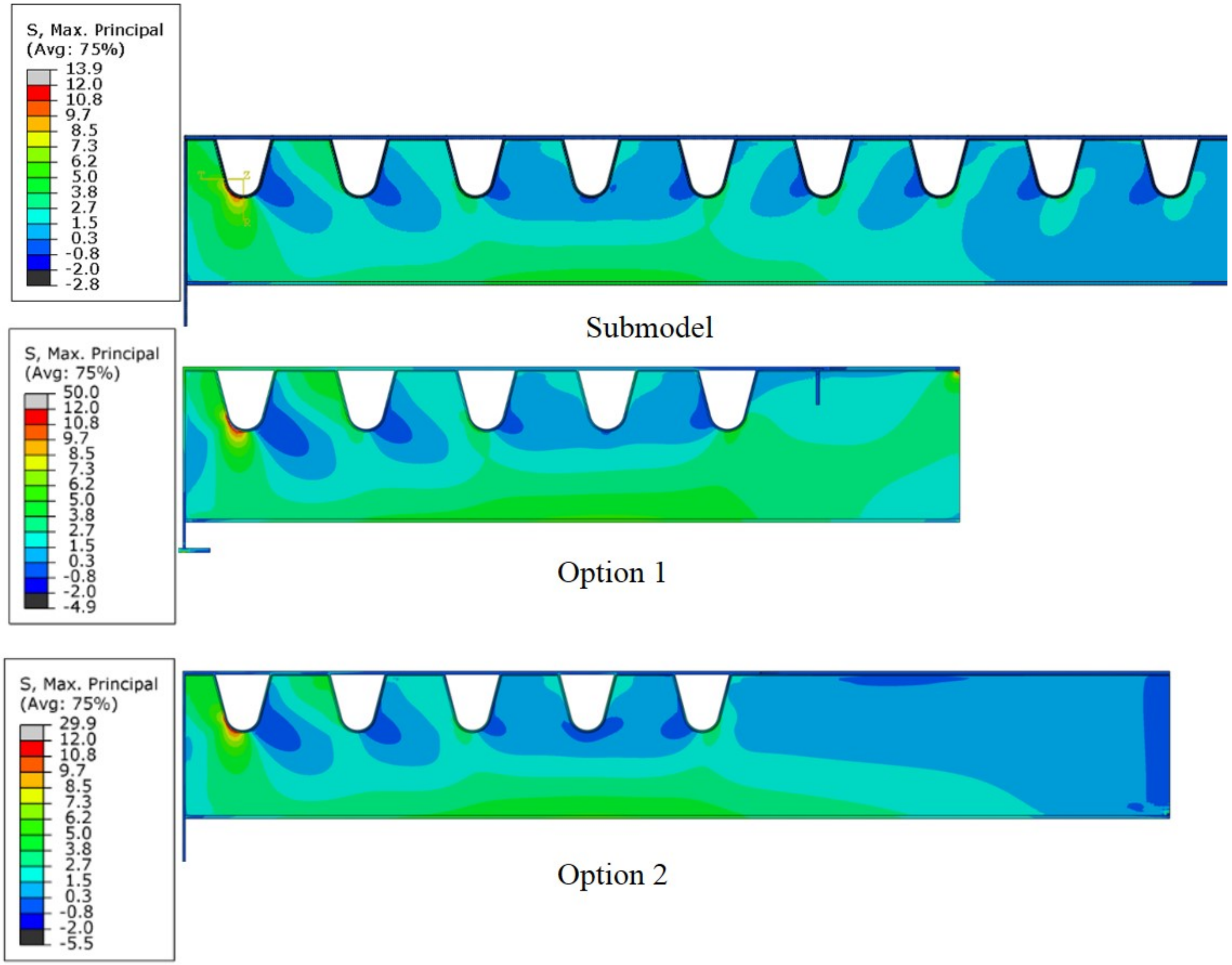

Submodel

Option 1

Option 2

Figure 243. Principal stress comparison for Option 1 and Option 2

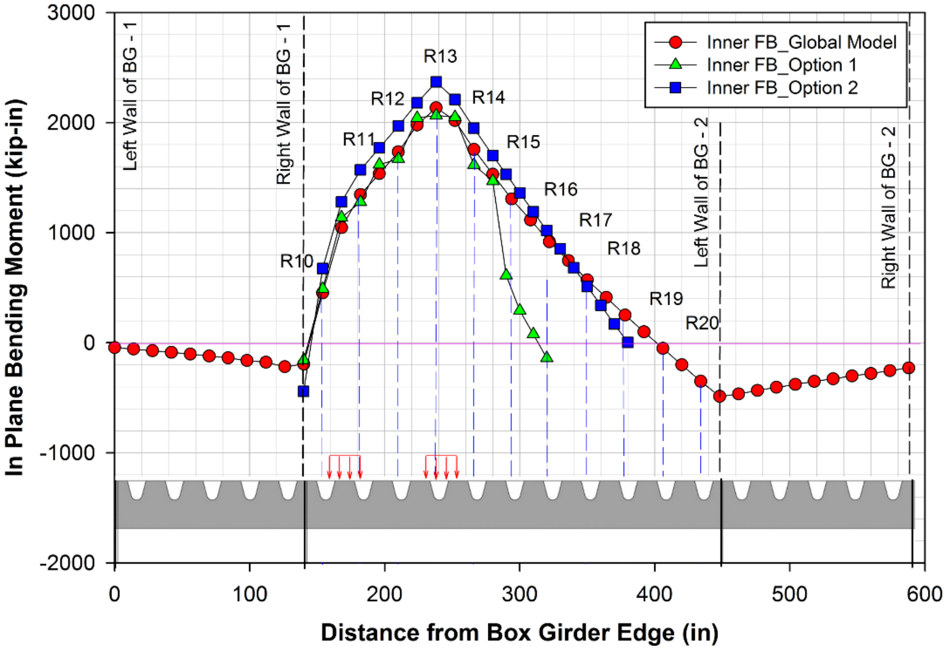

Figure 244. Comparison of in-plane bending moment of inner FB in Option 1 and Option 2 with global model

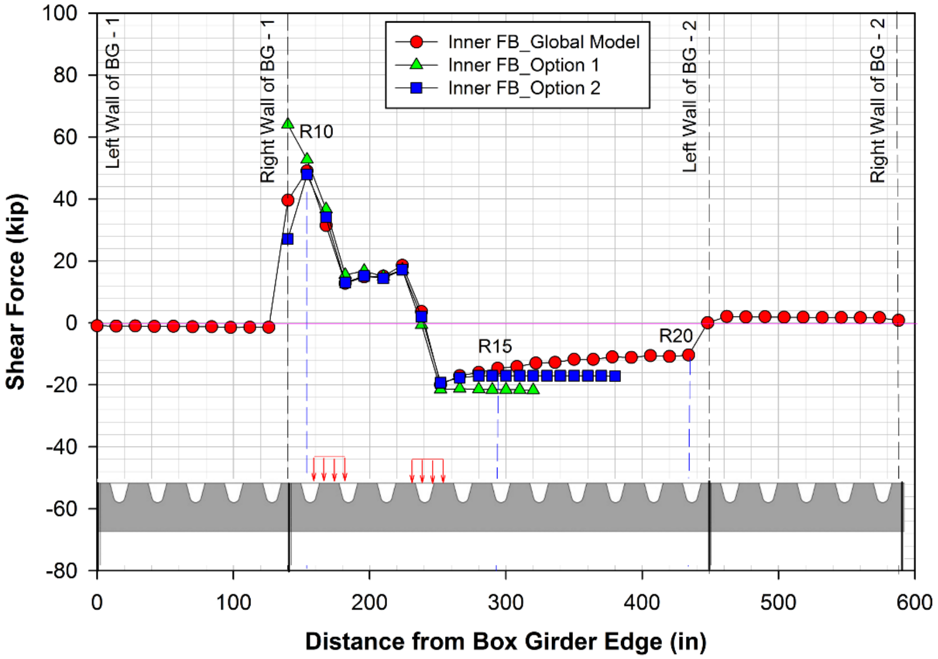

Figure 245. Comparison of shear in inner FB in Option 1 and Option 2 with global model

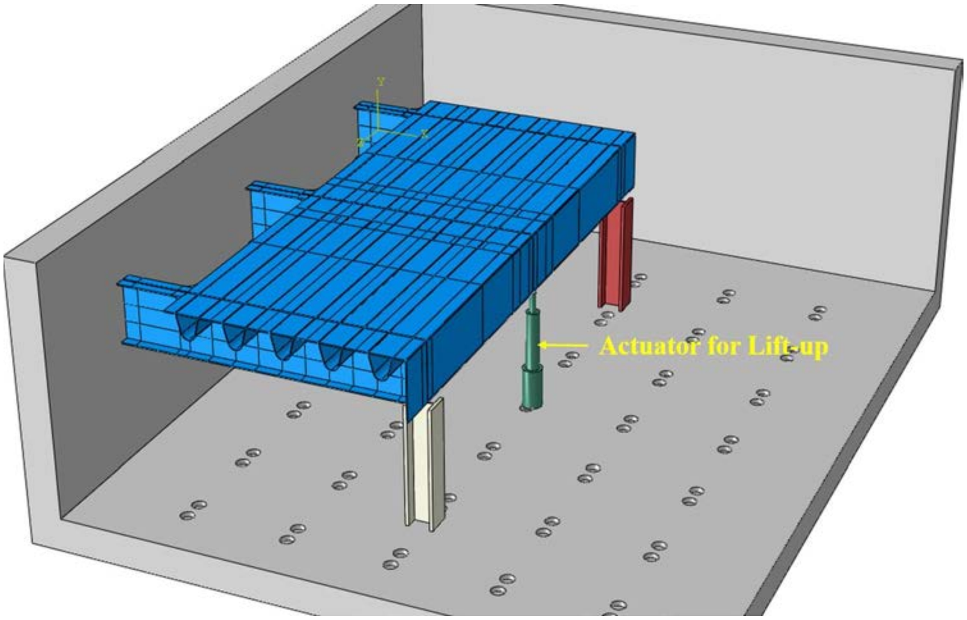

Figure 246. Conceptual figure showing installation of Option 1 in the laboratory

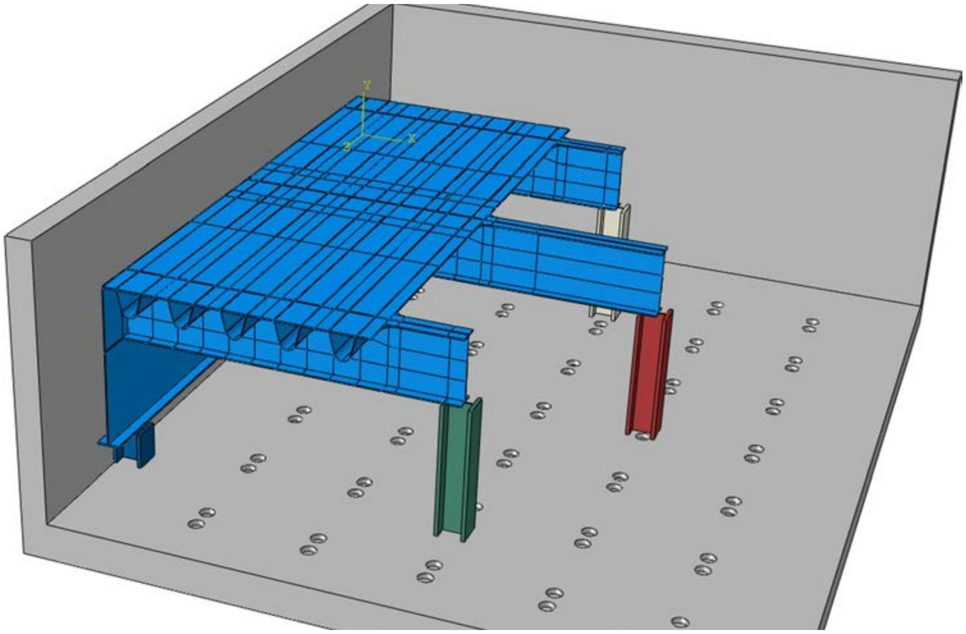

Figure 247. Conceptual figure showing installation of Option 2 in the laboratory

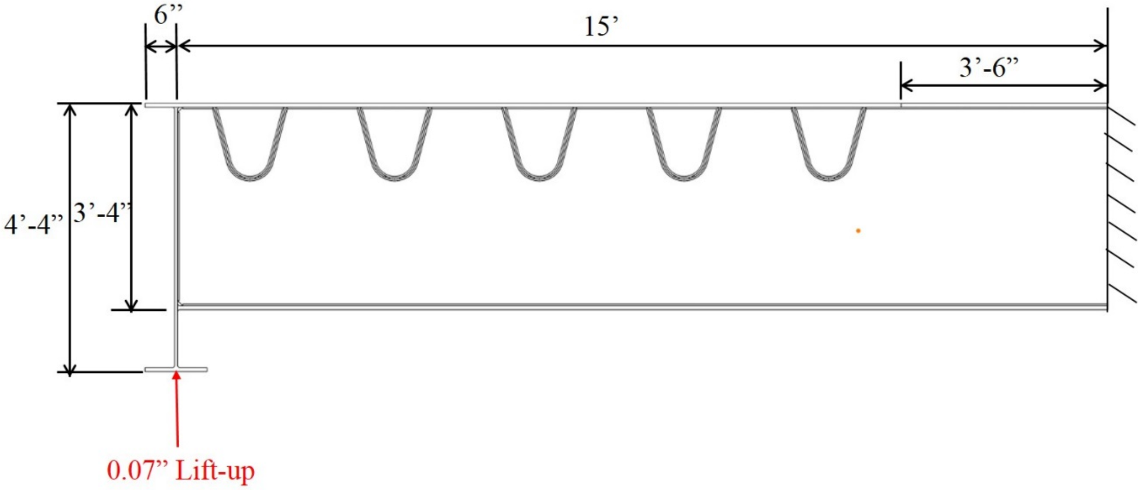

Figure 248. Sectional elevation of modified Option 1

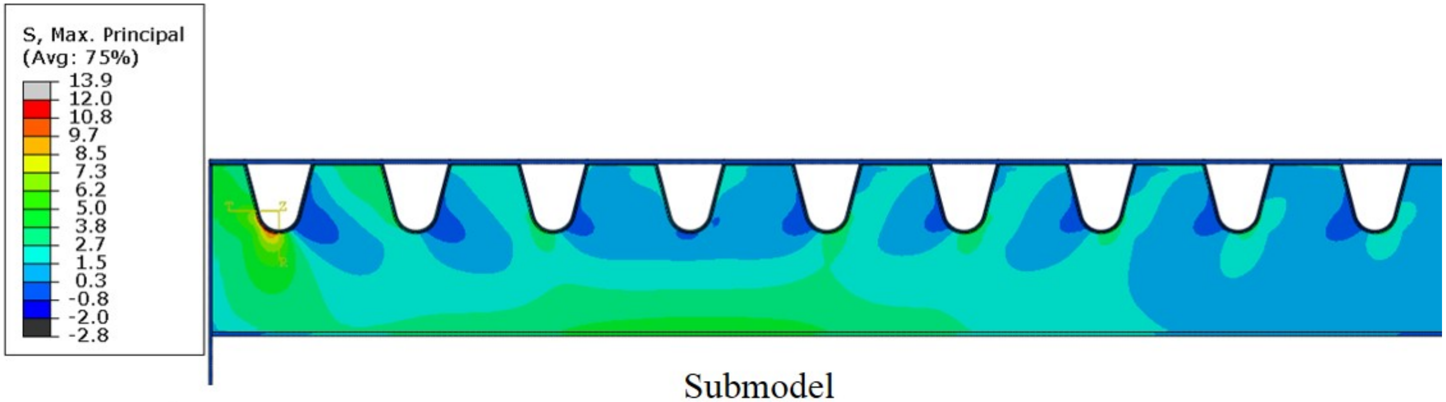

Submodel

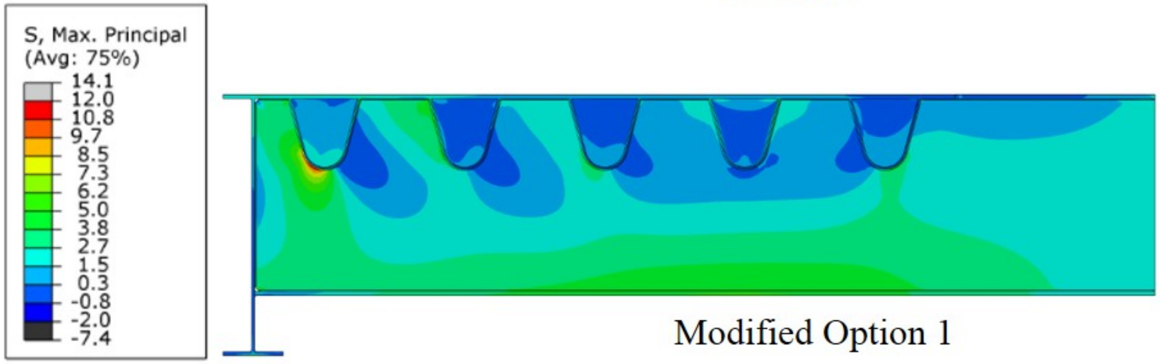

Modified Option 1

Figure 249. Principal stress comparison for Modified Option 1

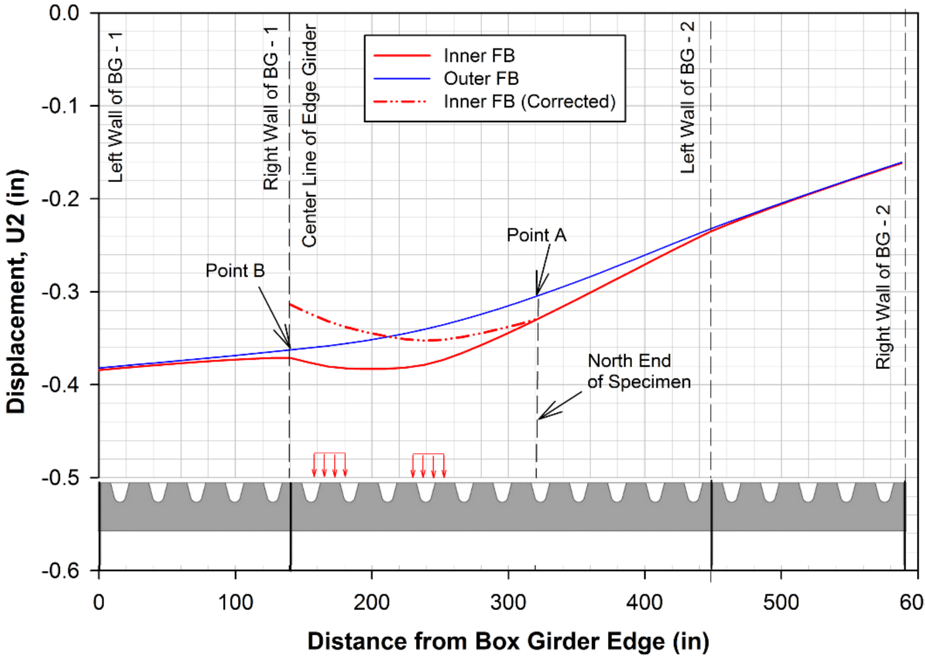

Figure 250. Deflected shape of inner floor beam after correction for rigid body rotation

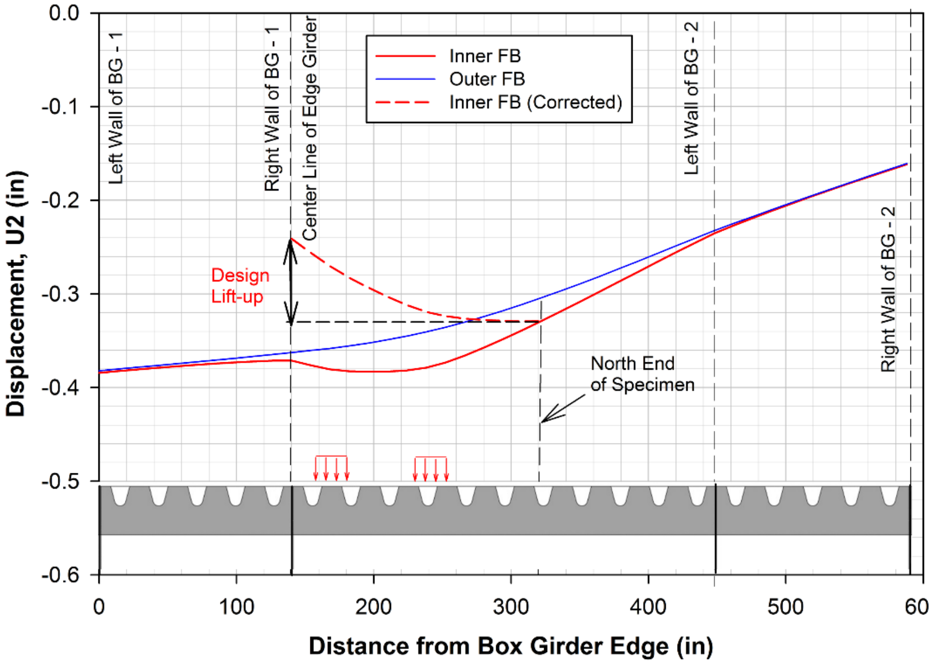

Figure 251. Calculation of design lift-up

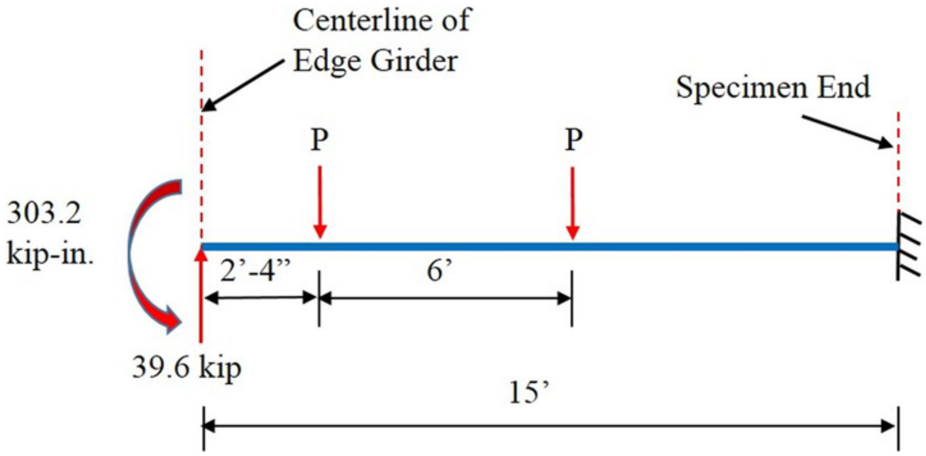

Figure 252. Calculation of lift-up from the reactions obtained from global model

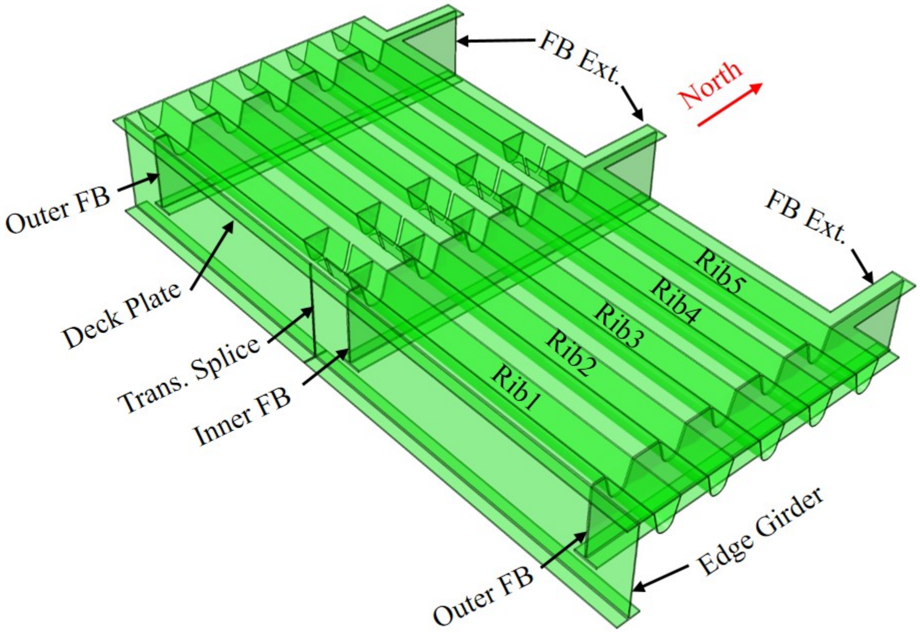

Figure 253. 3D View of the specimen

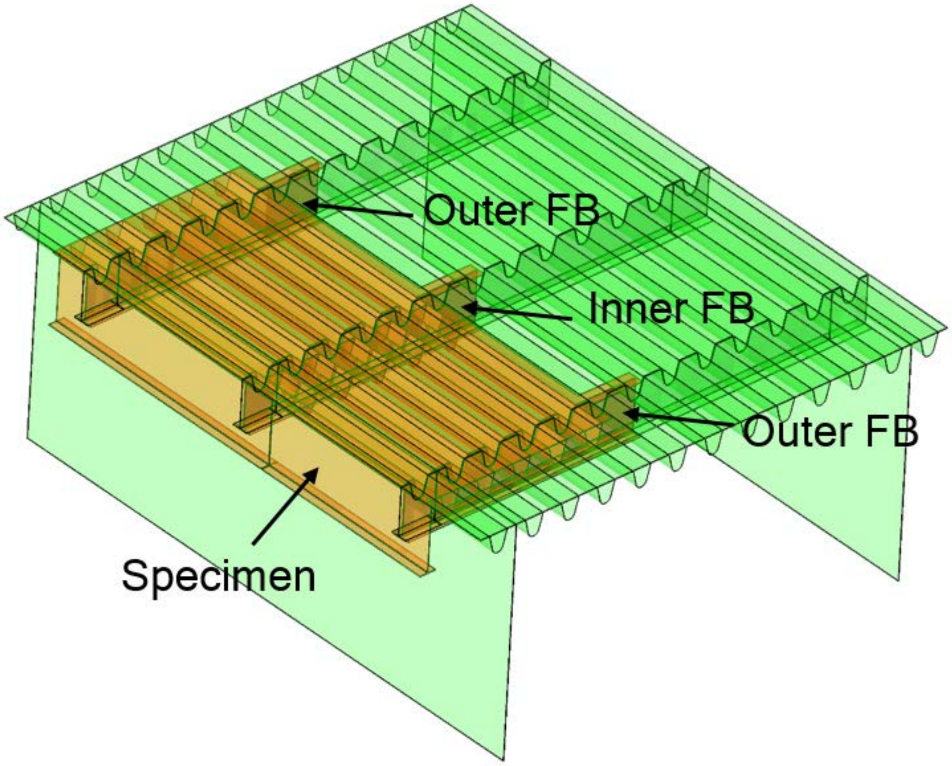

Figure 254. Top view of submodel showing extent of specimen model

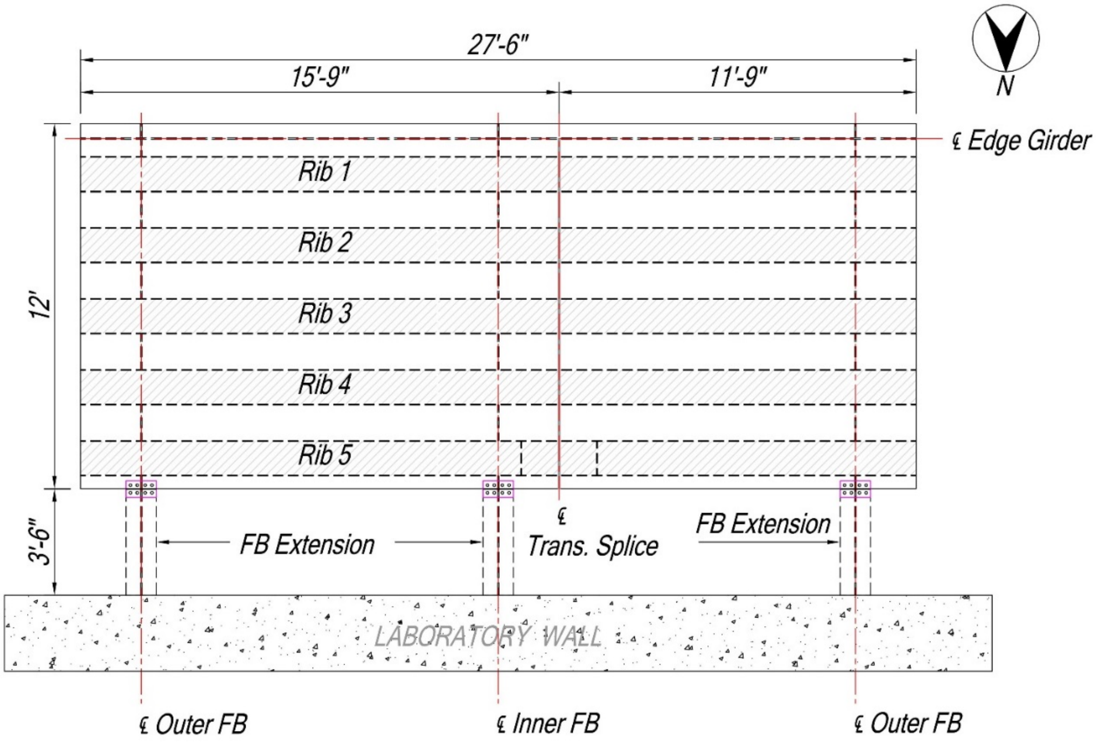

Figure 255. Plan view of the specimen

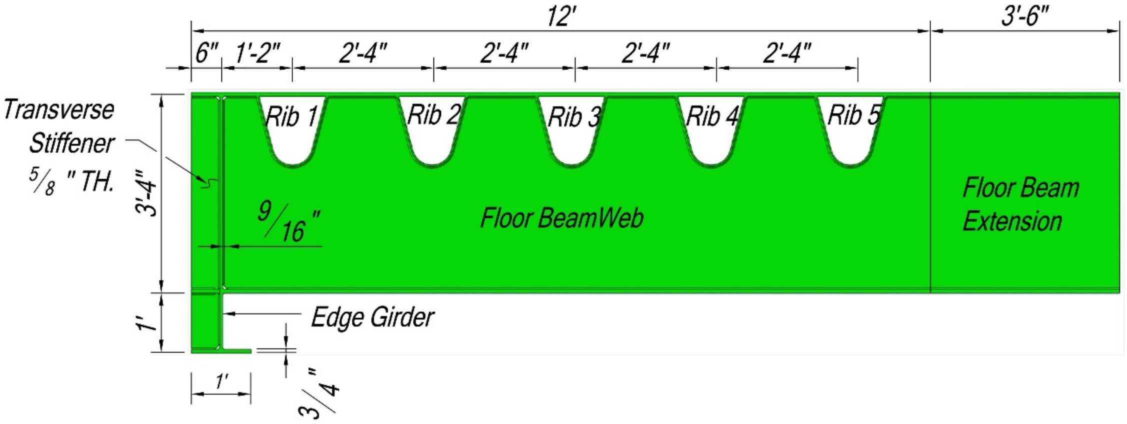

Figure 256. Sectional elevation of the specimen

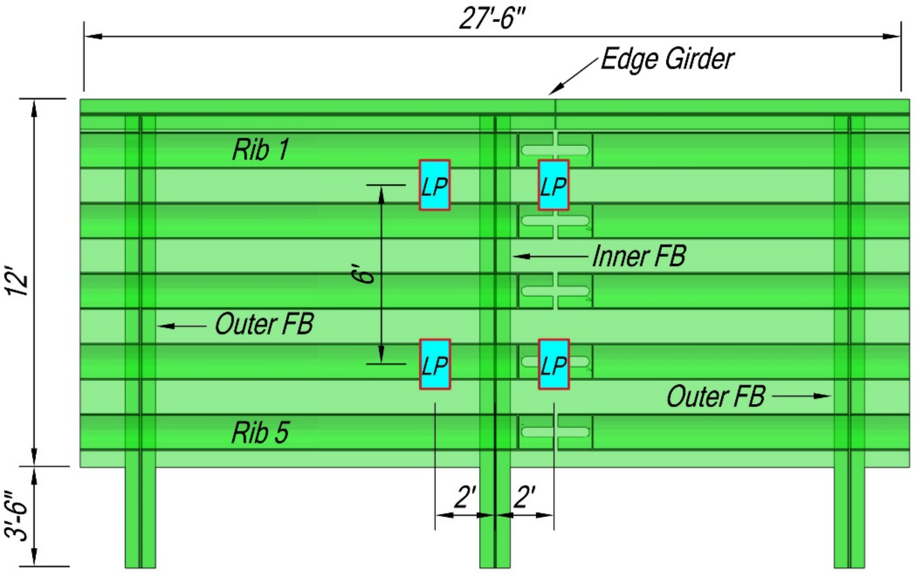

Figure 257. Top view of the specimen model with load positions shown (identified as LP)

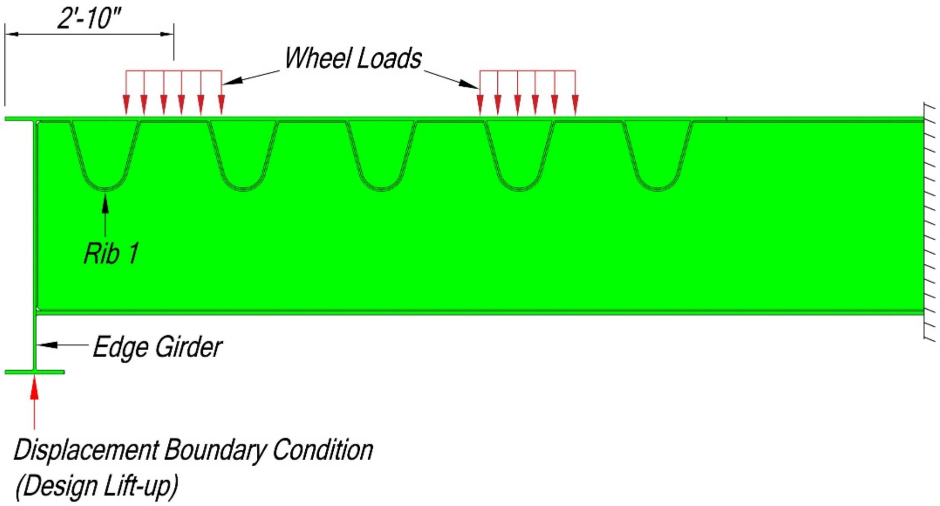

Figure 258. Sectional elevation of the specimen model showing the load position

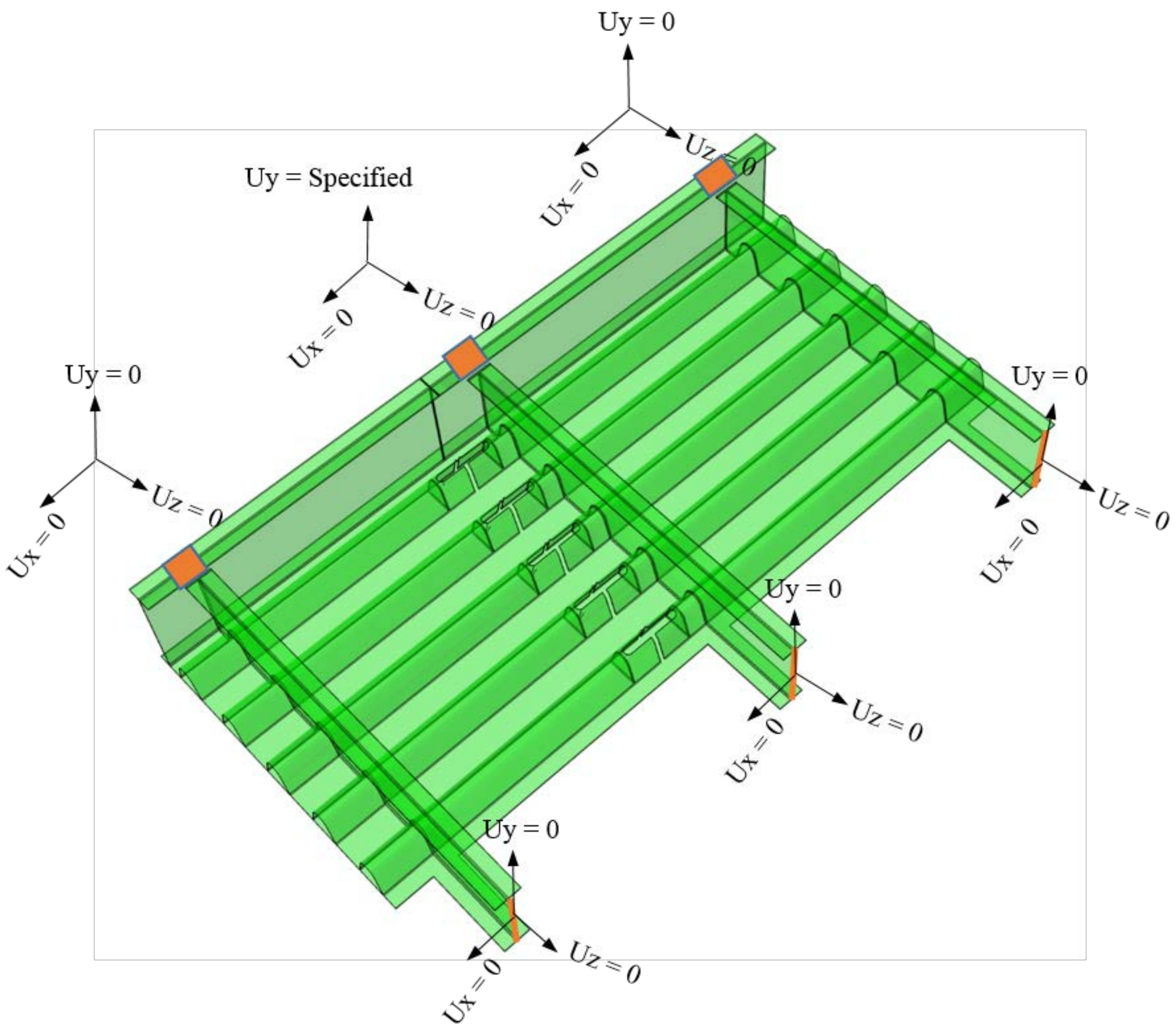

Figure 259. Underside view of the specimen model showing the applied boundary conditions

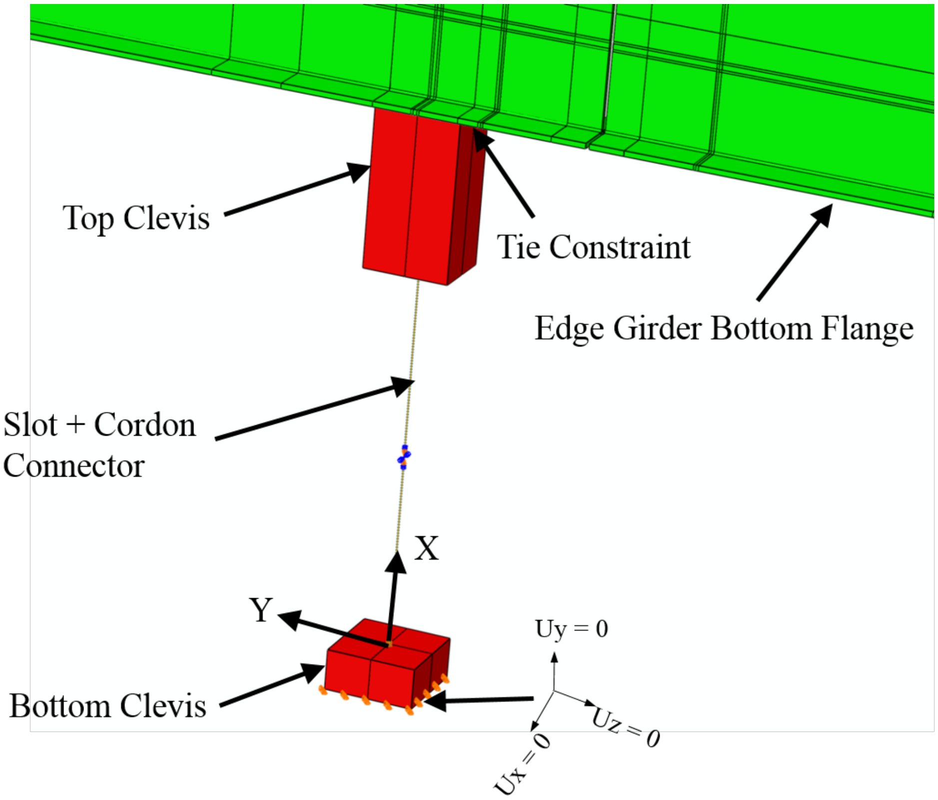

Figure 260. Under-deck actuator arrangement in specimen model

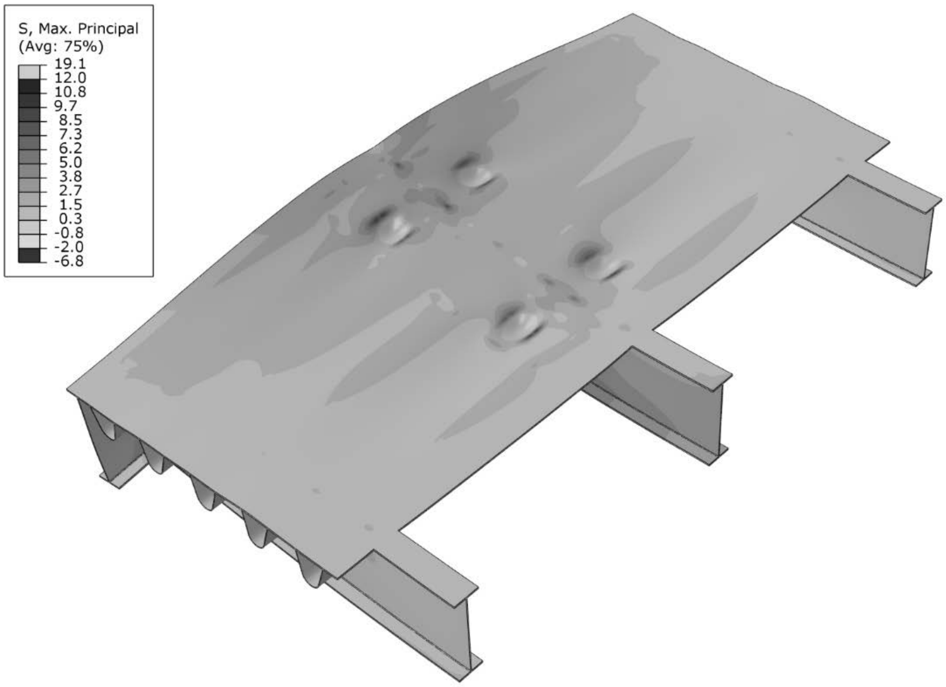

Figure 261. 3D top view of the specimen showing the principal stress contour

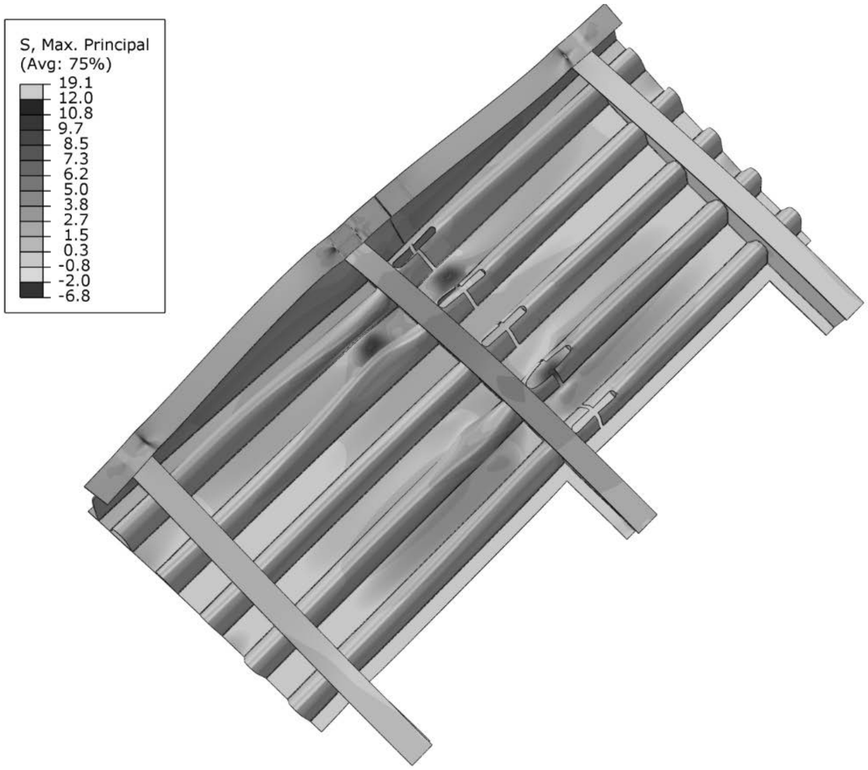

Figure 262. 3D underside view showing principal stress contour

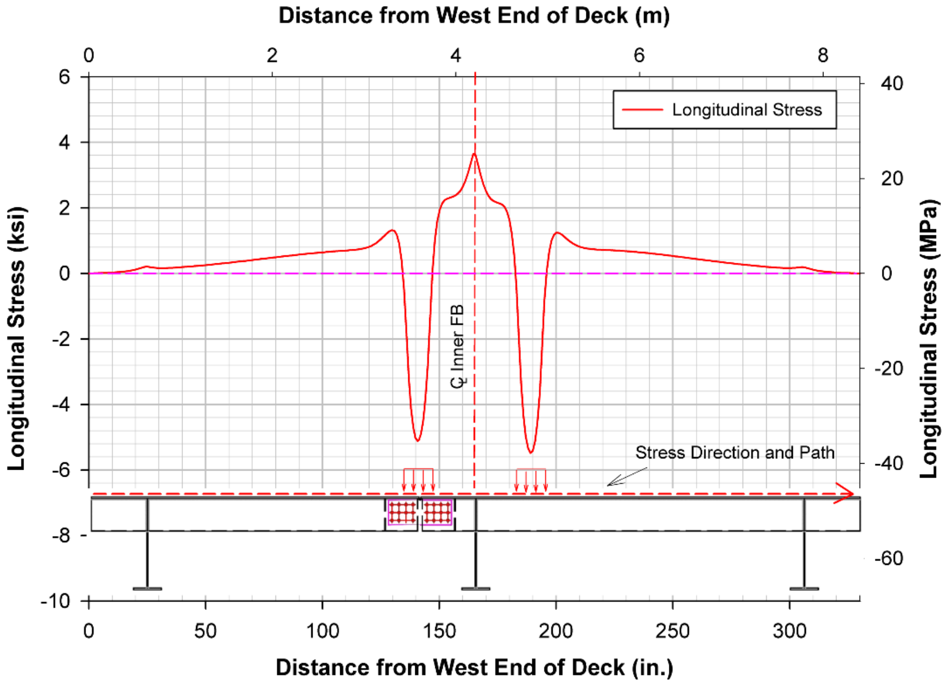

Figure 263. Variation of longitudinal stress on the top of the deck plate along a path through the south load pads

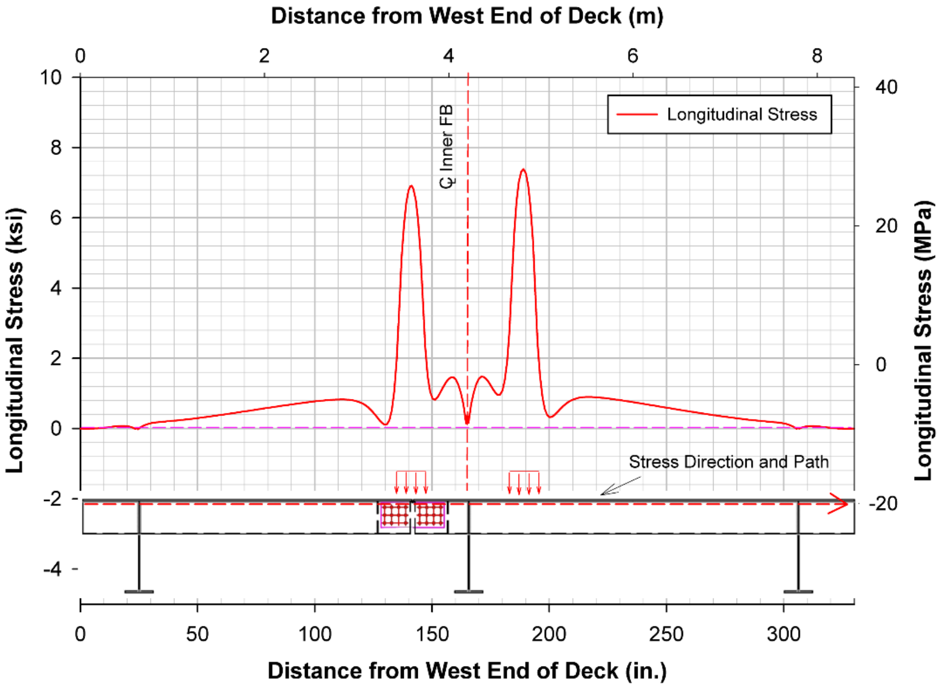

Figure 264. Variation of longitudinal stress on the bottom of the deck plate along a path through the south load pads

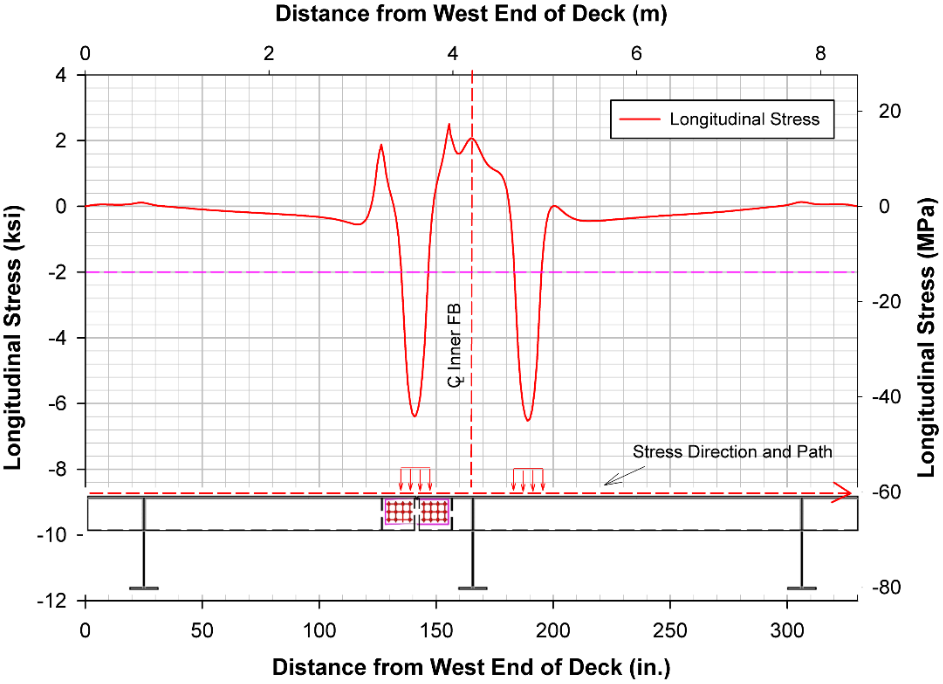

Figure 265. Variation of longitudinal stress on the top of the deck plate along a path through the north load pads

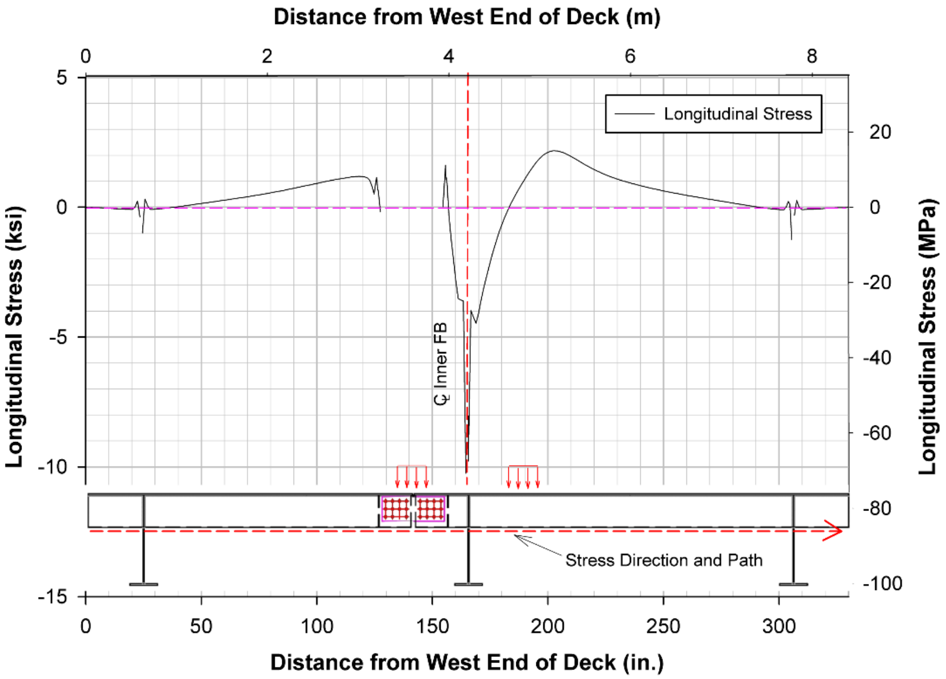

Figure 266. Variation of longitudinal stress on the bottom of Rib 4 along a path through the north load pads

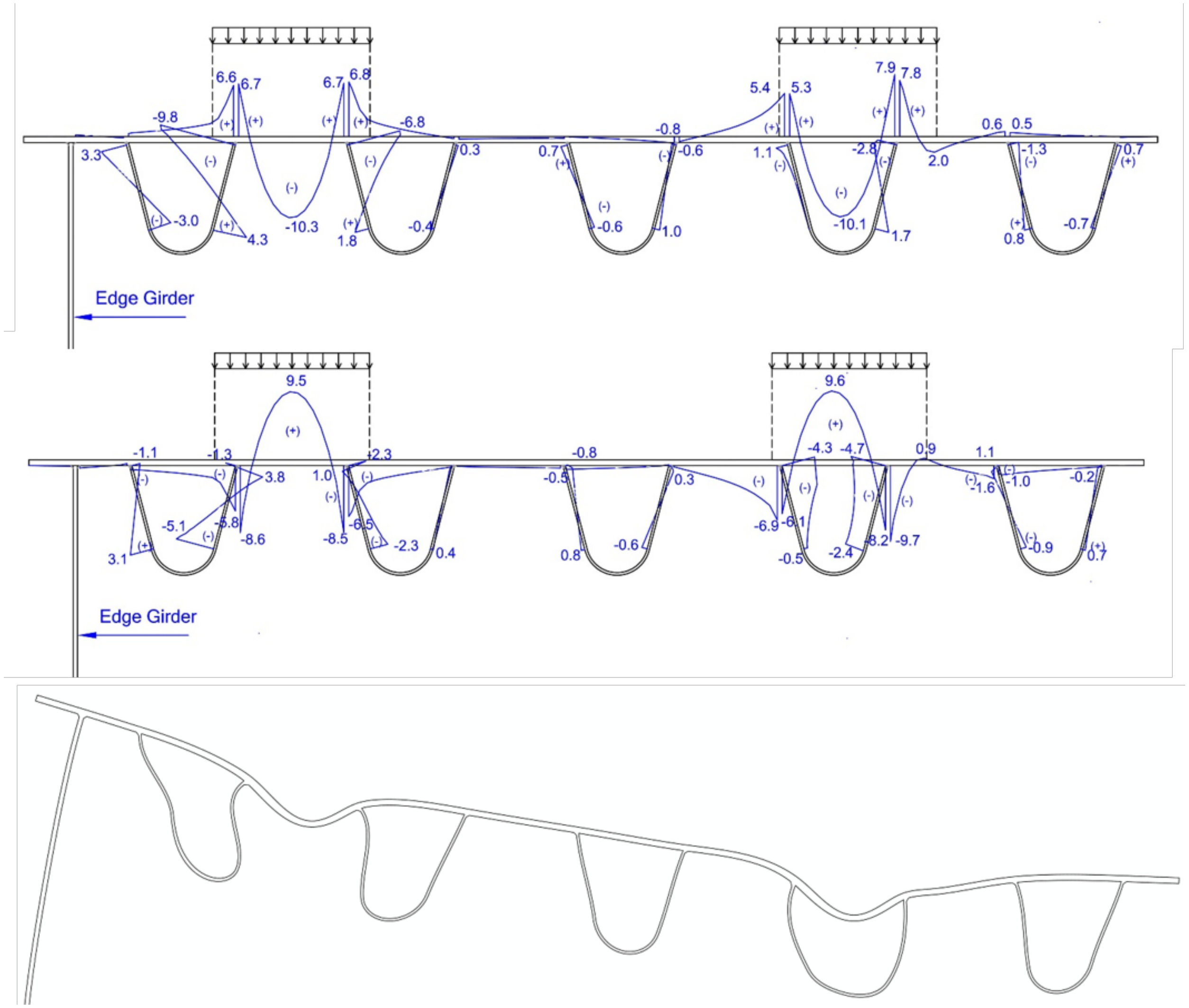

Figure 267. Transverse stresses and deformation of deck at a section through the load patches

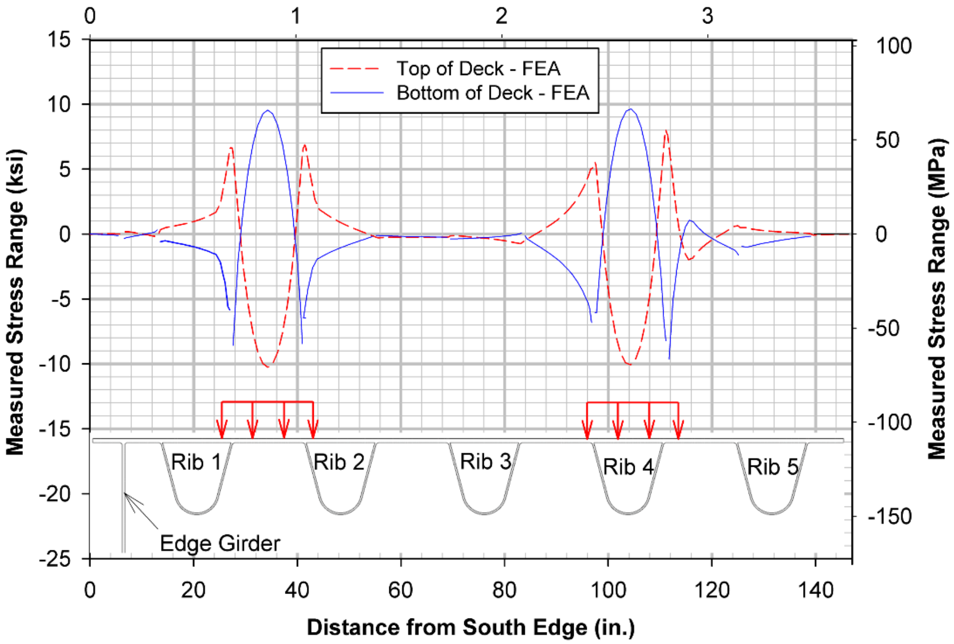

Figure 268. Transverse stress distribution of deck plate at a section through the load pads

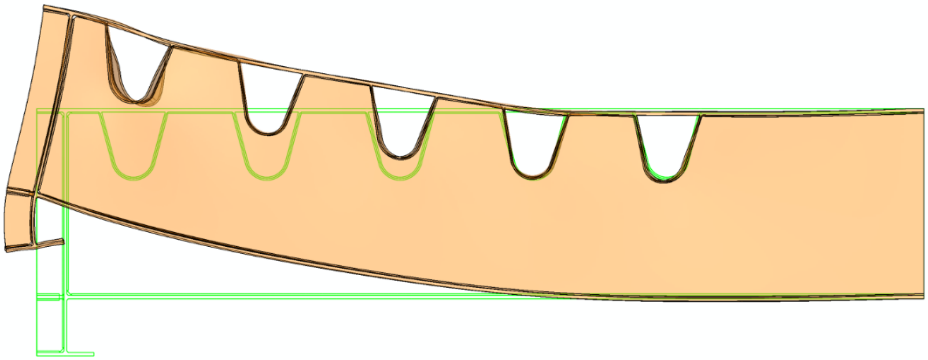

Figure 269. Deformed configuration of inner floor beam overlaid on undeformed configuration

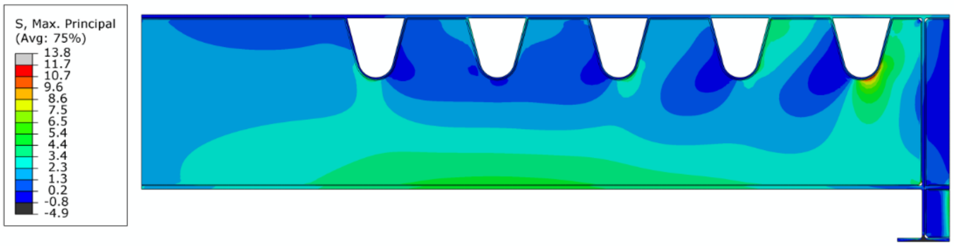

Figure 270. Maximum principal stress contour on floor beam web

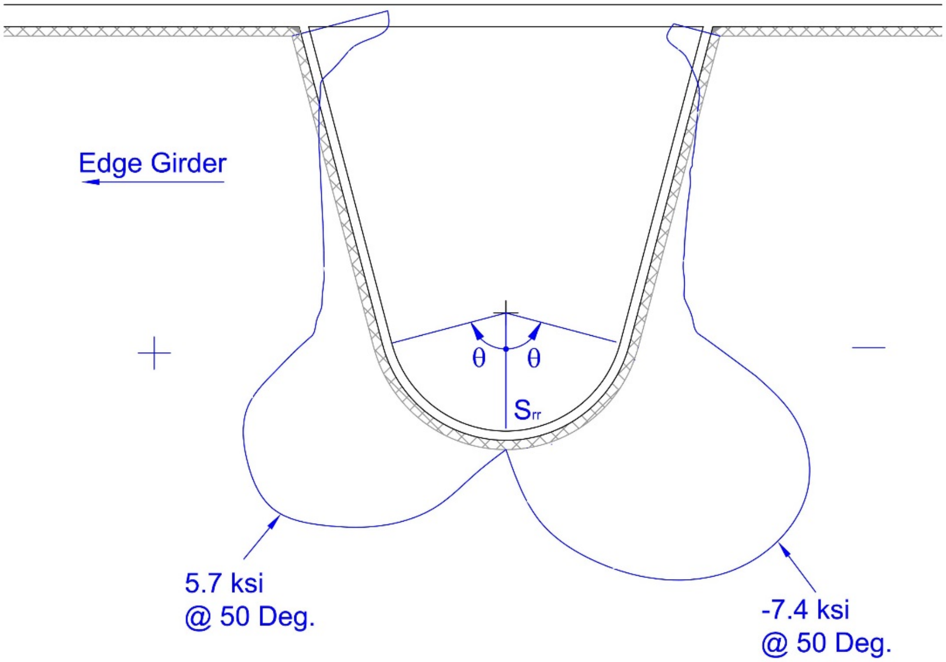

Figure 271. Variation of stress normal to weld toe at the weld toe

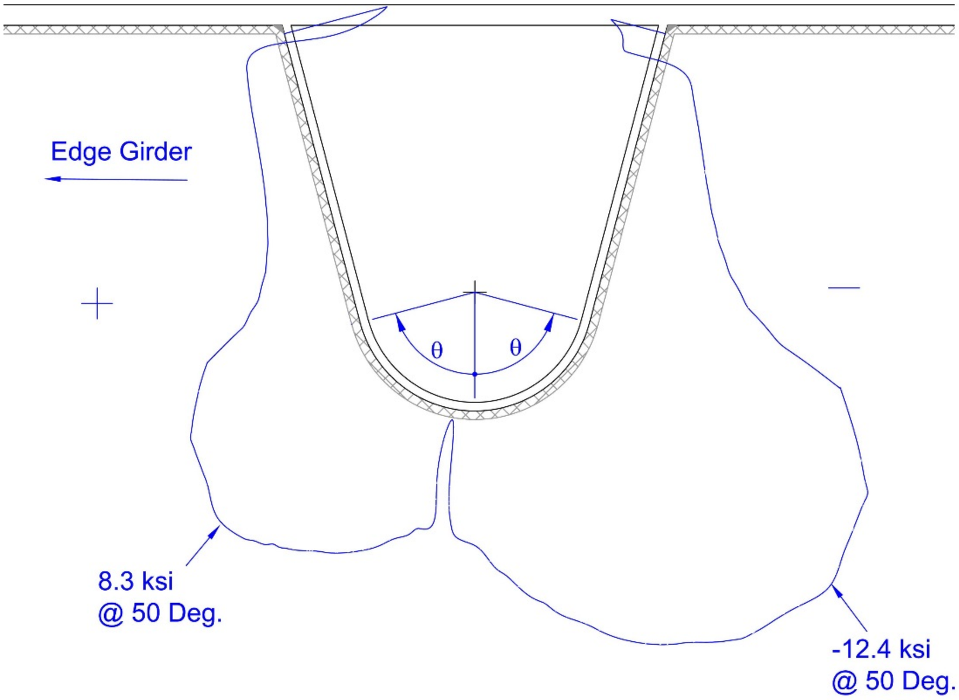

Figure 272. Variation of maximum principal stress at weld root

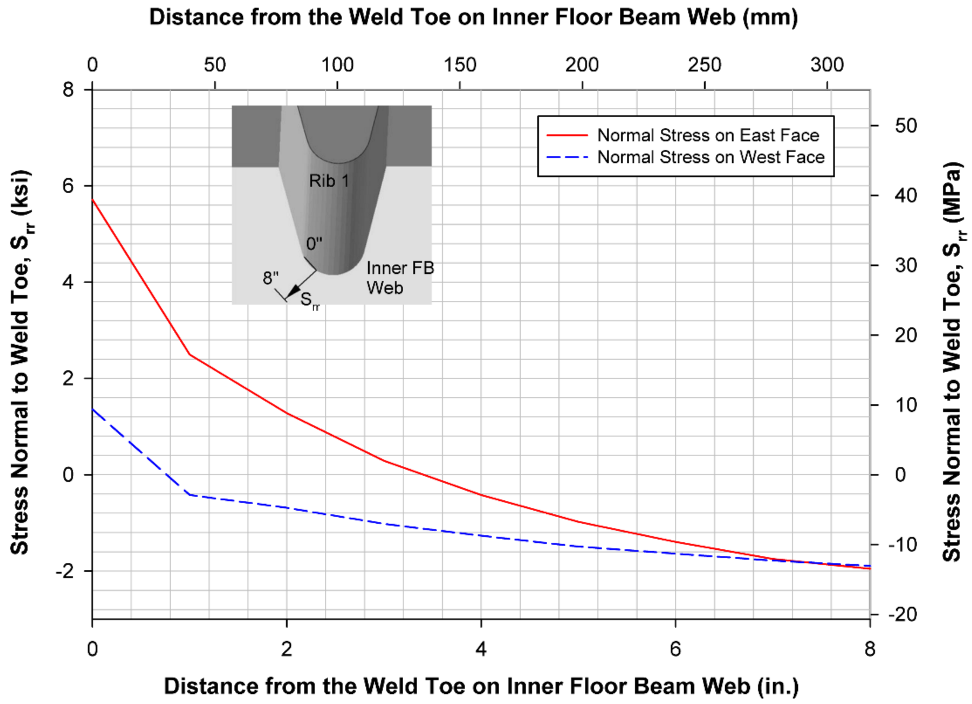

Figure 273. Out-of-plane bending of inner floor beam web

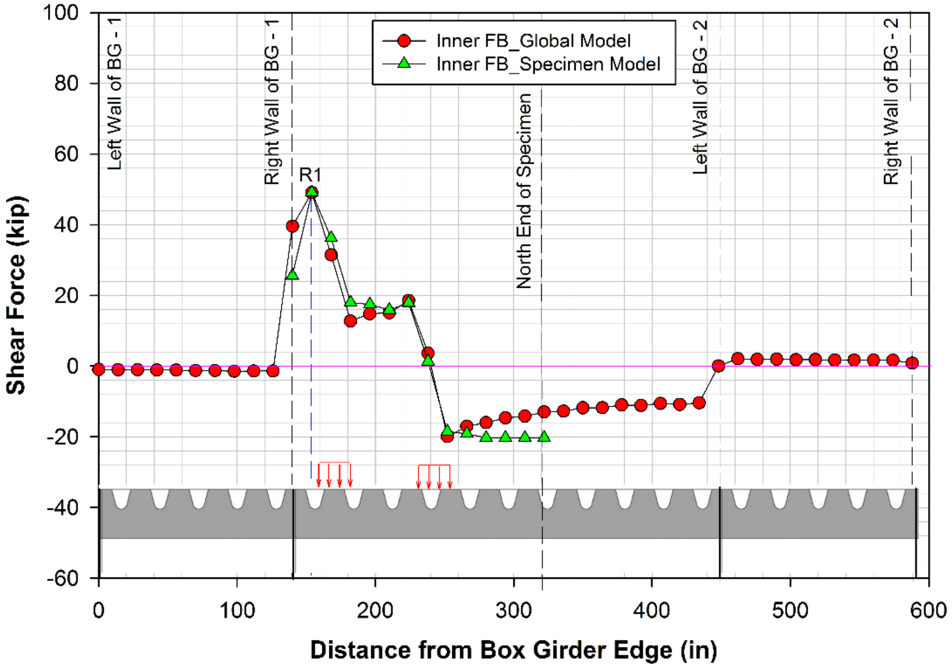

Figure 274. Comparison of shear force in global model and specimen model

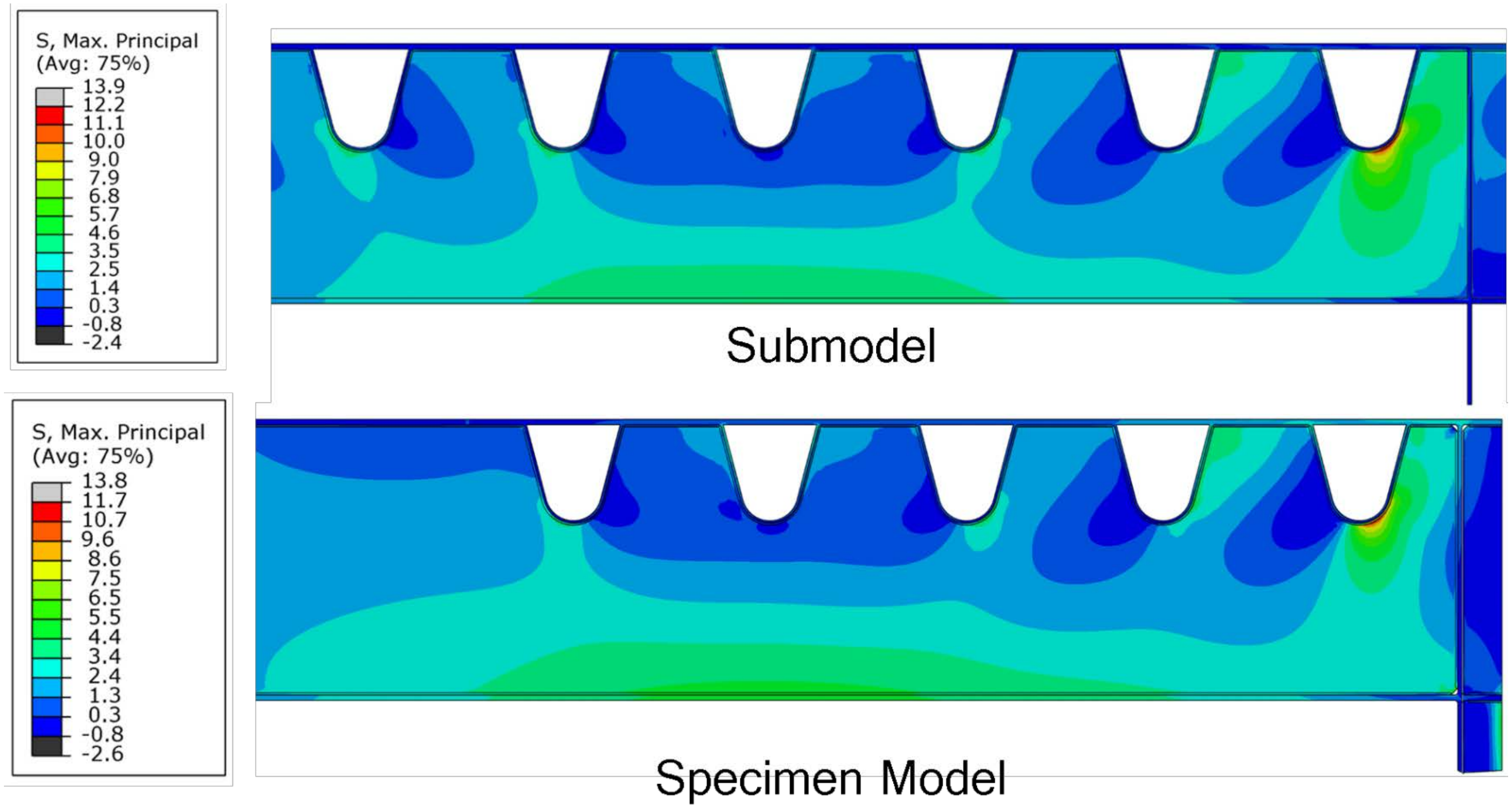

Figure 275. Principal stress comparison between specimen model and submodel

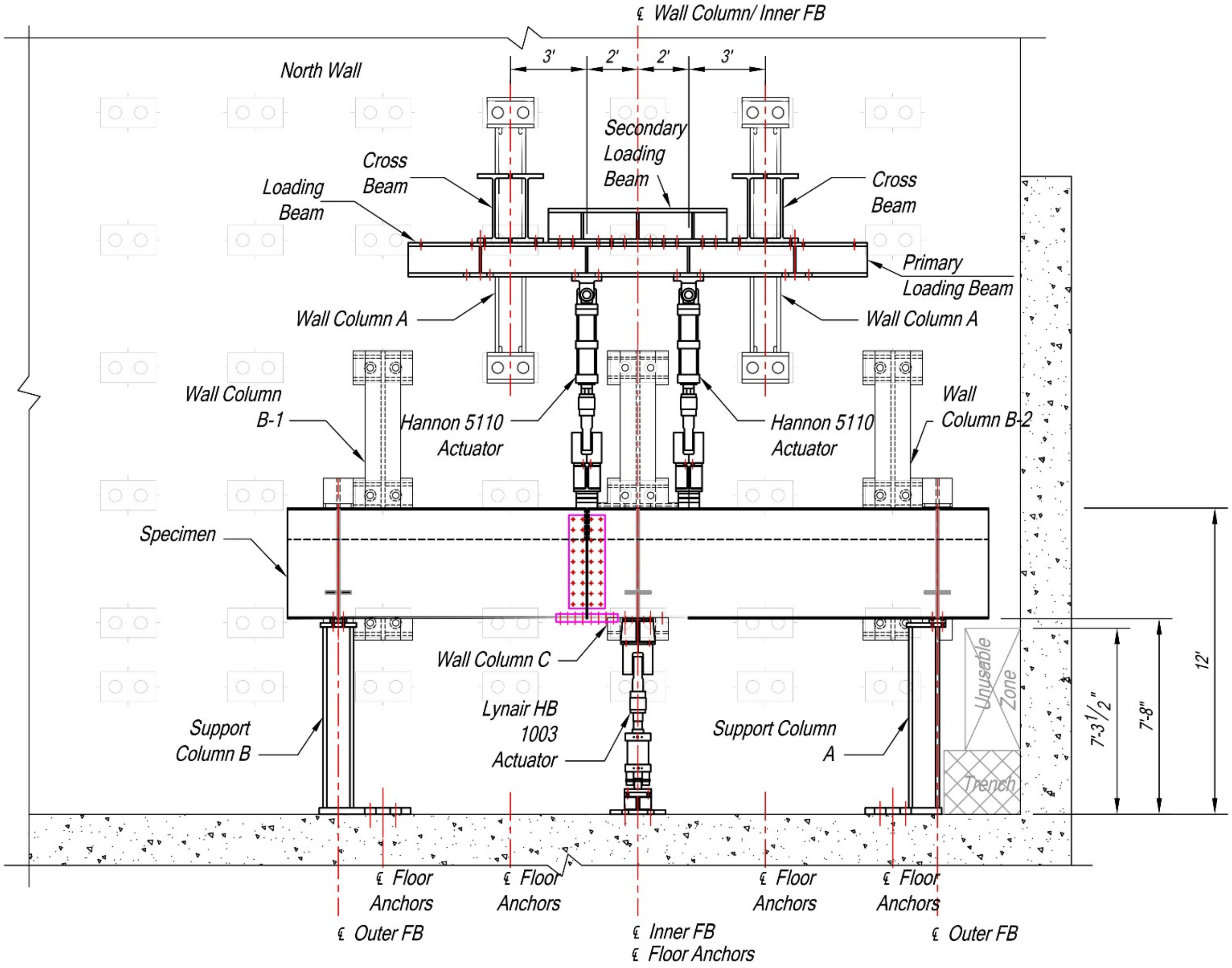

Figure 276. North elevation of the test setup

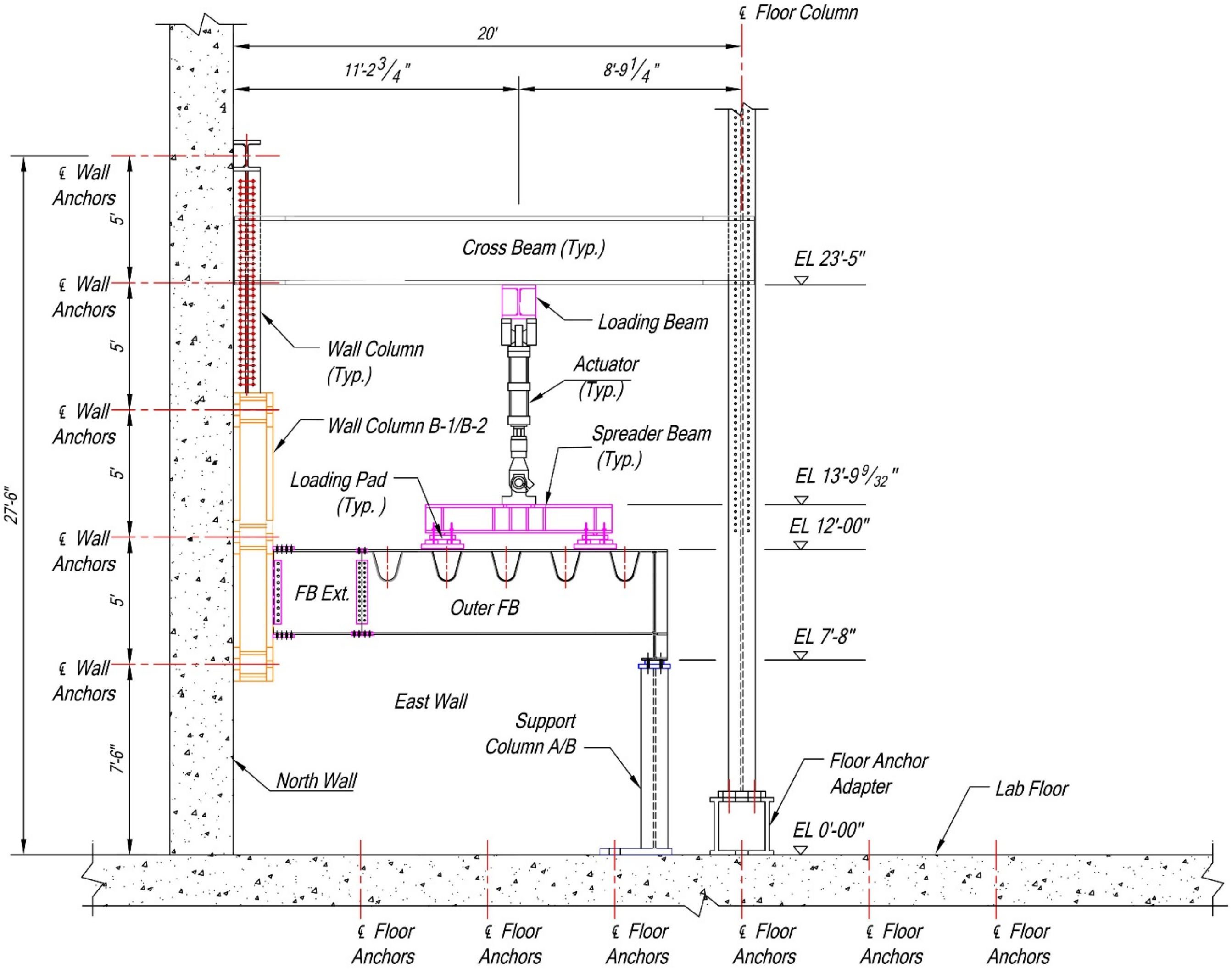

Figure 277. Side elevation of the test setup (looking east)

7. FABRICATION OF FULL-SIZE SPECIMEN

7.1 Overview

The activities undertaken in Task 7 of the research project related to fabrication of the full-size specimen are reported in this chapter. According to NJDOT's directive (provided via email dated March 19, 2013 and other discussions), the details of the full-size prototype orthotropic deck were specified as follows. The rib-to-deck plate connection was specified as an 80% PJP weld with minimum of 70% DOP and a fit-up gap not exceeding 0.020 in. (0.5 mm) The rib-to-floor beam connection was specified as $^{5}/_{16}$ in. (8 mm) fillet weld with fit-up gap not exceeding $^{1}/_{16}$ in. (1.5 mm). It was also specified to develop suitable weld procedure specifications (WPS) for achieving the desired fabrication quality and to demonstrate their success by destructive evaluation of mockups prior to fabricating the full-size specimen. In addition, it was proposed to measure the DOP of rib-to-deck plate welds by PAUT and to verify against the destructive evaluations. The transverse deck splice was specified as a CJP weld at the deck plate and bolted splice at the ribs, with a tolerance of $^{1}/_{16}$ in. (1.5 mm) for vertical and horizontal misalignments. In addition, it was specified to perform the weld using a backing bar and to remove the backing bar after welding is done, and to back gouge and back weld the root and to inspect the quality by 100% UT. Any reinforcement and local defects above $^{1}/_{8}$ in. (3 mm) were specified to be ground flush with the top surface of the deck plate. The deviation from flatness in any direction of the deck was specified as ¼ in. (6 mm) at all sections, except at either end of the splice where it was specified as $^{1}/_{8}$ in. (3 mm). The full-size specimen was fabricated using the qualified WPS duly approved by NJDOT. The prototype deck was fabricated by High Steel Structures at their Lancaster facility. Valuable lessons were learnt during the fabrication of the full-size specimen that may be utilized for cost-effective fabrication of the orthotropic deck for the Wittpenn Bridge.

7.2 Development of Welding Procedures

WPS for the rib-to-deck plate welds were developed and qualified by fabricating several mockups with different welding parameters and in one case a different joint preparation, and subsequent evaluation of weld penetrations and weld profiles on macro-etched sections. In addition, the weld penetration was investigated non-destructively by PAUT for 2 mockups. For rib-to-floor beam connections, the WPS was developed on a mockup panel containing 3 ribs and 3 floor beams, and subsequently qualified by evaluating macro-etched cross sections.

7.2.1 <u>WPS for Rib-to-Deck Plate Welds</u>

25 ft. Single Rib Mockup

A preliminary WPS for rib-to-deck plate PJP welds was developed by High Steel that was evaluated on a 25 ft. long mockup containing a single rib and deck plate as per the Specifications for Large Size Prototype Orthotropic Deck. This mockup is identified as MU4 and will be referred accordingly. The thickness of the rib and the deck plate was identical to the full-size prototype. This WPS involved semi-automatic welding of the rib to the deck plate using a single pass of SAW process in 2G position with Voltage (V) = 34 Volts, Current (A) = 600 Ampere and travel speed of 21 in./min. There was no joint preparation and the rib was square ended producing a natural bevel due to inclination of the rib wall.

MU4 was fabricated on July 26, 2013 using an overhead gantry (Figure 278). A rib, bent to the required profile in a brake press by Greiner Inc. of Mount Joy, PA, was procured and inspected as per the specifications. The rib was pressed down on the deck plate in an inverted position, and was tack welded to the deck plate (on both sides of the rib) at uneven spacing. The maximum and the minimum spacing of the tack welds were 17 in. (432 mm) and 7 in. (178 mm) respectively. The fit-up gap between the rib and the deck plate over the entire length was inspected using a feeler gauge. Subsequently, the rib-to-deck plate weld was made simultaneously on both sides of the rib.

Subsequent to the fabrication of MU4, the rib was sectioned at every 1 ft. (305 mm) after leaving an initial space of 1 in., resulting in 25 segments. The locations of the sections and the tack welds, along with the welding parameters are shown in Figure 279. The rib-to-deck plate section at the beginning of each segment on both sides of the rib (identified as Side A and Side B) was destructively evaluated, except for segment 5 where the sections at the end of the segment was evaluated by mistake. Consequently, the rib-to-deck plate weld sections in segment 5 and 6 were essentially at the same location. In this report, the rib-to-deck plate sections are identified by the mockup identification (MU4) suffixed by the side of the rib (e.g., A or B) and then suffixed by the location of the section from the end where cutting of MU4 was started (e.g., 1, 13, 25, 37, etc.). Total 50 cross sections were prepared, with 25 sections on each side of MU4.

The rib-to-deck plate weld sections were etched at High Steel facility with 5% Nital. The macro-etched sections were then digitally photographed. The dimensional parameters of the rib-to-deck plate weld were measured from the digital photographs of the macro-etched sections at Lehigh University as described in the following. The photographs were imported into AutoCAD 2014 (Autodesk, Inc.), a commercially available CAD program. The nominal rib thickness was considered as the basis for the measurement. A scaling factor was computed as the ratio of the nominal rib thickness to the rib thickness measured from the digital photographs in AutoCAD. The other measured dimensional parameters were multiplied with this scaling factor to obtain the respective sizes. The dimensional parameters are shown in Figure 280. The measured dimensional parameters were: (a) the lack of penetration of the weld along the deck plate surface from the opposite edge of the rib wall, *LOP* and (b) the weld leg on the deck plate with respect to the extension of the rib surface, *D*. The length of the weld penetration along the deck plate surface, P, was estimated by subtracting LOP from the horizontal projected rib thickness (0.3235 in.) as shown in the following:

$$P = 0.3235 - LOP \tag{1}$$

Finally, the weld penetration, WP, was estimated as,

$$WP\ (\%) = \frac{P}{0.3235} \times 100 \tag{2}$$

Prior to sectioning, the rib-to-deck weld penetration was non-destructively estimated by PAUT on July 9, 2013. The testing was performed by Baker Testing Services at High Steel's facility, and was conducted from the deck plate side or Side C as defined by AWS D1.5 Bridge Welding Code (AASHTO/AWS D1.5M/D1.5, 2008) with reference to ultrasonic testing. The sides for ultrasonic testing as per AWS D1.5 are identified in Figure 281. The test setup that was used for the PAUT scanning is shown in Figures 282 and 283. After fabricating MU4, it was turned upside down so that the deck plate was on the top (Figure 282). A guide was then mounted on the deck plate to keep the scan in line. Two Olympus 5L60 probes were mounted onto two Olympus SPWZ1-OC-IHC zero degree wedges. Use of two probes enabled scanning both sides of the rib simultaneously. The probe-wedge combination was mounted to a fixing which was connected to a magnetic encoder, and was pressed onto the deck plate using springs which were integrated in the fixing. The sound couplant was applied automatically during the scan process using tubes which were connected to the wedges. The fixing with attached probes and wedges was moved over the deck plate using the magnetic encoder. The data was collected using an Olympus OmniScan MX1 phased array equipment. The settings of the OmniScan MX1 equipment used during the process is shown in Table 12.

The procedure for determining the weld penetrating using PAUT is discussed in the following. A schematic of scanning procedure is shown in Figure 284. Since a zero degree wedge was used, the ultrasound beams were steered into the deck plate normal to the surface. Once the ultrasound beams traveled through the entire deck plate, some of it was reflected back to the probe by the back wall of the deck plate. In the region were the weld was connecting the deck plate to the rib, the ultrasound beams were not reflected back to the probe. The area in which the sound was reflected back to the probe showed up as saturated reflection (high amplitude reflection) in S-Scan as shown in Figure 285. However, the area which didn't reflect any sound back to the probe showed up blank. This blank area was the sum of the weld leg and the weld penetration. Decibel (dB) drop technique was used for determining the dimension of the blank area. With respect to the maximum amplitude in the S-scan, the location of two points on either side of the centerline of the scan whose amplitude was 50% of the maximum (equivalent to 6 dB drop) were located (two vertical lines as shown in Figure 285). The weld penetration was then determined by subtracting the weld leg.

The macro-etched sections for MU4 are shown in Figures E-1 to E-52. The destructive weld measurements on macro-etched sections are tabulated in Table 13. On side A, the weld penetration ranged between 61% and 100%, with a mean penetration of about 75% and a coefficient of variation (COV) of about 10.5%. However, a smaller variation was noted on side B, where the penetration ranged between 63% and 83% with a mean penetration of about 73% and a COV of about 6.7%. Sections MU4_A_61, MU4_A_109, MU4_A_157 & MU4_A_289 on side A and sections MU4_B_97, MU4_B_145 &

MU4_B_205 on side B were at the tack weld locations. All these sections achieved the minimum penetration of 70% except sections MU4_B_145 & MU4_B_205 on side B.

The discrete measures of weld penetration along the length of MU4 for both sides A and B are graphically presented in Figure 286. Also shown on the figure are the specified and the minimum weld penetrations. Only 3 sections (out of 25) on side A achieved the target penetration of 80%, whereas, on side B only 2 sections (out of 25) achieved the target penetration of 80%. The minimum specified penetration of 70% was achieved by 19 sections (out of 25) of each of side A and B respectively. As the rib-to-deck plate weld was performed on both sides simultaneously using the same weld parameters, their combined penetration data is statistically shown in Figure 287 as bar chart. As it can be seen from the figure, 82% of the sections (41 out of 50) achieved the minimum penetration of 70%, however, only 10% of the sections (5 out of 50) achieved the target penetration of 80%.

The weld penetration measurements by PAUT on sides A and B are compared with the destructive measurements in Tables 14 and 15 respectively. Initial PAUT measurements were done based on an assumed weld leg of 0.31 in. So a significant variation was observed in the PAUT measurements with respect to the destructive measurements. The variation was due to the variation in size of the actual weld leg, measured from the cross sections. When the PAUT data was corrected for the actual weld leg at each section, the weld penetration from PAUT was more consistent with the destructive measurements, however, the difference was still very high at few sections. The maximum difference was about 35% and 69% for sides A and B respectively.

A typical macro-etched section of the rib-to-deck plate weld for MU4 is shown in Figure 288. The photo macrographs of all the sections are presented in Appendix D, contained in Volume VII. The weld profiles were still similar to the Phase 2 studies, showing “washout” at the rib end, and splay near the surface. This kind of profile was indicative of a higher heat input that was used for achieving the specified penetration without a joint preparation. Weld meld through condition was noted at one location on side A (Figure 289). Blow through condition was also noted at one location on both sides of the rib (Figures 290 and 291). Blow through condition was unacceptable as per the specifications, however, no repair procedure was developed during that phase. Blow through condition was again noted during the fabrication of the full-size specimen. Accordingly, a repair procedure was developed which is discussed in detail in section 7.3.

The DOP of the rib-to-deck plate welds at most of the sections (19 out of 25 for each side) achieved the minimum penetration of 70%. However, only few sections achieved the target penetration of 80%, and, the weld profile was still similar to the Phase 2 studies. Accordingly, the existing WPS for the rib-to-deck plate welds was further evaluated in one of the ribs in the following 3 rib mockup, which was fabricated to evaluate the WPS of the rib-to-floor beam weld also. In the other two ribs, alternative procedures were evaluated for improvement of the weld quality. The evaluation of the 3 rib mockup is discussed in the following section.

3 Rib Mockup

The 3 rib mockup consisted of 3 ribs (Rib 1, Rib 2 and Rib 3), 3 floor beams and deck plate. The specimen is identified as MU5 and will be referred accordingly. The thickness of the ribs, the floor beams and the deck plate and spacing between the ribs were identical to the full-size prototype. However, the spacing between the floor beams was reduced to 5 ft. 6 in. (1.7 m) to restrict the length of the mockup. The overall dimensions of MU5 were 15 ft. in length and 7 ft. in width. The rib-to-deck plate welds for ribs 1 and 2 were fabricated employing the preliminary WPS without any joint preparation on the rib wall (square ended rib). The welding parameters for Rib 1 was same as that of 25 ft. mockup. However, the welding parameters were changed in Rib 2 to reduce the heat input, and Voltage (V) = 33 Volts, Current (A) = 580 Ampere and travel speed of 21 in./min were used. The rib-to-deck plate welds for Rib 3 were fabricated with a joint preparation on the rib wall that included a bevel of 50° on the rib wall (including the natural bevel due to the inclination of the rib wall) and a landing of $^1/_8$ in. (3 mm). The rib-to-deck plate weld for Rib 3 was done with Voltage (V) = 33 Volts, Current (A) = 480 Ampere and travel speed of 21 in./min. The rib-to-deck plate weld details for ribs 1, 2 and 3 are shown in Figures 292, 293, and 294 respectively. The WPS for the 3 ribs involved semi-automatic welding of the ribs to the deck plate using a single pass of SAW process.

MU5 was fabricated using an overhead gantry following the same procedure as MU4. Subsequent to the fabrication of MU5, the ribs were sectioned at every 1 ft. (305 mm) interval after leaving an initial and a final space of 6 in., resulting in 14 segments. Additional two sections were taken at 84 in. and 156 in. The locations of the sections and the tack welds are shown in Figure 295. The rib-to-deck plate section at the beginning of each segment on both sides of the ribs (identified as Side A and Side B) was destructively evaluated. In this report, the rib-to-deck plate sections are identified by the rib identification (e.g., R1, R2 or R3) suffixed by the side of the rib (e.g., A or B) and then suffixed by the location of the section from the end where cutting of MU5 was started (e.g., 6, 18, 30 etc.). Some of the sections were not taken exactly at 1 in. interval, however while naming the sections, their location was rounded to the next integer (e.g. 53.875 rounded to 54). Total 32 cross sections were prepared for each rib, with 16 sections on each side of the ribs. As in MU4, the weld penetration was estimated in MU5 both non-destructively (using PAUT) and destructively following the same procedures of MU4. The PAUT and the destructive measurements were done by Baker Testing Services and Lehigh University respectively.

The macro-etched sections for MU5 are shown in Appendices E, F and G, contained in Volume VII, for ribs 1, 2 and 3 respectively. The destructive weld measurements on macro-etched sections are tabulated in Tables 16, 17, and 18 for ribs 1, 2 and 3 respectively. For Rib 1, on side A, the weld penetration ranged between 62% and 72%, with a mean penetration of about 68% and a COV of about 4.3%. However, larger penetrations were noted on side B, where the penetration ranged between 65% and 77% with a mean penetration of about 71% and a COV of about 4.8%. For Rib 2, the distribution of weld penetration was lower. On side A, the weld penetration ranged between 54% and 67%, with a mean penetration of about 63% and a COV of about

4.6%. A larger variation was noted on side B, where the penetration ranged between 57% and 81%, with a mean penetration of about 68% and a COV of about 8.3%. The distribution of weld penetration in Rib 3 which was fabricated with a joint preparation, was the lowest of all the ribs. On side A, the weld penetration ranged between 54% and 81%, with a mean penetration of about 62% and a COV of about 10.1%. On side B, the weld penetration ranged between 55% and 72%, with a mean penetration of about 63% and a COV of about 6.8%.

The discrete measures of weld penetration along the length of MU5 for both sides A and B are graphically presented in Figures 296, 297, and 298 for ribs 1, 2 and 3 respectively. Also shown on the figure are the specified and the minimum weld penetrations. None of the sections for Rib 1 achieved the target penetration of 80%, whereas only 1 section for each of ribs 2 and 3 achieved the target penetration. The minimum specified penetration of 70% was achieved by 7 sections (out of 16) on side A and 12 sections (out of 16) for side B of Rib 1. However for rib 2, none of the sections on side A and 4 sections (out of 16) on side B achieved the minimum penetration. Similar to Rib 2, only 1 section (out of 16) for each side of Rib 3 achieved the minimum penetration. As the rib-to-deck plate weld was performed on both sides of each rib simultaneously using the same weld parameters, their combined penetration data is statistically shown as bar charts in Figures 299, 301, and 302 for ribs 1, 2 and 3 respectively. As it can be seen for Rib 1, 59% of the sections (19 out of 30) achieved the minimum penetration of 70%, however, none of the sections achieved the target penetration of 80%. Since, the weld parameters for Rib 1 and 25 ft. single rib mockup was identical, their combined penetration data is statistically shown in Figure 300. As it can be seen from the figure, 70% of the sections (57 out of 82) achieved the minimum penetration of 70%, whereas only 6% of the sections (5 out of 82) achieved the target penetration. For ribs 2 and 3, the distribution of weld penetration showed low penetrations values. Only 12.5% (5 out of 32) and 6% (2 out of 32) achieved the minimum penetration of 70% for ribs 2 and 3 respectively. For both ribs 2 and 3, only 3% of the sections (1 out of 32) achieved the target penetration of 80%.

The weld penetration measurements by PAUT on sides A and B for the ribs are compared with the destructive measurements in: Tables 19 and 20 for Rib 1; Tables 21 and 22 for Rib 2 and Tables 23 and 24 for Rib 3. The weld penetration obtained from PAUT, although significantly different from the destructive measurements at certain sections, were generally in good agreement. In almost all cases, the PAUT under estimated the weld penetration. The maximum difference noted was 23% (1.9 mm) at a section on side B for Rib 2. The penetration by PAUT was determined based on the weld leg dimensions obtained by the Bridge welding gauge. Some of the differences in penetration between the PAUT and the destructive measurements was attributed to this difference in the measured weld sizes. Other source of the difference was in the PAUT process, which could not be ascertained without a detailed methodology.

A typical macro-etched section of the rib-to-deck plate weld for ribs 1, 2 and 3 is shown in Figures 303, 304, and 305 respectively. The photo macrographs of all the sections are presented in Appendices E, F and G, contained in Volume VII, respectively. The macro etched sections of ribs 1 and 2 showed similar wash down profile (bulging at the deck plate end and under fill at the rib end) as MU4 and the mock up specimens of Phase 2, which is indicative of higher heat input that was used to achieve penetration without a joint preparation. The macro etched sections of Rib 3, which was welded with a lower heat input, did not exhibit the wash down profile. However, severe undercutting was noted at the rib end. Apparently, welding of this rib was not adequately performed, which was also evident by meandering of the welds between 156 in. and 180 in. on side A that was observed during PAUT measurements. The weld cross section for all ribs showed more inclination towards the deck plate, and a splay near the surface. Such splayed cross section is indicative of AC welding process that was used for these rib fabrication, and/or higher heat input or slower welding speed, as was explained in the Phase 2 studies (section 5.2, contained in Volume II).

As is evident, for all the ribs the rib-to-deck plate weld didn’t meet the specification, with ribs fabricated with no joint preparation using reduced heat input and with joint preparation showing lower values of weld penetration. In addition, the weld profiles were unacceptable. Accordingly, in the following 12 ft. single rib mockups (2 numbers), four different combinations of welding parameters were evaluated where the rib-to-deck plate welds were fabricated as per the specifications without any joint preparation on the rib wall. The evaluation of the 12 ft. single rib mockups is discussed in the following section.

12 ft. Single Rib Mockups

Two 12 ft. 2 in. mockups were fabricated containing a single rib and deck plate as per the Specifications for Large Size Prototype Orthotropic Deck. The mockups are identified as MU6 and MU7 and will be referred accordingly. Four different combinations of welding parameters including: voltage, current, wire angle, polarity balance and travel speed were tried with one combination on each side of the ribs (identified as Side A and Side B). The different weld combinations are tabulated in Table 25. The rib-to-deck plate welds were performed semi-automatically using a single pass of SAW process.

MU6 and MU7 were also fabricated using an overhead gantry similar to the previous mockups. The DOP in these ribs was subsequently evaluated by cutting sections and etching them. During fabrication of these mockups, significant blow through occurred over the initial portion in both MU6 and MU7 due to gantry malfunctioning. The portions containing the blow through were discarded and remaining portions were sectioned for destructive evaluation. MU6 was sectioned into 9 segments 12 in. apart and MU7 was sectioned into 12 segments 12 in. apart. Since the destructive measurements were done at High Steel, the exact locations of the segments were not known. In this report, the rib-to-deck plate sections are identified by the mockup identification (e.g., MU6 or MU7) suffixed by the side of the rib (e.g., A or B) and then suffixed by the section number from start (e.g., 1, 2, 3, etc.). Total 18 sections were prepared for MU6 with 9 sections on each side of the rib. And for MU7, total 24 sections were prepared with 12 sections on each side of the rib.

The destructive weld measurements on macro-etched sections are tabulated in Tables 26 and 27, respectively for MU6 and MU7. For MU6, on side A, the weld penetration ranged between 74% and 83%, with a mean penetration of about 79% and a COV of about 3.6%. However, lesser penetrations were noted on side B, where the penetration ranged between 70% and 82% with a mean penetration of about 74% and a COV of about 5.7%. All the sections for both sides A and B in MU6 achieved the minimum penetration of 70%. The specified penetration of 80% was achieved by 4 sections (out of 9) and 1 section (out of 9) for sides A and B respectively. For MU7, on side A, the weld penetration ranged between 78% and 89%, with a mean penetration of about 84% and a COV of about 3.9%. However, lesser penetrations were noted on side B, where the penetration ranged between 64% and 84% with a mean penetration of about 77% and a COV of about 7.7%. All the sections on side A achieved the minimum penetration of 70%, and 11 sections (out of 12) achieved the target penetration of 80%. However on side B, 11 sections (out of 12) achieved the minimum penetration and 5 sections (out of 12) achieved the target penetration.

A typical macro-etched section of the rib-to-deck plate weld for sides A and B for MU6 and MU7 is shown in Figures 306, 307, 308 and 309 respectively. The macro etched sections showed similar wash down profile (bulging at the deck plate end and under fill at the rib end) as the other mockups. However, the wash down was the least for MU7 side A.

The weld penetrations in MU7 side A was the best among the 4 trials, as only 1 section (out of 12) didn't achieve the target penetration but all the sections achieved the minimum penetration of 70%. Accordingly, High Steel issued a WPS for the rib-to-deck plate welds based on the results of MU7 side A. The WPS and the functioning of the gantry was verified in the following 16 ft. single rib mockup. The evaluation of the 16 ft. single rib mockup is discussed in the following section.

16 ft. Single Rib Mockup

A 16 ft. mockup was fabricated containing a single rib and deck plate as per the Specifications for Large Size Prototype Orthotropic Deck. The mockup is identified as MU8 and will be referred accordingly. The rib was $^{5}/_{16}$ in. (8 mm) thick, but trapezoidal in shape. The cross section of the rib didn't adhere to the specifications, because spare trapezoidal rib was readily available at High Steel and the specimen was fabricated for evaluation purpose only. The rib-to-deck welds were performed following the WPS, developed based on the results of MU7 side A, which involved semi-automatic welding of the rib to the deck plate using a single pass of SAW process. There was no joint preparation on the rib wall (square ended rib). The rib-to-deck plate weld detail along with the welding parameters is shown in Figure 310.

Similar to other mockups, MU8 was also fabricated using an overhead gantry similar to the previous mockups. The rib was sectioned at every 1 ft. interval, resulting in 16 segments. The locations of the sections are shown in Figure 311. The rib-to-deck plate section at the end of each segment on both sides of the rib (identified as Side A and Side B) was destructively evaluated at Lehigh University. In this report, the rib-to-deck plate sections are identified by the mockup identification (MU8) suffixed by the side of the rib (e.g., A or B) and then suffixed by the location of the section from the end where cutting of MU4 was started (e.g., 12, 24, 36, 48, etc.). Total 32 cross sections were prepared, with 16 sections on each side of MU4.

The macro-etched sections for MU8 are shown in Figures 621 to 652. The destructive weld measurements on macro-etched sections are tabulated in Table 28. On side A, the weld penetration ranged between 72% and 85%, with a mean penetration of about 77% and a COV of about 3.5%. On side B, the penetration ranged between 74% and 85% with a mean penetration of about 80% and a COV of about 4.4%.

The discrete measures of weld penetration along the length of MU8 for both sides A and B are graphically presented in Figure 312. Also shown on the figure are the specified and the minimum weld penetrations. All the sections on sides A and B achieved the minimum penetration of 70%. The target penetration of 80% was achieved by 2 sections (out of 16) and 9 sections (out of 16) on side A and side B respectively. As the rib-to-deck plate weld was performed on both sides simultaneously using the same weld parameters, their combined penetration data is statistically shown in Figure 313 as bar chart. As it can be seen from the figure, 100% of the sections (32 out of 32) achieved the minimum penetration of 70% and 34% of the sections (11 out of 32) achieved the target penetration of 80%. A summary of the weld penetrations for MU8 is tabulated in Table 29.

A typical macro-etched section of the rib-to-deck plate weld for MU8 is shown in Figure 314. The photo macrographs of all the sections are presented in Appendix H, contained in Volume VII. Although, the weld profile showed a slight wash down due to welding in 2G position with relatively high heat input required for joints without any preparation, the typical weld cross section showed a much improved profile than what was accomplished in the earlier mockups.

WPS for the Full-size Specimen

Based on the findings of MU8, the latest WPS was approved by NJDOT for fabricating the full-size deck specimen. The rib-to-deck plate weld detail was as per the Specifications for Large Size Prototype Orthotropic Deck which specified an 80% PJP weld with a minimum DOP of 70% and a fit-up gap not exceeding 0.020 in. (0.5 mm). The WPS involved semi-automatic welding of the rib-to-deck plate weld using SAW process with V = 550-650 Volts, A = 32-35 Ampere, electrode angle of 60° and a travel speed of 17-23 in./min. The approved WPS is provided as Appendix I, contained in Volume VII.

7.2.2 <u>WPS for Rib-to-Floor Beam Welds</u>

3 Rib Mockup (MU5)

The WPS for rib-to-floor beam fillet welds was evaluated in MU5 which had three floor beams and three ribs, resulting in nine rib-to-floor beam connections. The description of MU5 has been already given earlier. The three floor beams were located at 2 ft., 7 ft. 6 in. and 13 ft., respectively from the end of MU5 from where the sectioning of rib-to-deck plate weld was started. The rib-to-floor beam welds were fabricated as per the

Specifications for Large Size Prototype Orthotropic Deck, except the maximum fit-up gap which was increased to $^3/_{32}$ in. (2.4 mm) with a target fit-up gap of $^1/_{16}$ in. (1.6 mm). This WPS involved manual welding of the rib to the floor beam using GMAW process by standing the deck on the rib ends. All the welds were done in 2F position, which was accomplished by flipping the deck after completing the welds on one side.

The nine rib-to-floor beam connections were cut out MU5 and shipped to ATLSS Center by High Steel. Each connection was further sectioned at 7 locations as shown in Figure 316. In this report, the rib-to-floor beam sections are identified by the rib identification (e.g., R1, R2 or R3) suffixed by the location of the floor beams (e.g., 24, 90 or 156) and then suffixed by the number of the section (e.g., 1, 2, 3, 4, etc.). Total 63 cross sections were prepared, with 7 sections at each rib location (3 ribs) for each floor beam (3 floor beams).

The rib-to-floor beam weld sections were etched at Lehigh University with 5% Nital. The macro-etched sections were then digitally photographed. The dimensional parameters of the rib-to-floor beam weld were measured from the digital photographs of the macro-etched sections as described in the following. The photographs were imported into AutoCAD 2014 (Autodesk, Inc.). The nominal floor beam thickness was considered as the basis for the measurement. A scaling factor was computed as the ratio of the nominal floor beam thickness to the floor beam thickness measured from the digital photographs in AutoCAD. The other measured dimensional parameters were multiplied with this scaling factor to obtain the respective sizes. The dimensional parameters are shown in Figure 317. The measured dimensional parameters were: (a) the lack of fusion of the weld, *LOF* and (b) the root opening or fit-up gap between the rib and the floor beam, *R*.

The macro-etched sections of the rib-to-floor beam welds in MU5 are shown in Figures 589 to 620. The destructive weld measurements on the macro-etched sections are tabulated in Tables Table 30 to Table 32 for connections with Rib 1, Tables 33 to 35 for connections with Rib 2 and Tables 36 to 38 for connections with Rib 3. Since all the connections were fabricated with same welding parameters, a summary of the destructive weld measurements is tabulated in Table 39. The value of R ranged between 0.006 in. and 0.117 in. (~$^1/_8$ in.), with a mean of 0.03 in. (~$^1/_{32}$ in.) and a large COV of 67.5%. Such large COV can be expected considering the small magnitude of R. The distribution of R is statistically shown in Figure 318. Out of 63 sections, the root gap at 59 sections (94%) was less than the target of $^1/_{16}$ in. (less than 2 mm). The largest root gap, exceeding $^3/_{32}$ in. occurred only at 1 section (R3_90_1). The LOF showed a lot less variance (COV of 12.5%), with a mean of 0.414 in., or mean fusion of 17.2%. The distribution of LOF is statistically shown in Figure 319. Such small fusion or large LOF is typical of fillet welded connections. At 2 sections (out of 63), the weld did not fuse the floor beam (R2_24_7 and R2_90_4). The larger fit-up gaps and the unfused floor beams mostly occurred at the intersection of the rib-to-deck plate and rib-to-floor beam welds. Only at R2_90_4, the floor beam was not fused at the rib soffit.

A typical-macro-etched section of the rib-to-floor beam weld is shown in Figure 320. The photo macrographs of all the sections are presented in Appendix J, contained in Volume

VII. The weld profiles were typical of manual fillet welds. At the rib-to-deck plate and the rib-to-floor beam intersections (Figure 321), however, the weld profiles were questionable.

WPS for the Full-size Specimen

The WPS for the rib-to-floor beam weld used for MU5 was approved for fabricating the full-size specimen, except the maximum fit-up gap was limited to $^1/_{16}$ in. following the Specifications for Large Size Prototype Orthotropic Deck. The approved WPS is provided in Appendix K, contained in Volume VII.

7.3 Fabrication of Full-size Specimen

The full-size specimen was fabricated by High Steel at their Lancaster facility, using the qualified WPS duly approved by NJDOT. The deck was fabricated in two panels 15 ft. 9 in. and 11 ft. 9 in. long respectively, to simulate the transverse field splice condition during fatigue testing. The two panels will be referred as long panel and short panel in subsequent texts. The panels were spliced at ATLSS Center and the splicing procedure is discussed in detail in Chapter 8. The rib-to-floor beam and rib-to-deck plate connection details used for the full-size specimen are shown in Figure 322.

The short panel was fabricated prior to the long panel. The rib-to-deck plate welds were performed from the innermost ribs outwards in the sequence of 3, 5, 2, 4 and then 1, by using single pass of SAW process simultaneously on each side of the ribs. During the welding of Rib 3 to the deck plate, blow through conditions were observed on both sides of the rib near the splice end. The dimensions of the blow troughs were 1 ½ in. and 2 in. respectively (Figures 324 and 325). To prevent the condition of blow through, the fabricator placed tack welds on both sides of the rib at the splice end for all of the remaining four ribs. With this measure, ribs 3 and 5 were successfully welded without any further blow through. However, undesirable weld profiles were observed for ribs 3 and 5. To correct the weld profile, the fabricator reduced the travel speed and increased the current during performing the rib-to-deck plate weld for Rib 2, however, both the parameters were within the allowable range of the WPS. The correction didn't brought about much improvement in the weld profile, but caused two blow through (5 in. and 6 in. respectively) on one side of Rib 2 towards the splice end. Welding of the rib-to-deck plate connection for Rib 2 was stopped with immediate effect and the welder in the machine was thoroughly examined. It was found out that the welder was out of calibration by more than two volts and this happened when the welder was switched from one production process to another at the beginning of the full-size deck fabrication. Once the welder was recalibrated and the welds were run within procedure, all the rib-to-deck plate welds were performed without any blow through and desired weld profile was observed. This was verified by welding several short calibration rib-to-deck welds on scarp material. Several of these were also cut and etched to ensure that adequate penetration was being maintained. All of the sections showed weld penetration more than the minimum specified of 70%. The measurements of the weld penetrations and the quality of the weld profiles in the full-size specimen are discussed in detail in Chapter 11, contained in Volume VII.

A repair procedure was developed for repairing the blow through portions of the rib-to-deck plate welds in ribs 3 and 2. The blow through portions in Rib 3 were excavated out by grinding (Figure 326) 4 in. of the weld. Magnetic Particle testing was used to verify the soundness of the remaining weld. 3 passes for GMAW process (Figure 327) were then applied to fill-up the excavated welds. For Rib 2 with larger blow through, the blow through portions were excavated out by using carbon arc (Figures 328 and 329). After verifying the soundness of the remaining weld by Magnetic Particle testing, 5 passes of GMAW process (Figure 330) was applied to fill-up the excavated welds. The repair procedure was documented and is provided in Appendix L, contained in Volume VII. The floor beams were then match cut (Figure 331) according to as-fabricated rib profile and were fitted around the ribs using tack welds, to the specified fit-up gap not exceeding $^{1}/_{16}$ in. (2 mm) as shown in Figure 331. The floor beams were them welded to the deck plate using $^{5}/_{16}$ in. (8 mm) fillet welds on both sides of the web. The rib-to-floor beam fillet welds were performed in 2F position (Figure 333) by a single pass continuously around the rib using GMAW process. The edge girder web was then connected to the deck plate using $^{5}/_{16}$ in. (8 mm) fillet welds on both sides of the web. Subsequent to this, the floor beam web was connected the edge girder web using $^{5}/_{16}$ in. (8 mm) fillet welds on both sides of the web. The floor beam flange-to-edge girder web CJP weld was then performed using multi-passes of SAW process.

The long panel was fabricated following same sequence of welding procedures as the short panel. While performing the rib-to-deck plate weld for Rib 1 in the long panel, the overhead welding gantry got stopped due to an error at approximately 34 in. from the end (Figure 334). As it was specified to remove all weld starts and stops, the fabricator proposed to start the welding from the end on the run off tab and then travel back to the stop location. This proposal was approved by NJDOT and this change in the procedure resulted in a single stop location on both sides of the rib instead of start and stop on each side.

Table 12 - OmniScan MXI Equipment Settings for Side C Scanning

Parameter	Value
Probe	Olympus 5L60
Wedge	Olympus SPWZ1-OC-IHC
Part material	Steel, mild
Ultrasound wave type	Shear wave (SW)
Groups	2
Probe Frequency	5 MHz
Available elements	60
Active elements	16
First element	1
Last element	16
Scan type used	Linear Scan
Minimum sector angle (Bottom boundary)	N/A
Maximum sector angle (Top boundary)	N/A
Stepping	0.5
Focus depth	0.75 in. (true depth focusing)
Measurement readings:	- A% (A-Scan amplitude in gate A)
Scan resolution	0.15 in.
	- DA^ (True depth distance)
	- PA^ (Horizontal distance from wedge)
	- SA^ (Sound path distance)
View setting used	A-Scan / S-Scan / C-Scan

Table 13 - Measured Dimensional Parameters of Rib-to-Deck Plate Weld for Sides A and B for MU4

	Side A				Side B			
SL. No.	ID[a]	LOP[b] (in.)	P[b] (in.)	Weld Penetration[c] [WP] (%)	ID[a]	LOP[b] (in.)	P[b] (in.)	Weld Penetration[c] [WP] (%)
1	MU4_A_1	0.094	0.229	71	MU4_B_1	0.090	0.234	72
2	MU4_A_13	0.054	0.269	83	MU4_B_13	0.055	0.268	83
3	MU4_A_25	0.037	0.286	88	MU4_B_25	0.072	0.252	78
4	MU4_A_37	0.073	0.251	77	MU4_B_37	0.072	0.252	78
5	MU4_A_61	0.093	0.231	71	MU4_B_61	0.082	0.242	75
6	MU4_A_61	0.083	0.241	74	MU4_B_61	0.084	0.240	74
7	MU4_A_73	0.082	0.242	75	MU4_B_73	0.091	0.232	72
8	MU4_A_85	0.069	0.254	79	MU4_B_85	0.109	0.215	66
9	MU4_A_97	0.086	0.237	73	MU4_B_97	0.092	0.232	72
10	MU4_A_109	0.068	0.256	79	MU4_B_109	0.081	0.242	75
11	MU4_A_121	0.070	0.253	78	MU4_B_121	0.121	0.202	63
12	MU4_A_133	0.113	0.210	65	MU4_B_133	0.093	0.231	71
13	MU4_A_145	0.090	0.233	72	MU4_B_145	0.102	0.222	68
14	MU4_A_157	0.074	0.250	77	MU4_B_157	0.075	0.249	77
15	MU4_A_169	0.089	0.235	73	MU4_B_169	0.097	0.227	70
16	MU4_A_181	0.075	0.248	77	MU4_B_181	0.091	0.233	72
17	MU4_A_193	0.115	0.208	64	MU4_B_193	0.066	0.257	79
18	MU4_A_205	0.110	0.213	66	MU4_B_205	0.107	0.216	67
19	MU4_A_217	0.070	0.254	78	MU4_B_217	0.072	0.252	78
20	MU4_A_229	0.084	0.240	74	MU4_B_229	0.100	0.223	69
21	MU4_A_241	0.127	0.196	61	MU4_B_241	0.057	0.266	82
22	MU4_A_253	0.076	0.247	76	MU4_B_253	0.095	0.229	71
23	MU4_A_265	0.089	0.234	72	MU4_B_265	0.090	0.234	72
24	MU4_A_277	0.000	0.324	100	MU4_B_277	0.096	0.227	70
25	MU4_A_289	0.072	0.252	78	MU4_B_289	0.096	0.227	70
	Maximum	0.127	0.324	100	Maximum	0.121	0.268	83
	Minimum	0.000	0.196	61	Minimum	0.055	0.202	63
	Mean	0.080	0.244	75	Mean	0.087	0.236	73
	Std. Dev.	0.026	0.026	7.9	Std. Dev.	0.016	0.016	4.9
	COV	32.1	10.5	10.5	COV	18.2	6.7	6.7

[a] Refer to Figure 279 for identification of sections

[b] Refer Figure 280 for identification of parameters

[c] Weld Penetration (%) is calculated as {(P)/0.3235}x100

Table 14 - Comparison of Weld Penetration between Destructive and PAUT Measurements for Side A of MU4

		Destructive Measurements		PAUT Measurements				
SL. No.	ID[a]	Measured Weld Leg[b] [D] (in.)	Weld Penetration (%)	Assumed Weld Leg[b] [D] (in.)	Weld Penetration with Assumed D (%)	Diff. (%)	Weld Penetration with Measured D (%)	Diff. (%)
1	MU4_A_1	0.456	71	0.31	--	--	--	--
2	MU4_A_13	0.376	83	0.31	90	7	68	-15
3	MU4_A_25	0.352	88	0.31	103	15	88	0
4	MU4_A_37	0.358	77	0.31	90	13	74	-3
5	MU4_A_61	0.347	71	0.31	96	25	84	13
6	MU4_A_61	0.36	74	0.31	90	16	73	-1
7	MU4_A_73	0.345	75	0.31	53	-22	40	-35
8	MU4_A_85	0.336	79	0.31	84	5	75	-4
9	MU4_A_97	0.33	73	0.31	78	5	70	-3
10	MU4_A_109	0.363	79	0.31	96	17	78	-1
11	MU4_A_121	0.336	78	0.31	84	6	75	-3
12	MU4_A_133	0.364	65	0.31	109	44	91	26
13	MU4_A_145	0.344	72	0.31	90	18	78	6
14	MU4_A_157	0.342	77	0.31	78	1	66	-11
15	MU4_A_169	0.333	73	0.31	90	17	82	9
16	MU4_A_181	0.329	77	0.31	78	1	71	-6
17	MU4_A_193	0.361	64	0.31	90	26	73	9
18	MU4_A_205	0.338	66	0.31	84	18	74	8
19	MU4_A_217	0.366	78	0.31	96	18	78	0
20	MU4_A_229	0.323	74	0.31	96	22	91	17
21	MU4_A_241	0.371	61	0.31	71	10	51	-10
22	MU4_A_253	0.39	76	0.31	84	8	57	-19
23	MU4_A_265	0.354	72	0.31	78	6	63	-9
24	MU4_A_277	0.221	100	0.31	78	-22	105	5
25	MU4_A_289	0.335	78	0.31	65	-13	56	-22
	Maximum	0.456	100	0.310	109	44	105	26
	Minimum	0.221	61	0.310	53	-22	40	-35
	Mean	0.349	75	0.310	85	--	73	--
	Std. Dev.	0.038	7.9	0.0	12.2	--	14.0	--
	COV (%)	10.8	10.5	0.0	14.2	--	19.0	--

[a] Refer to Figure 279 for identification of sections

[b] Refer Figure 280 for identification of parameters

Table 15 - Comparison of Weld Penetration between Destructive and PAUT Measurements for Side B of MU4

		Destructive Measurements		PAUT Measurements				
SL. No.	ID[a]	Measured Weld Leg[b] [D] (in.)	Weld Penetration (%)	Assumed Weld Leg[b] [D] (in.)	Weld Penetration with Assumed D (%)	Diff. (%)	Weld Penetration with Measured D (%)	Diff. (%)
1	MU4_B_1	0.354	72	0.31	--	--	--	--
2	MU4_B_13	0.329	83	0.31	90	7	83	0
3	MU4_B_25	0.336	78	0.31	71	-7	62	-16
4	MU4_B_37	0.342	78	0.31	84	6	73	-5
5	MU4_B_61	0.334	75	0.31	153	78	144	69
6	MU4_B_61	0.327	74	0.31	78	4	71	-3
7	MU4_B_73	0.328	72	0.31	71	-1	65	-7
8	MU4_B_85	0.358	66	0.31	78	12	61	-5
9	MU4_B_97	0.328	72	0.31	78	6	71	-1
10	MU4_B_109	0.336	75	0.31	96	21	87	12
11	MU4_B_121	0.37	63	0.31	71	8	51	-12
12	MU4_B_133	0.35	71	0.31	71	0	58	-13
13	MU4_B_145	0.335	68	0.31	103	35	94	26
14	MU4_B_157	0.328	77	0.31	71	-6	65	-12
15	MU4_B_169	0.357	70	0.31	84	14	68	-2
16	MU4_B_181	0.336	72	0.31	96	24	87	15
17	MU4_B_193	0.315	79	0.31	78	-1	75	-4
18	MU4_B_205	0.347	67	0.31	71	4	59	-8
19	MU4_B_217	0.331	78	0.31	78	0	70	-8
20	MU4_B_229	0.33	69	0.31	103	34	95	26
21	MU4_B_241	0.325	82	0.31	78	-4	72	-10
22	MU4_B_253	0.358	71	0.31	71	0	55	-16
23	MU4_B_265	0.343	72	0.31	78	6	66	-6
24	MU4_B_277	0.354	70	0.31	78	8	63	-7
25	MU4_B_289	0.328	70	0.31	71	1	65	-5
	Maximum	0.370	83	0.310	153	78	144	69
	Minimum	0.315	63	0.310	71	-7	51	-16
	Mean	0.339	73	0.310	83	--	73	--
	Std. Dev.	0.014	4.9	0.0	18.0	--	19.0	--
	COV (%)	4.0	6.8	0.0	21.6	--	26.0	--

[a] Refer to Figure 279 for identification of sections

[b] Refer Figure 280 for identification of parameters

Table 16 - Measured Dimensional Parameters of Rib-to-Deck Plate Weld for Rib 1 of MU5

			Side A				Side B			
SL. No.	ID[b]	Section Location[b] (in.)	LOP[a] (in.)	P[a] (in.)	WP[c] (%)	D[a] (in.)	LOP[a] (in.)	P[a] (in.)	WP[c] (%)	D[a] (in.)
1	R1_A_6	6.125	0.097	0.227	70	0.359	0.099	0.225	69	0.358
2	R1_A_18	18.125	0.098	0.225	70	0.358	0.098	0.225	70	0.343
3	R1_A_30	30	0.101	0.223	69	0.357	0.095	0.229	71	0.336
4	R1_A_42	41.875	0.091	0.232	72	0.366	0.098	0.226	70	0.349
5	R1_A_54	53.875	0.113	0.211	65	0.368	0.089	0.235	73	0.342
6	R1_A_66	65.75	0.096	0.228	70	0.358	0.076	0.248	77	0.345
7	R1_A_78	78.4375	0.117	0.207	64	0.341	0.095	0.229	71	0.335
8	R1_A_84	83.875	0.094	0.229	71	0.364	0.088	0.235	73	0.325
9	R1_A_96	96	0.109	0.215	66	0.342	0.093	0.230	71	0.332
10	R1_A_108	108	0.092	0.232	72	0.349	0.109	0.214	66	0.329
11	R1_A_120	120	0.091	0.233	72	0.360	0.081	0.242	75	0.336
12	R1_A_132	132	0.101	0.223	69	0.352	0.096	0.227	70	0.331
13	R1_A_144	144	0.123	0.200	62	0.357	0.085	0.239	74	0.357
14	R1_A_150	150	0.103	0.220	68	0.354	0.113	0.210	65	0.338
15	R1_A_162	162	0.106	0.217	67	0.357	0.073	0.250	77	0.338
16	R1_A_174	174	0.105	0.218	67	0.364	0.103	0.220	68	0.349
		Maximum	0.123	0.233	72	0.368	0.113	0.250	77	0.358
		Minimum	0.091	0.200	62	0.341	0.073	0.210	65	0.325
		Mean	0.102	0.221	68	0.357	0.093	0.230	71	0.340
		Std. Dev.	0.010	0.010	2.9	0.008	0.011	0.011	3.4	0.010
		COV (%)	9.3	4.3	4.3	2.1	11.8	4.8	4.8	2.8

[a] Refer to Figure 280 for identification of weld parameters

[b] Refer to Figure 295 for identification of sections

[c] Weld Penetration (WP in %) is calculated as {(P)/0.3235}x100

Table 17 - Measured Dimensional Parameters of Rib-to-Deck Plate Weld for Rib 2 of MU5

			Side A				Side B			
SL. No.	ID[b]	Section Location[b] (in.)	LOP[a] (in.)	P[a] (in.)	WP[c] (%)	D[a] (in.)	LOP[a] (in.)	P[a] (in.)	WP[c] (%)	D[a] (in.)
1	R2_A_6	6.125	0.124	0.200	62	0.346	0.114	0.209	65	0.367
2	R2_A_18	18.125	0.116	0.208	64	0.341	0.101	0.222	69	0.338
3	R2_A_30	30	0.125	0.199	61	0.358	0.108	0.216	67	0.334
4	R2_A_42	41.875	0.119	0.205	63	0.354	0.106	0.217	67	0.334
5	R2_A_54	53.875	0.127	0.197	61	0.352	0.140	0.183	57	0.340
6	R2_A_66	65.75	0.112	0.211	65	0.346	0.121	0.202	63	0.337
7	R2_A_78	78.4375	0.116	0.208	64	0.342	0.104	0.220	68	0.330
8	R2_A_84	83.875	0.120	0.203	63	0.376	0.109	0.214	66	0.342
9	R2_A_96	96	0.126	0.197	61	0.348	0.103	0.221	68	0.341
10	R2_A_108	108	0.115	0.208	64	0.333	0.116	0.207	64	0.346
11	R2_A_120	120	0.117	0.206	64	0.346	0.104	0.220	68	0.332
12	R2_A_132	132	0.119	0.205	63	0.361	0.075	0.249	77	0.333
13	R2_A_144	144	0.107	0.217	67	0.347	0.093	0.230	71	0.324
14	R2_A_150	150	0.131	0.193	60	0.332	0.063	0.261	81	0.314
15	R2_A_162	162	0.148	0.176	54	0.369	0.084	0.240	74	0.327
16	R2_A_174	174	0.117	0.207	64	0.345	0.107	0.216	67	0.348
		Maximum	0.148	0.217	67	0.376	0.140	0.261	81	0.367
		Minimum	0.107	0.176	54	0.332	0.063	0.183	57	0.314
		Mean	0.121	0.202	63	0.350	0.103	0.220	68	0.337
		Std. Dev.	0.009	0.009	2.9	0.012	0.018	0.018	5.6	0.012
		COV (%)	7.7	4.6	4.6	3.4	17.7	8.3	8.3	3.5

[a] Refer to Figure 280 for identification of weld parameters

[b] Refer to Figure 295 for identification of sections

[c] Weld Penetration (WP in %) is calculated as {(P)/0.3235}x100

Table 18 - Measured Dimensional Parameters of Rib-to-Deck Plate Weld for Rib 3 of MU5

			Side A				Side B			
SL. No.	ID[b]	Section[b] Location (in.)	LOP[a] (in.)	P[a] (in.)	WP[c] (%)	D[a] (in.)	LOP[a] (in.)	P[a] (in.)	WP[c] (%)	D[a] (in.)
1	R3_A_6	6.125	0.114	0.209	65	0.319	0.109	0.214	66	0.282
2	R3_A_18	18.125	0.129	0.195	60	0.302	0.103	0.221	68	0.280
3	R3_A_30	30	0.149	0.174	54	0.337	0.102	0.222	69	0.289
4	R3_A_42	41.875	0.129	0.195	60	0.331	0.109	0.215	66	0.301
5	R3_A_54	53.875	0.131	0.192	59	0.355	0.133	0.190	59	0.320
6	R3_A_66	65.75	0.115	0.208	64	0.334	0.091	0.232	72	0.315
7	R3_A_78	78.4375	0.131	0.192	59	0.345	0.117	0.207	64	0.307
8	R3_A_84	83.875	0.136	0.188	58	0.350	0.125	0.199	62	0.314
9	R3_A_96	96	0.127	0.196	61	0.352	0.124	0.199	62	0.290
10	R3_A_108	108	0.125	0.199	61	0.339	0.132	0.191	59	0.304
11	R3_A_120	120	0.119	0.204	63	0.334	0.123	0.200	62	0.302
12	R3_A_132	132	0.136	0.187	58	0.334	0.128	0.195	60	0.307
13	R3_A_144	144	0.138	0.185	57	0.344	0.131	0.193	60	0.310
14	R3_A_150	150	0.110	0.214	66	0.342	0.144	0.180	55	0.315
15	R3_A_162	162	0.061	0.263	81	0.306	0.116	0.207	64	0.291
16	R3_A_174	174	0.100	0.224	69	0.338	0.112	0.211	65	0.334
		Maximum	0.149	0.263	81	0.355	0.144	0.232	72	0.334
		Minimum	0.061	0.174	54	0.302	0.091	0.180	55	0.280
		Mean	0.122	0.202	62	0.335	0.119	0.205	63	0.304
		Std. Dev.	0.020	0.020	6.3	0.015	0.014	0.014	4.3	0.015
		COV (%)	16.7	10.1	10.1	4.5	11.7	6.8	6.8	4.8

[a.] Refer to Figure 280 for identification of weld parameters

[b.] Refer to Figure 295 for identification of sections

[c.] Weld Penetration (WP in %) is calculated as {(P)/0.324}x100

Table 19 - Comparison of Weld Penetration between Destructive and PAUT Measurements for Rib 1 of MU5: Side A

			Weld Penetration (WP)		
SL. No.	ID[a]	Section Location[a] (in.)	Destructive Measurements by Lehigh (%)	PAUT Measurements by Baker (%)	Difference in WP (%)
1	R1_A_6	6.125	70	58	-12
2	R1_A_18	18.125	70	58	-12
3	R1_A_30	30	69	59	-10
4	R1_A_42	41.875	72	65	-7
5	R1_A_54	53.875	65	59	-6
6	R1_A_66	65.75	70	57	-14
7	R1_A_78	78.4375	64	63	-1
8	R1_A_84	83.875	71	57	-14
9	R1_A_96	96	66	57	-10
10	R1_A_108	108	72	62	-10
11	R1_A_120	120	72	68	-4
12	R1_A_132	132	69	67	-2
13	R1_A_144	144	62	60	-2
14	R1_A_150	150	68	62	-6
15	R1_A_162	162	67	49	-18
16	R1_A_174	174	67	68	-1
	Maximum		72	68	-1
	Minimum		62	49	-18
	Mean		68	60	--
	Std. Dev.		2.9	5.0	--
	COV (%)		4.3	8.2	--

[a.] Refer to Figure 280 for identification of sections

Table 20 - Comparison of Weld Penetration between Destructive and PAUT Measurements for Rib 1 of MU5: Side B

SL. No.	ID[a]	Section Location[a] (in.)	Weld Penetration (WP) Destructive Measurements by Lehigh (%)	Weld Penetration (WP) PAUT Measurements by Baker (%)	Difference in WP (%)
1	R1_B_6	6.125	69	60	-9
2	R1_B_18	18.125	70	76	-6
3	R1_B_30	30	71	57	-14
4	R1_B_42	41.875	70	71	1
5	R1_B_54	53.875	73	64	-9
6	R1_B_66	65.75	77	67	-10
7	R1_B_78	78.4375	71	69	-2
8	R1_B_84	83.875	73	62	-11
9	R1_B_96	96	71	62	-9
10	R1_B_108	108	66	64	-2
11	R1_B_120	120	75	69	-5
12	R1_B_132	132	70	69	-1
13	R1_B_144	144	74	70	-4
14	R1_B_150	150	65	59	-6
15	R1_B_162	162	77	75	-2
16	R1_B_174	174	68	64	-4
	Maximum		77	76	1
	Minimum		65	57	-14
	Mean		71	66	--
	Std. Dev.		3.4	5.6	--
	COV (%)		4.8	8.5	--

[a] Refer to Figure 280 for identification of sections

Table 21 - Comparison of Weld Penetration between Destructive and PAUT Measurements for Rib 2 of MU5: Side A

			Weld Penetration (WP)		
SL. No.	ID[a]	Section Location[a] (in.)	Destructive Measurements by Lehigh (%)	PAUT Measurements by Baker (%)	Difference in WP (%)
1	R2_A_6	6.125	62	63	1
2	R2_A_18	18.125	64	51	-13
3	R2_A_30	30	61	58	-4
4	R2_A_42	41.875	63	58	-5
5	R2_A_54	53.875	61	52	-9
6	R2_A_66	65.75	65	66	1
7	R2_A_78	78.438	64	59	-5
8	R2_A_84	83.875	63	64	1
9	R2_A_96	96	61	64	3
10	R2_A_108	108	64	63	-1
11	R2_A_120	120	64	53	-11
12	R2_A_132	132	63	60	-3
13	R2_A_144	144	67	57	-10
14	R2_A_150	150	60	69	10
15	R2_A_162	162	54	51	-4
16	R2_A_174	174	64	64	0
	Maximum		67	69	0
	Minimum		54	51	-13
	Mean		63	60	--
	Std. Dev.		2.9	5.7	--
	COV (%)		4.6	9.5	--

[a] Refer to Figure 280 for identification of sections

Table 22 - Comparison of Weld Penetration between Destructive and PAUT Measurements for Rib 2 of MU5: Side B

			Weld Penetration (WP)		
SL. No.	ID[a]	Section Location[a] (in.)	Destructive Measurements by Lehigh (%)	PAUT Measurements by Baker (%)	Difference in WP (%)
1	R2_B_6	6.125	65	55	-10
2	R2_B_18	18.125	69	60	-9
3	R2_B_30	30	67	62	-5
4	R2_B_42	41.875	67	60	-7
5	R2_B_54	53.875	57	55	-1
6	R2_B_66	65.75	63	62	0
7	R2_B_78	78.4375	68	63	-5
8	R2_B_84	83.875	66	63	-3
9	R2_B_96	96	68	58	-10
10	R2_B_108	108	64	65	1
11	R2_B_120	120	68	69	1
12	R2_B_132	132	77	63	-13
13	R2_B_144	144	71	66	-5
14	R2_B_150	150	81	57	-23
15	R2_B_162	162	74	58	-16
16	R2_B_174	174	67	75	8
	Maximum		81	75	8
	Minimum		57	55	-23
	Mean		68	62	--
	Std. Dev.		5.6	5.2	--
	COV (%)		8.3	8.5	--

[a.] Refer to Figure 280 for identification of sections

Table 23 - Comparison of Weld Penetration between Destructive and PAUT Measurements for Rib 3 of MU5: Side A

SL. No.	ID[a]	Section Location[a] (in.)	Weld Penetration (WP) Destructive Measurements by Lehigh (%)	Weld Penetration (WP) PAUT Measurements by Baker (%)	Difference in WP (%)
1	R3_A_6	6.125	65	67	2
2	R3_A_18	18.125	60	62	1
3	R3_A_30	30	54	68	14
5	R3_A_42	41.875	60	64	4
6	R3_A_54	53.875	59	62	3
7	R3_A_66	65.75	64	63	-2
9	R3_A_78	78.438	59	63	-4
10	R3_A_84	83.875	58	63	5
11	R3_A_96	96	61	63	2
12	R3_A_108	108	61	69	8
13	R3_A_120	120	63	62	-1
14	R3_A_132	132	58	62	5
15	R3_A_144	144	57	59	2
16	R3_A_150	150	66	65	-1
18	R3_A_162	162	81	80	-1
19	R3_A_174	174	69	65	-4
	Maximum		81	80	14
	Minimum		54	59	-4
	Mean		62	65	--
	Std. Dev.		6.3	4.9	--
	COV (%)		10.1	7.5	--

[a] Refer to Figure 280 for identification of sections

Table 24 - Comparison of Weld Penetration between Destructive and PAUT Measurements for Rib MU5: Side B

SL. No.	ID[a]	Section Location[a] (in.)	Weld Penetration (WP)		Difference in WP (%)
			Destructive Measurements by Lehigh (%)	PAUT Measurements by Baker (%)	
1	R3_B_6	6.125	66	65	-1
2	R3_B_18	18.125	68	63	-6
3	R3_B_30	30	69	54	-15
5	R3_B_42	41.875	66	63	-3
6	R3_B_54	53.875	59	68	9
7	R3_B_66	65.75	72	67	-4
9	R3_B_78	78.438	64	61	-3
10	R3_B_84	83.875	62	61	-0
11	R3_B_96	96	62	67	5
12	R3_B_108	108	59	55	-4
13	R3_B_120	120	62	55	-7
14	R3_B_132	132	60	61	1
15	R3_B_144	144	60	68	8
16	R3_B_150	150	55	68	12
18	R3_B_162	162	64	66	2
19	R3_B_174	174	65	69	4
	Maximum		72	69	15
	Minimum		55	54	-7
	Mean		63	63	--
	Std. Dev.		4.3	5.1	--
	COV (%)		6.8	8.1	--

[a] Refer to Figure 280 for identification of sections

Table 25 - Welding parameters for Rib-to-Deck Plate Welds of MU6 and MU7

Weld Parameters	MU6		MU7	
	Side A	Side B	Side A	Side B
Voltage (v)	34	35	34	34
Current (A)	600	650	625	600
Wire Angle (°)	60	65	60	65
Polarity Balance	66/34	66/34	66/34	70/30
Travel Speed (in./min)	18	18	20	20

Table 26 - Measured Penetration of Rib-to-Deck Plate Weld of MU6

	Side A		Side B	
SL. No.	ID	Weld Penetration[a] [WP] (%)	ID	Weld Penetration[a] [WP] (%)
1	MU6_A_1	82	MU6_B_1	76
2	MU6_A_2	76	MU6_B_2	76
3	MU6_A_3	83	MU6_B_3	78
4	MU6_A_4	79	MU6_B_4	70
5	MU6_A_5	78	MU6_B_5	72
6	MU6_A_6	74	MU6_B_6	70
7	MU6_A_7	80	MU6_B_7	82
8	MU6_A_8	78	MU6_B_8	73
9	MU6_A_9	80	MU6_B_9	70
	Maximum	83	Maximum	82
	Minimum	74	Minimum	70
	Mean	79	Mean	74
	Std. Dev.	2.8	Std. Dev.	4.2
	COV	3.6	COV	5.7

[a] Weld Penetration (%) is calculated as {(P)/0.3235}x100

Table 27 - Measured Penetration of Rib-to-Deck Plate Weld of MU7

	Side A		Side B	
SL. No.	ID	Weld Penetration[a] [WP] (%)	ID	Weld Penetration[a] [WP] (%)
1	MU7_A_1	85	MU7_B_1	64
2	MU7_A_2	87	MU7_B_2	70
3	MU7_A_3	78	MU7_B_3	77
4	MU7_A_4	89	MU7_B_4	78
5	MU7_A_5	80	MU7_B_5	76
6	MU7_A_6	83	MU7_B_6	82
7	MU7_A_7	87	MU7_B_7	80
8	MU7_A_8	83	MU7_B_8	80
9	MU7_A_9	87	MU7_B_9	84
10	MU7_A_10	82	MU7_B_10	81
11	MU7_A_11	83	MU7_B_11	70
12	MU7_A_12	86	MU7_B_12	79
	Maximum	89	Maximum	84
	Minimum	78	Minimum	64
	Mean	84	Mean	77
	Std. Dev.	3.2	Std. Dev.	5.9
	COV	3.9	COV	7.7

[a] Weld Penetration (%) is calculated as {(P)/0.3235}x100

Table 28 - Measured Dimensional Parameters Rib-to-Deck Plate Weld of MU8

SL. No.	ID[b]	Section[b] Location (in.)	Side A LOP[a] (in.)	Side A P[a] (in.)	Side A WP[c] (%)	Side B LOP[a] (in.)	Side B P[a] (in.)	Side B WP[c] (%)
1	MU8_A_12	12	0.076	0.248	77	0.060	0.263	81
2	MU8_A _24	24	0.072	0.251	78	0.059	0.264	82
3	MU8_A_36	36	0.074	0.250	77	0.059	0.265	82
4	MU8_A_48	48	0.077	0.246	76	0.071	0.253	78
5	MU8_A_60	60	0.089	0.234	72	0.068	0.255	79
6	MU8_A_72	72	0.075	0.249	77	0.065	0.258	80
7	MU8_A_84	84	0.070	0.253	78	0.070	0.254	78
8	MU8_A_96	96	0.066	0.258	80	0.055	0.268	83
9	MU8_A_108	108	0.080	0.243	75	0.053	0.271	84
10	MU8_A_120	120	0.073	0.251	78	0.047	0.276	85
11	MU8_A_132	132	0.085	0.239	74	0.084	0.239	74
12	MU8_A_144	144	0.067	0.256	79	0.054	0.269	83
13	MU8_A_156	156	0.077	0.246	76	0.067	0.257	79
14	MU8_A_168	168	0.050	0.274	85	0.085	0.238	74
15	MU8_A_180	180	0.072	0.251	78	0.055	0.268	83
16	MU8_A_192	192	0.075	0.248	77	0.079	0.244	76
		Maximum	0.089	0.274	85	0.085	0.276	85
		Minimum	0.050	0.234	72	0.047	0.238	74
		Mean	0.074	0.250	77	0.065	0.259	80
		Std. Dev.	0.009	0.009	2.7	0.011	0.011	3.5
		COV (%)	11.8	3.5	3.5	17.5	4.4	4.4

[a] Refer Figure 280 for identification of parameters

[b] Refer Figure 311 for identification of sections

[c] Weld Penetration (%) is calculated as {(P)/0.3235}x100

Table 29 - Summary of Measured Weld Penetration of Rib-to-Deck Plate Weld of MU8

	Destructive Measurements by Lehigh		
	LOP[a] (in.)	P[a] (in.)	WP[b] (%)
Maximum	0.089	0.276	85
Minimum	0.047	0.234	72
Mean	0.069	0.254	79
Std. Dev.	0.011	0.011	3.4
COV (%)	15.8	4.3	4.3

[a.] Refer to Figure 280 for identification of weld parameters

[b.] Weld Penetration (%) is calculated as {(P)/0.3235}x100

Table 30 - Measured Dimensional Parameters of Rib 1-to-FB Weld for MU5: Section Location at 24 in.

		Destructive Measurements by Lehigh	
SL. No.	ID[b]	LOF[a] (in.)	R[a] (in.)
1	R1_24_1	0.380	0.039
2	R1_24_2	0.433	0.019
3	R1_24_3	0.368	0.021
4	R1_24_4	0.418	0.017
5	R1_24_5	0.410	0.014
6	R1_24_6	0.418	0.022
7	R1_24_7	0.449	0.042
	Maximum	0.449	0.042
	Minimum	0.368	0.014
	Mean	0.411	0.025
	Std. Dev.	0.028	0.011
	COV (%)	6.9	44.0

[a.] Refer to Figure 317 for identification of weld parameters.

[b.] Refer to Figure 316 for identification of sections.

Table 31 - Measured Dimensional Parameters of Rib 1-to-FB Weld for MU5: Section Location at 90 in.

		Destructive Measurements by Lehigh	
SL. No.	ID[b]	LOF[a] (in.)	R[a] (in.)
1	R1_90_1	0.401	0.020
2	R1_90_2	0.421	0.024
3	R1_90_3	0.367	0.032
4	R1_90_4	0.382	0.028
5	R1_90_5	0.384	0.044
6	R1_90_6	0.360	0.030
7	R1_90_7	0.400	0.027
	Maximum	0.421	0.044
	Minimum	0.360	0.020
	Mean	0.388	0.029
	Std. Dev.	0.021	0.008
	COV (%)	5.5	26.5

[a] Refer to Figure 317 for identification of weld parameters.
[b] Refer to Figure 316 for identification of sections.

Table 32 - Measured Dimensional Parameters of Rib 1-to-FB Weld for MU5: Section Location at 156 in.

		Destructive Measurements by Lehigh	
SL. No.	ID[b]	LOF[a] (in.)	R[a] (in.)
1	R1_156_1	0.488	0.006
2	R1_156_2	0.404	0.027
3	R1_156_3	0.373	0.025
4	R1_156_4	0.295	0.027
5	R1_156_5	0.412	0.029
6	R1_156_6	0.347	0.037
7	R1_156_7	0.478	0.089
	Maximum	0.488	0.089
	Minimum	0.295	0.006
	Mean	0.400	0.034
	Std. Dev.	0.069	0.026
	COV (%)	17.3	75.9

[a] Refer to Figure 317 for identification of weld parameters.
[b] Refer to Figure 316 for identification of sections.

Table 33 - Measured Dimensional Parameters of Rib 2-to-FB Weld for MU5: Section Location at 24 in.

		Destructive Measurements by Lehigh	
SL. No.	ID[b]	LOF[a] (in.)	R[a] (in.)
1	R2_24_1	0.493	0.020
2	R2_24_2	0.447	0.021
3	R2_24_3	0.458	0.008
4	R2_24_4	0.434	0.011
5	R2_24_5	0.380	0.038
6	R2_24_6	0.463	0.021
7	R2_24_7	0.500	0.041
	Maximum	0.500	0.041
	Minimum	0.380	0.008
	Mean	0.453	0.023
	Std. Dev.	0.040	0.012
	COV (%)	8.8	54.8

[a] Refer to Figure 317 for identification of weld parameters.

[b] Refer to Figure 316 for identification of sections.

Table 34 - Measured Dimensional Parameters of Rib 2-to-FB Weld for MU5: Section Location at 90 in.

		Destructive Measurements by Lehigh	
SL. No.	ID[b]	LOF[a] (in.)	R[a] (in.)
1	R2_90_1	0.437	0.043
2	R2_90_2	0.413	0.024
3	R2_90_3	0.363	0.072
4	R2_90_4	0.500	0.015
5	R2_90_5	0.312	0.019
6	R2_90_6	0.425	0.026
7	R2_90_7	0.475	0.020
	Maximum	0.500	0.072
	Minimum	0.312	0.015
	Mean	0.418	0.031
	Std. Dev.	0.064	0.020
	COV (%)	15.3	64.6

[a] Refer to Figure 317 for identification of weld parameters.

[b] Refer to Figure 316 for identification of sections.

Table 35 - Measured Dimensional Parameters of Rib 2-to-FB Weld for MU5: Section Location at 156 in.

		Destructive Measurements by Lehigh	
SL. No.	ID[b]	LOF[a] (in.)	R[a] (in.)
1	R2_156_1	0.439	0.030
2	R2_156_2	0.319	0.045
3	R2_156_3	0.427	0.024
4	R2_156_4	0.267	0.030
5	R2_156_5	0.401	0.037
6	R2_156_6	0.446	0.030
7	R2_156_7	0.479	0.006
	Maximum	0.479	0.045
	Minimum	0.267	0.006
	Mean	0.397	0.029
	Std. Dev.	0.076	0.012
	COV (%)	19.2	42.3

[a.] Refer to Figure 317 for identification of weld parameters.

[b.] Refer to Figure 316 for identification of sections.

Table 36 - Measured Dimensional Parameters of Rib 3-to-FB Weld for MU5: Section Location at 24 in.

		Destructive Measurements by Lehigh	
SL. No.	ID[b]	LOF[a] (in.)	R[a] (in.)
1	R3_24_1	0.408	0.050
2	R3_24_2	0.379	0.046
3	R3_24_3	0.443	0.006
4	R3_24_4	0.379	0.034
5	R3_24_5	0.352	0.028
6	R3_24_6	0.355	0.012
7	R3_24_7	0.426	0.059
	Maximum	0.443	0.059
	Minimum	0.352	0.006
	Mean	0.392	0.034
	Std. Dev.	0.035	0.020
	COV (%)	8.9	58.2

[a.] Refer to Figure 317 for identification of weld parameters.

[b.] Refer to Figure 316 for identification of sections.

Table 37 - Measured Dimensional Parameters of Rib 3-to-FB Weld for MU5: Section Location at 90 in.

		Destructive Measurements by Lehigh	
SL. No.	ID[b]	LOF[a] (in.)	R[a] (in.)
1	R3_90_1	0.454	0.117
2	R3_90_2	0.430	0.012
3	R3_90_3	0.411	0.010
4	R3_90_4	0.462	0.020
5	R3_90_5	0.371	0.027
6	R3_90_6	0.450	0.021
7	R3_90_7	0.391	0.085
	Maximum	0.462	0.117
	Minimum	0.371	0.010
	Mean	0.424	0.042
	Std. Dev.	0.034	0.042
	COV (%)	8.1	100.3

[a] Refer to Figure 317 for identification of weld parameters.

[b] Refer to Figure 316 for identification of sections.

Table 38 - Measured Dimensional Parameters of Rib 3-to-FB Weld for MU5: Section Location at 156 in.

		Destructive Measurements by Lehigh	
SL. No.	ID[b]	LOF[a] (in.)	R[a] (in.)
1	R3_156_1	0.484	0.024
2	R3_156_2	0.432	0.024
3	R3_156_3	0.433	0.017
4	R3_156_4	0.410	0.011
5	R3_156_5	0.383	0.028
6	R3_156_6	0.419	0.029
7	R3_156_7	0.442	0.011
	Maximum	0.484	0.029
	Minimum	0.383	0.011
	Mean	0.429	0.021
	Std. Dev.	0.031	0.008
	COV (%)	7.2	36.8

[a] Refer to Figure 317 for identification of weld parameters.

[b] Refer to Figure 316 for identification of sections.

Table 39 - Summary of Measured Dimensional Parameters for Rib-to-FB Weld for Ribs 1, 2 and 3 for MU5

	Destructive Measurements by Lehigh	
	LOF[a] (in.)	R[a] (in.)
Maximum	0.500[b]	0.117
Minimum	0.267	0.006
Mean	0.412	0.030
Std. Dev.	0.049	0.020
COV (%)	11.9	67.5

[a.] Refer to Figure 317 for identification of weld parameters.

[b.] Floor beam was not fused with the weld on both sides.

[c.] Total 63 sections considered for the study, 21 sections for each rib.

[d.] Out of 63 sections, 4 sections had R value greater than the target of $^1/_{16}$ in.

[e.] Only one section had R value greater than the maximum specified of $^3/_{32}$ in.

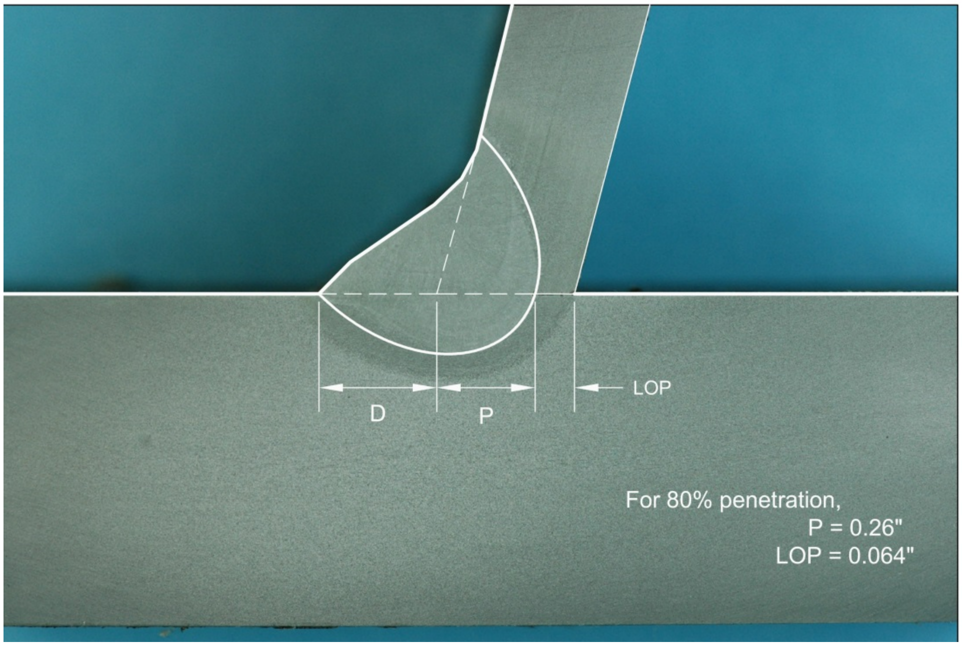

Figure 278. Fabrication of rib-to-deck plate weld for MU4

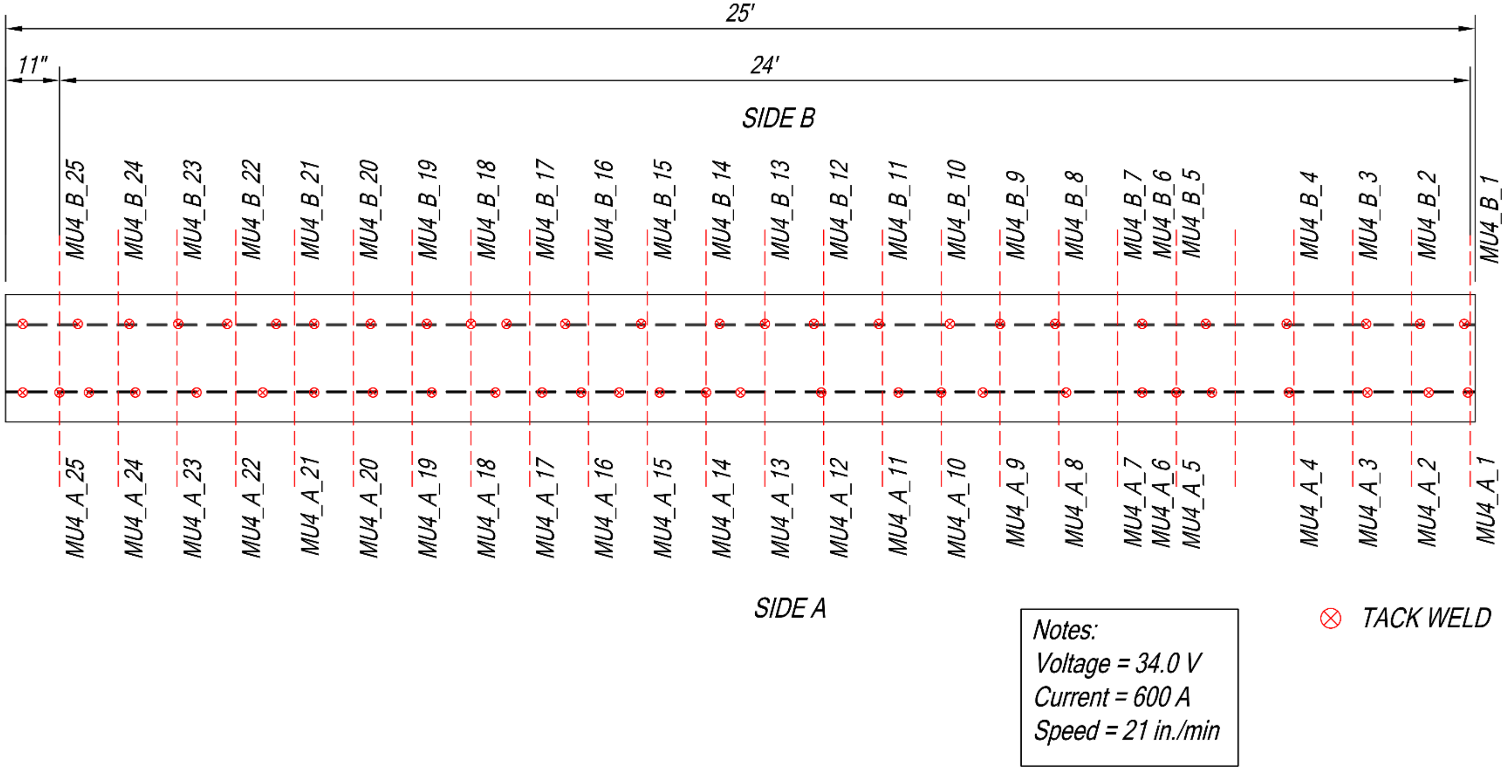

Notes:
Voltage = 34.0 V
Current = 600 A
Speed = 21 in./min

Figure 279. Specimen and section identification for MU4

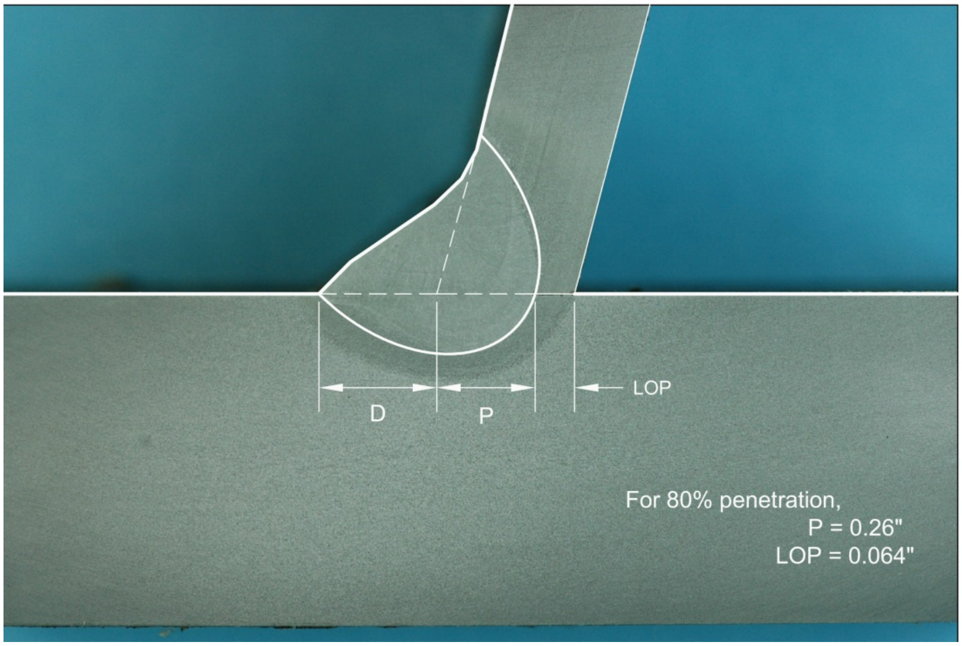

Figure 280. Schematic for rib-to-deck plate weld

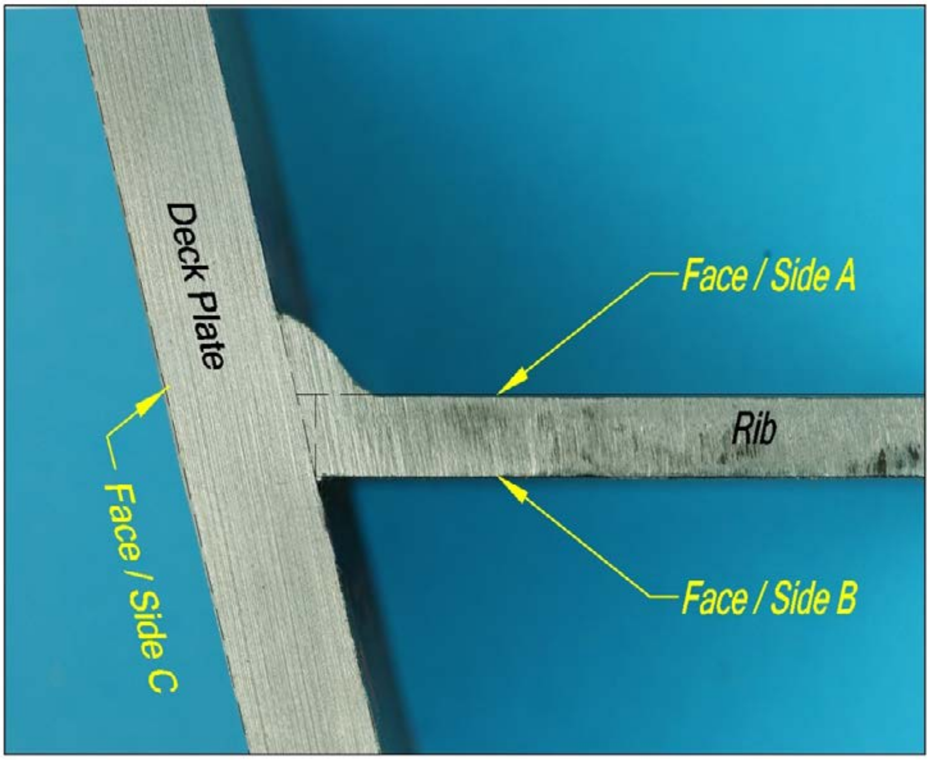

Figure 281. Sides for PAUT scanning

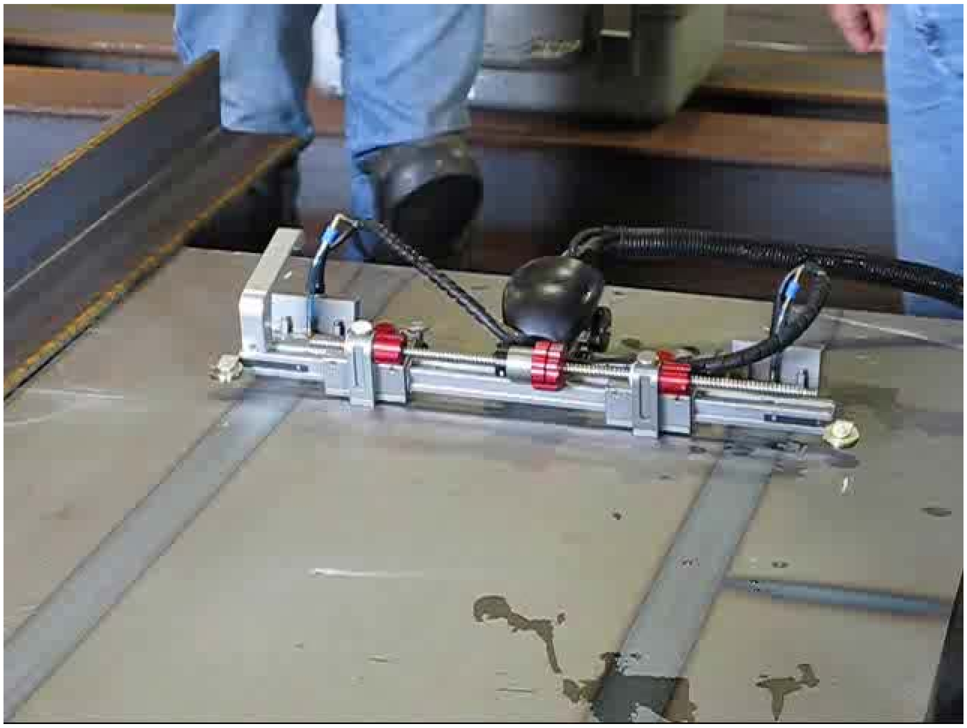

Figure 282. Scanning setup

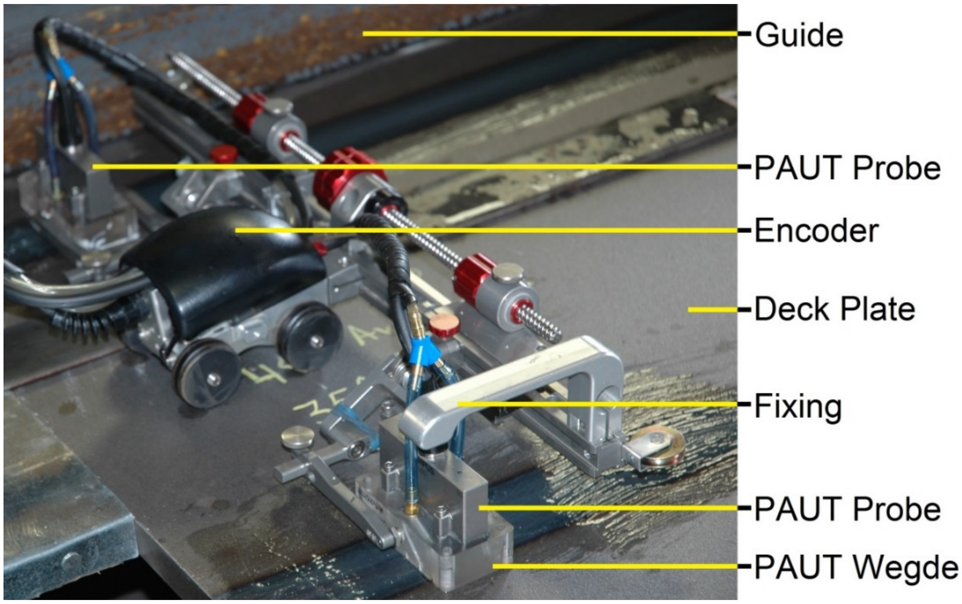

Figure 283. Details of the scanning setup

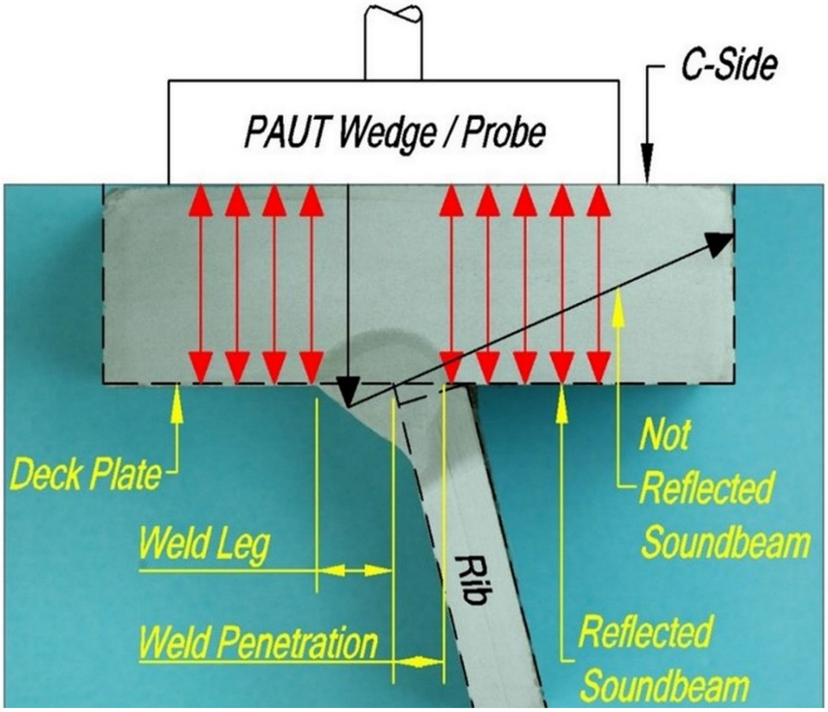

Figure 284. Schematic of scanning procedure from Side C

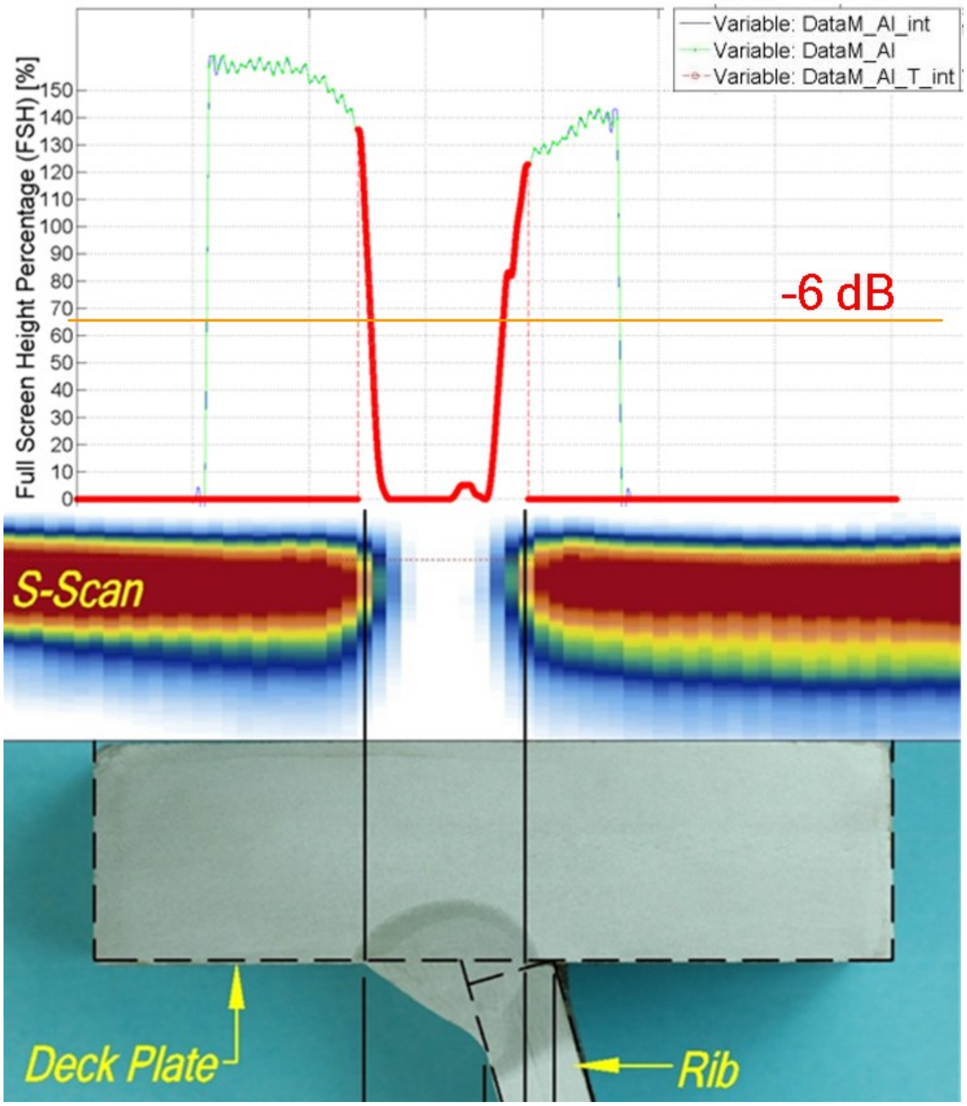

Figure 285. Procedure for determination of weld penetration

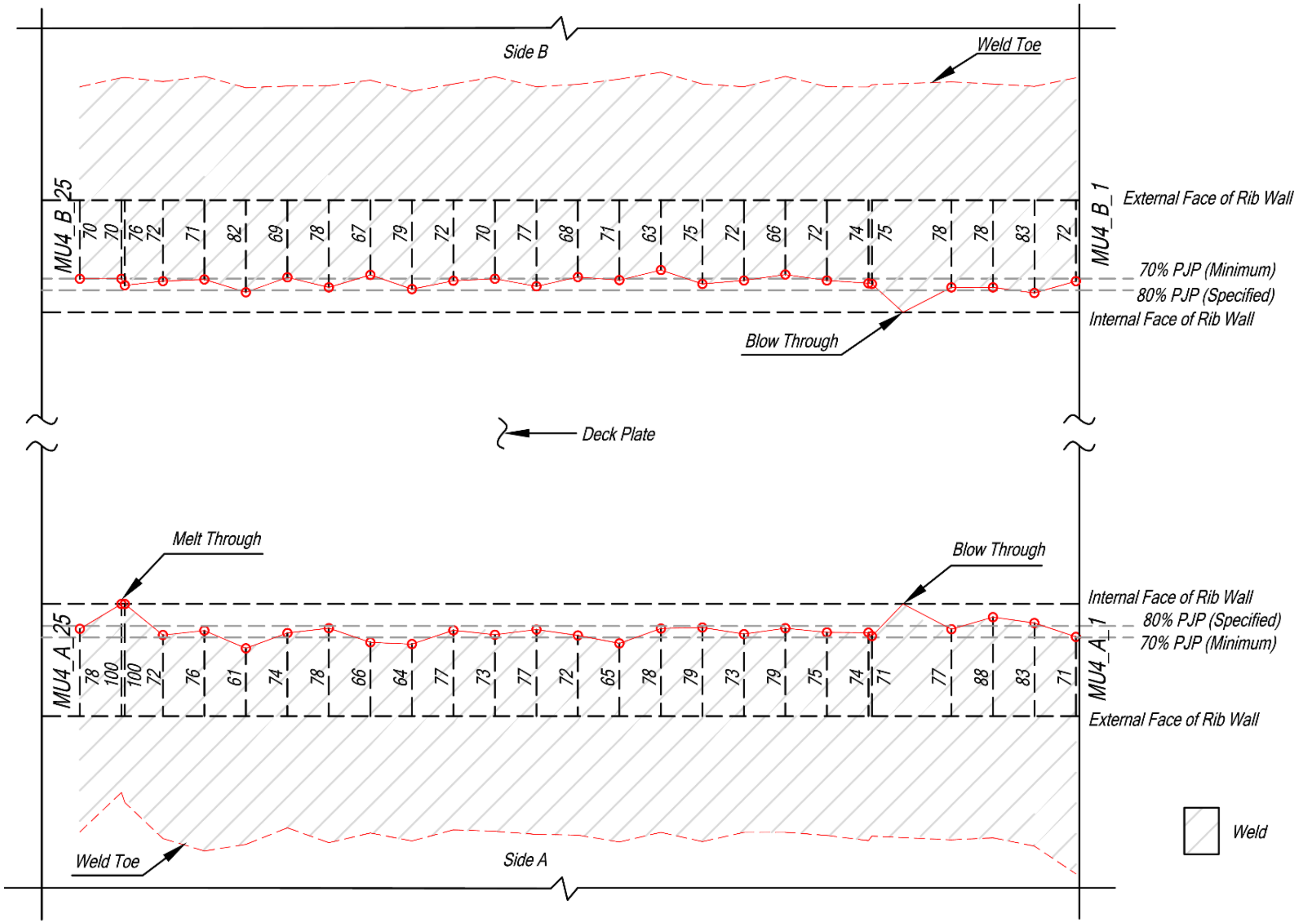

Figure 286. Distribution of weld penetrations (%) for rib-to-deck plate weld along the length of the rib for MU4

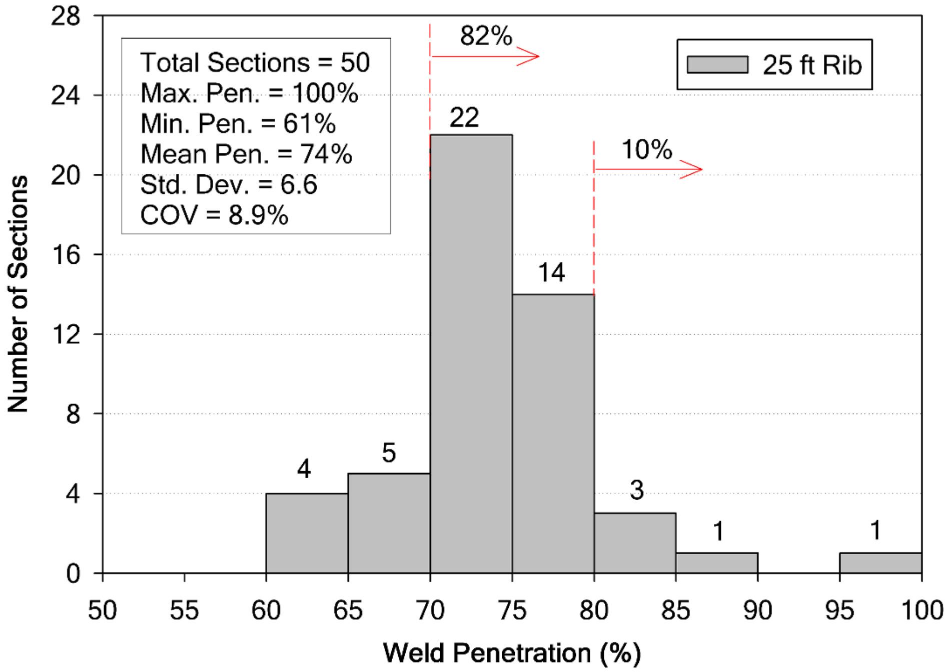

Figure 287. Statistical distribution of weld penetration for MU4

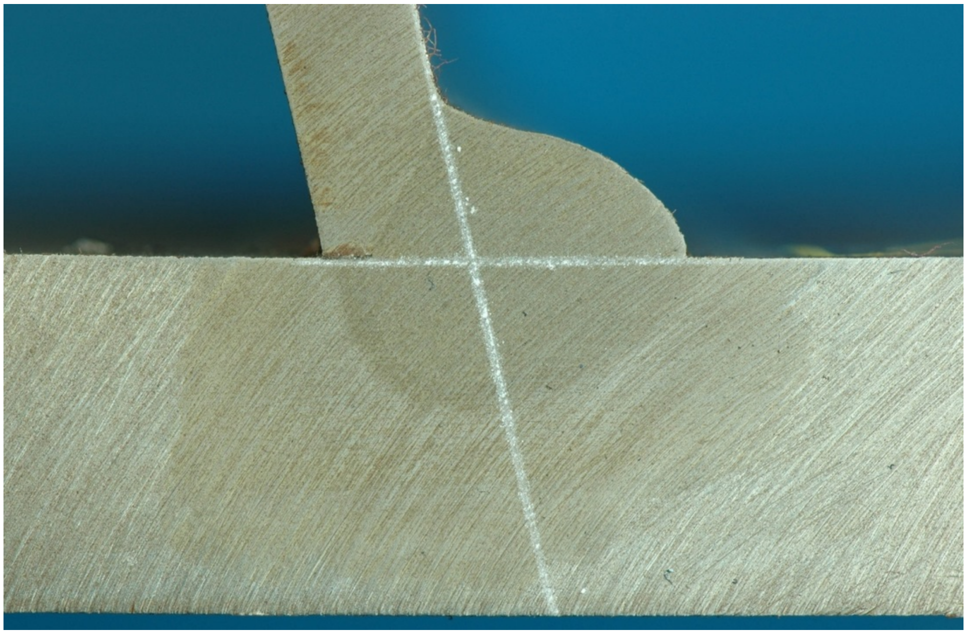

Figure 288. A typical macro-etched section for MU4

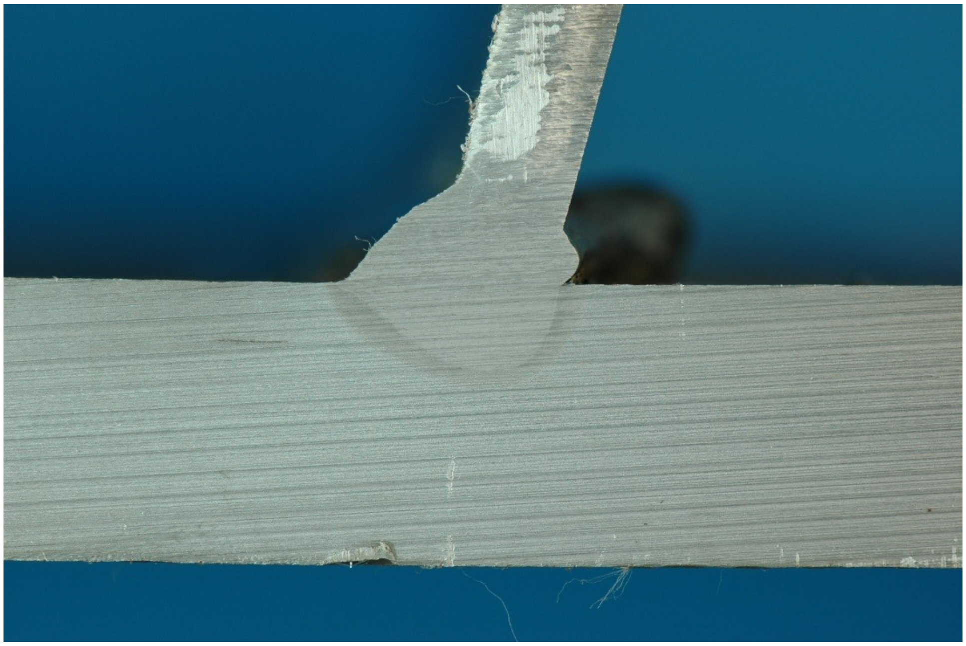

Figure 289. Melt through in Side A for MU4

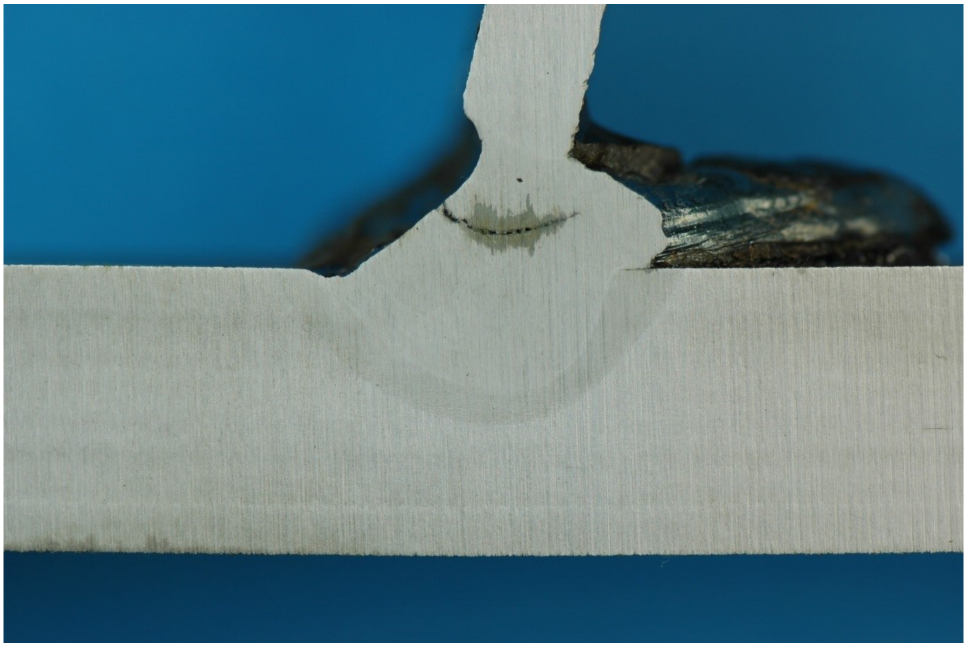

Figure 290. Blow through in Side A for MU4

Figure 291. Blow through in Side B for MU4

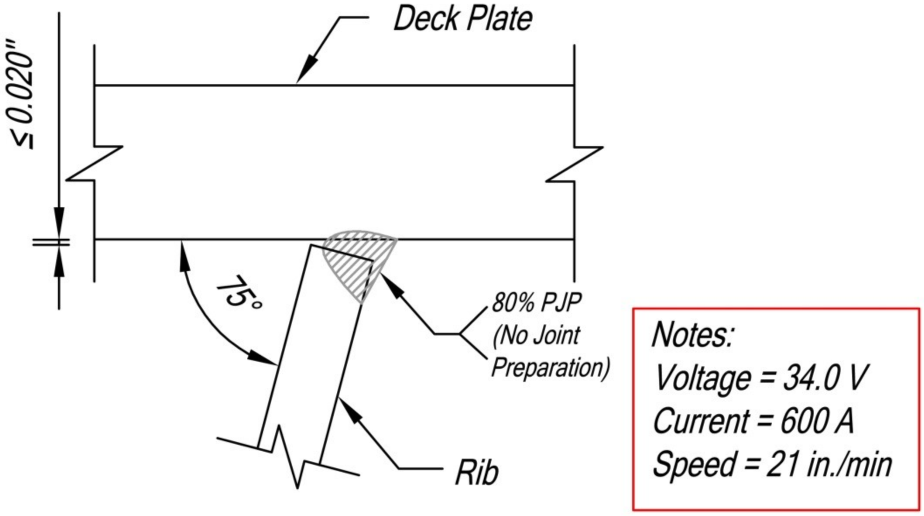

Figure 292. Detail of Rib 1-to-deck plate weld for MU5

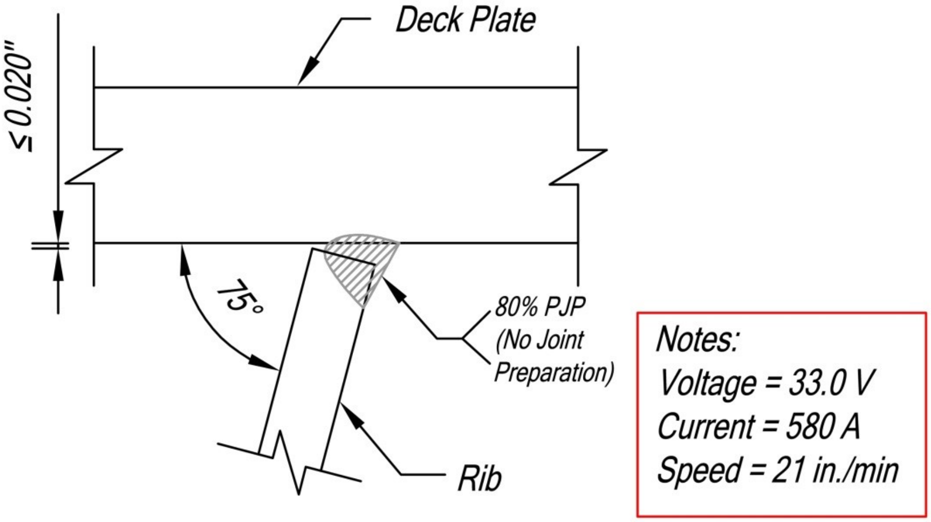

Notes:
Voltage = 33.0 V
Current = 580 A
Speed = 21 in./min

Figure 293. Detail of Rib 2-to-deck plate weld for MU5

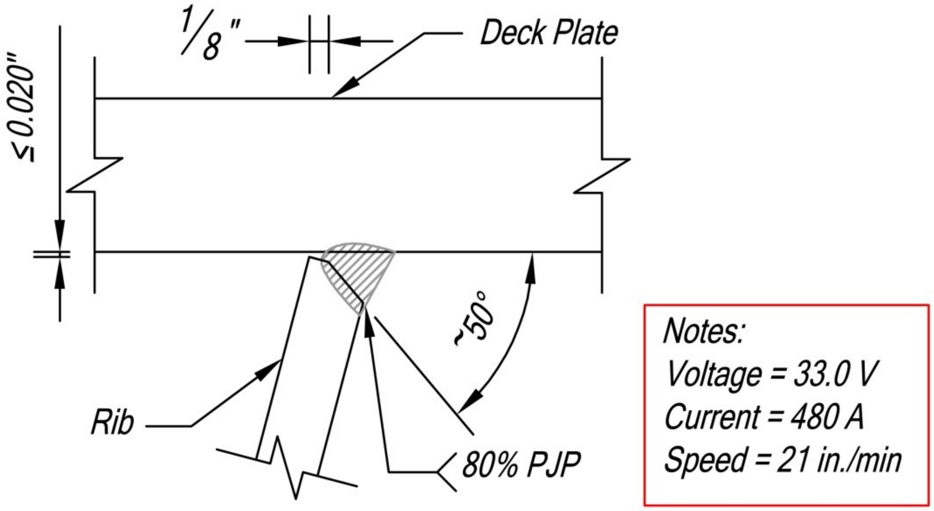

Notes:
Voltage = 33.0 V
Current = 480 A
Speed = 21 in./min

Figure 294. Detail of Rib 3-to-deck plate weld for MU5

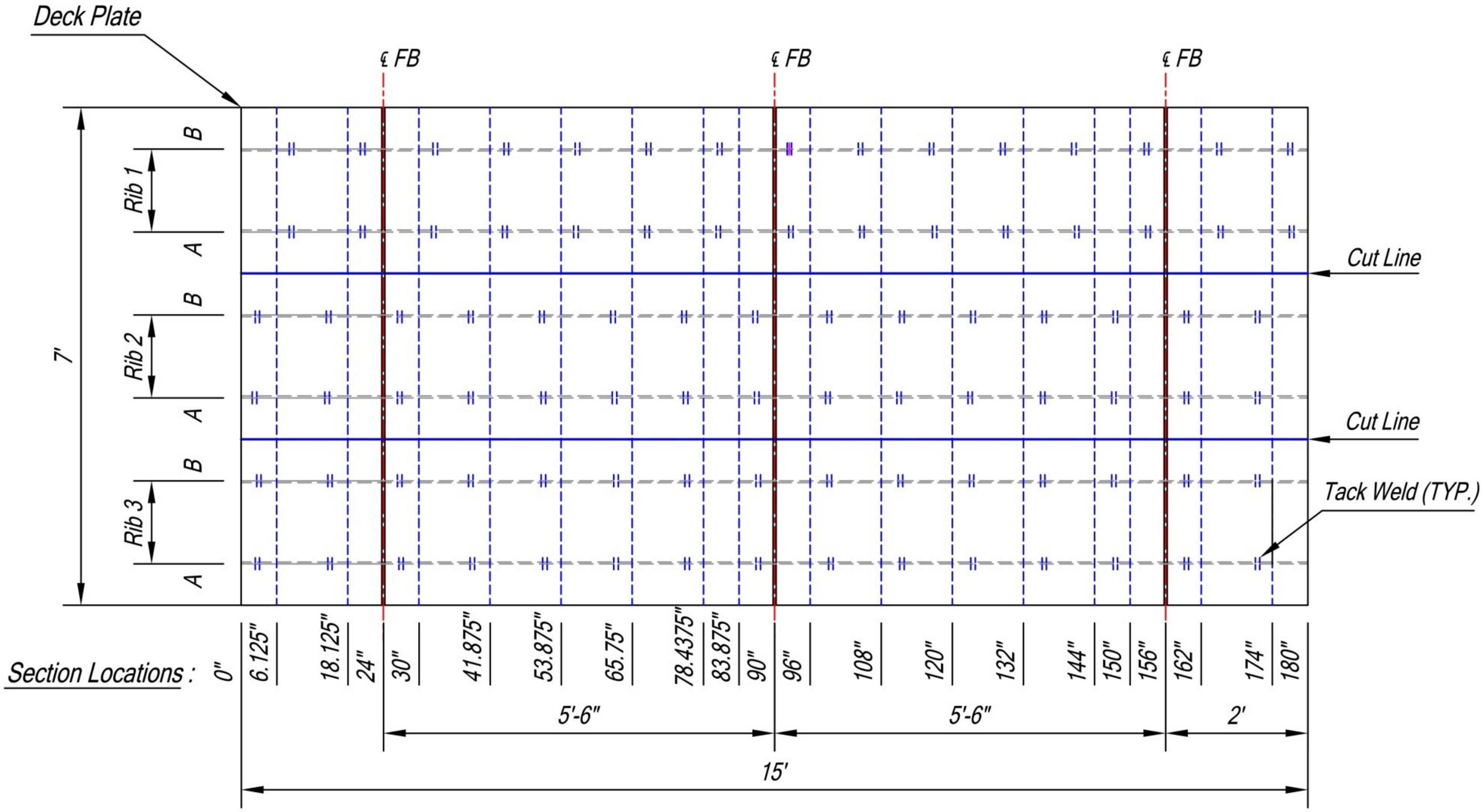

Figure 295. Section identification for MU5

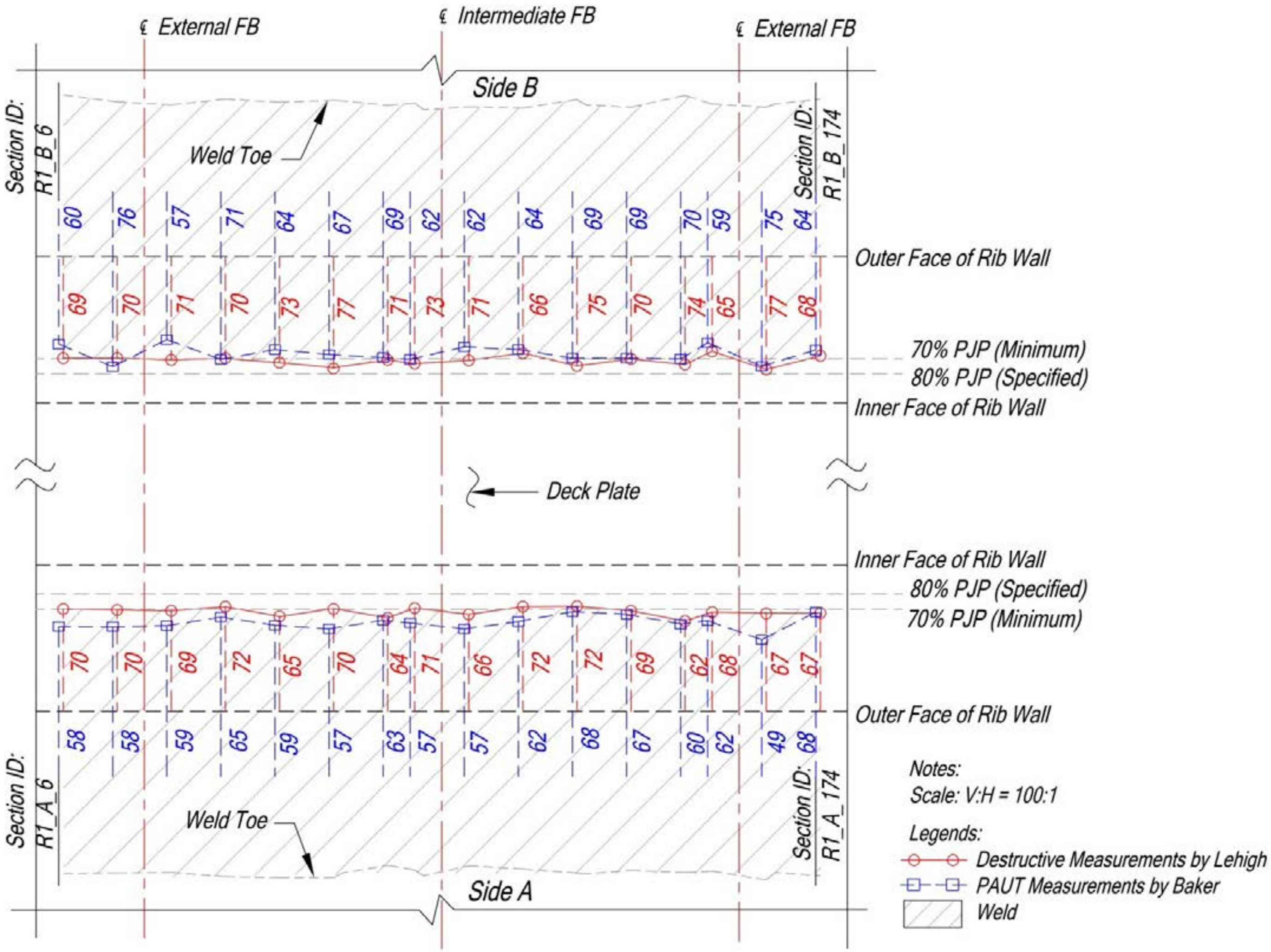

Figure 296. Distribution of weld penetrations (%) for rib-to-deck plate weld along the length for Rib1 of MU5

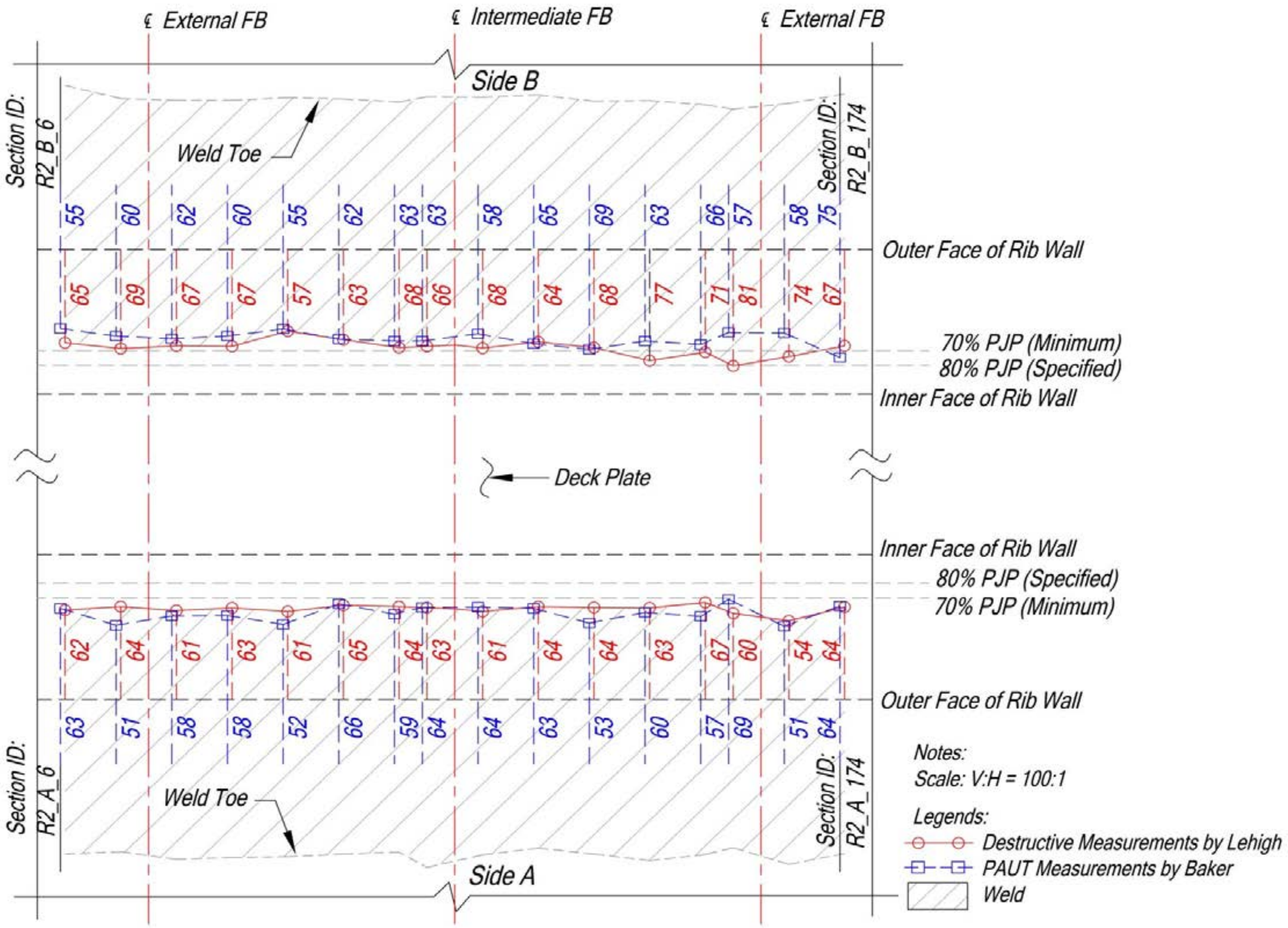

Figure 297. Distribution of weld penetrations (%) for rib-to-deck plate weld along the length for Rib2 of MU5

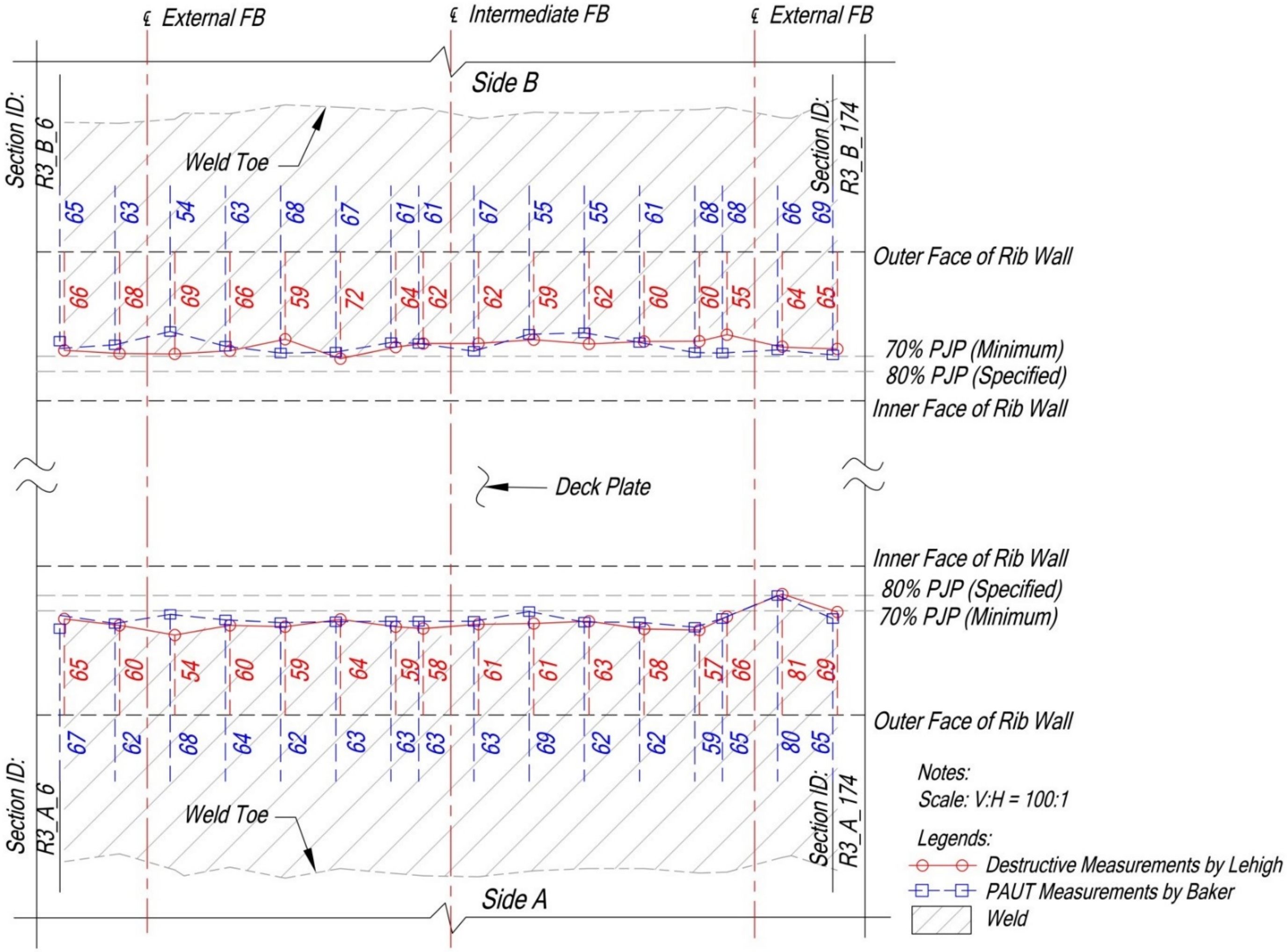

Figure 298. Distribution of weld penetrations (%) for rib-to-deck plate weld along the length for Rib3 of MU5

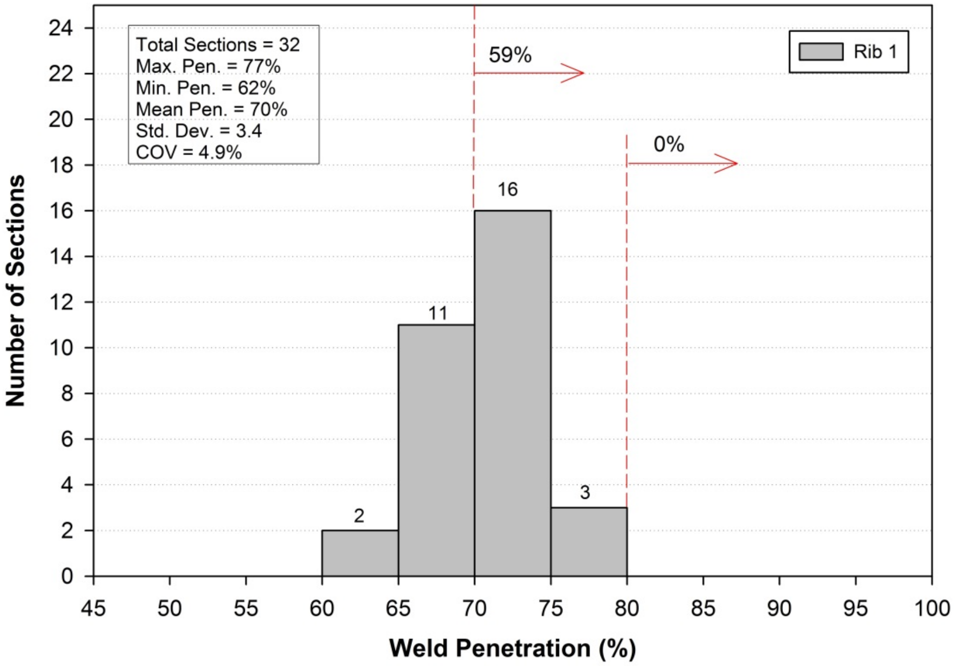

Figure 299. Distribution of weld penetrations (%) for Rib1 of MU5

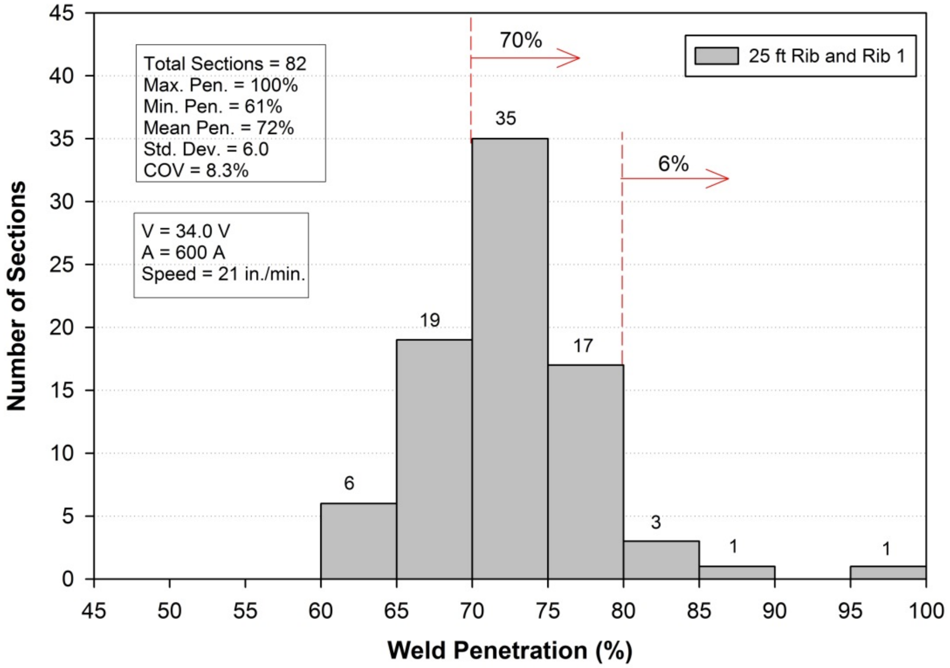

Figure 300. Distribution of weld penetrations (%) for Rib 1 and 25 ft. rib

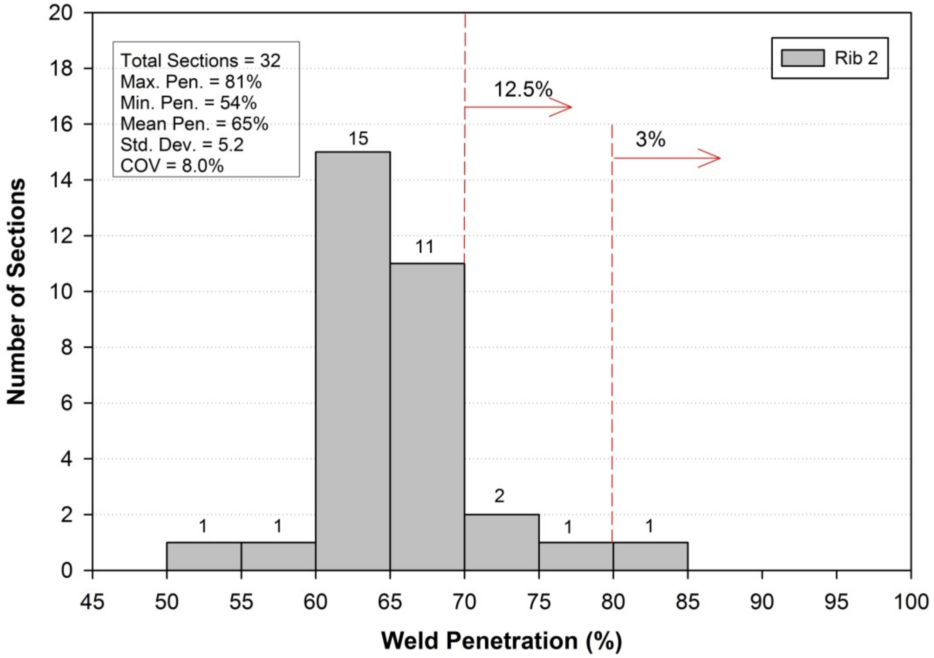

Figure 301. Distribution of weld penetrations (%) for Rib2 of MU5

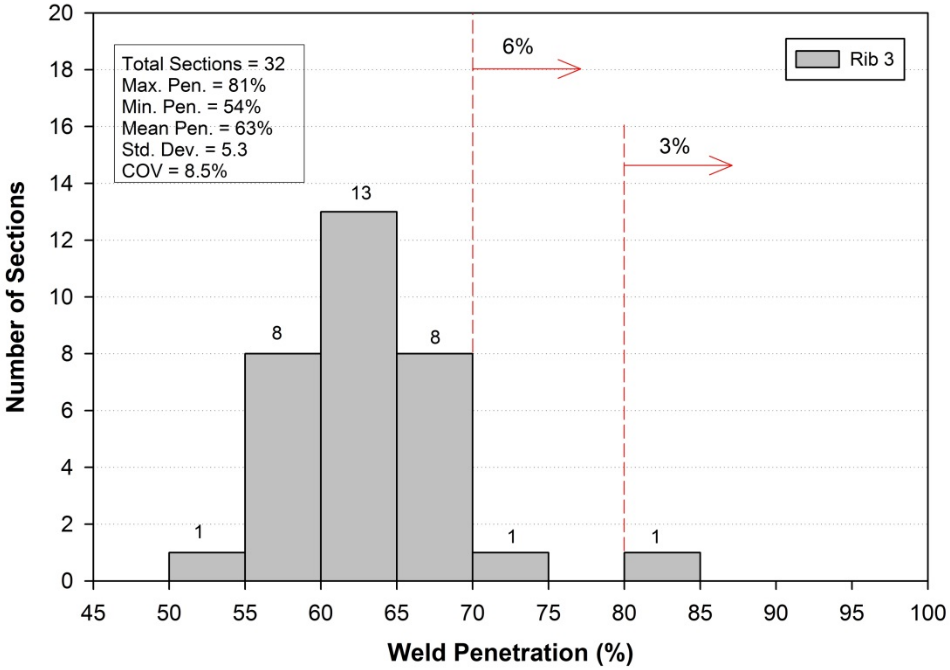

Figure 302. Distribution of weld penetrations (%) for Rib3 of MU5

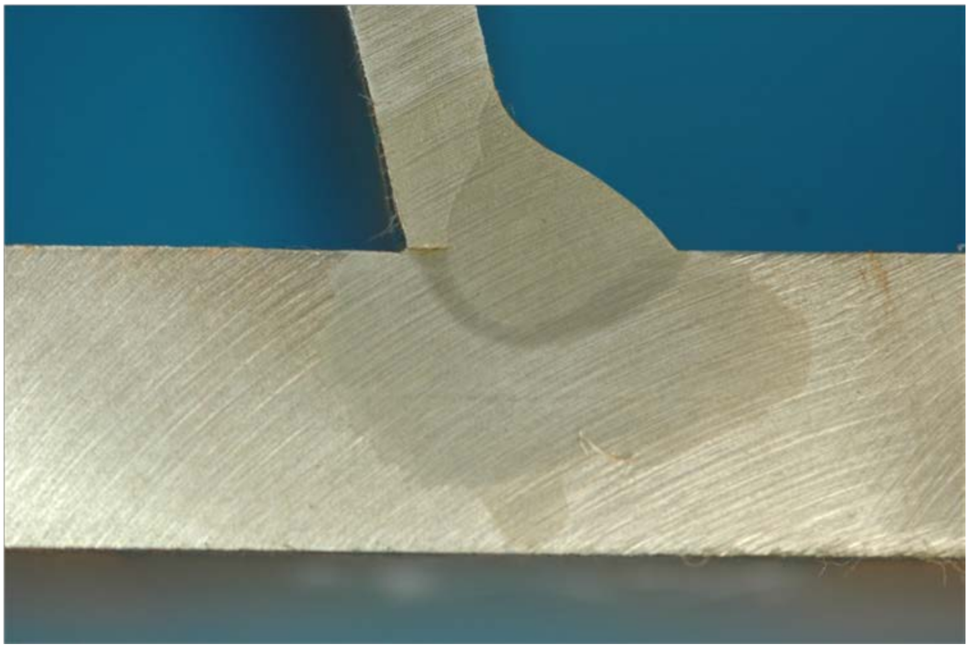

Figure 303. A typical macro-etched section for Rib 1 in MU5

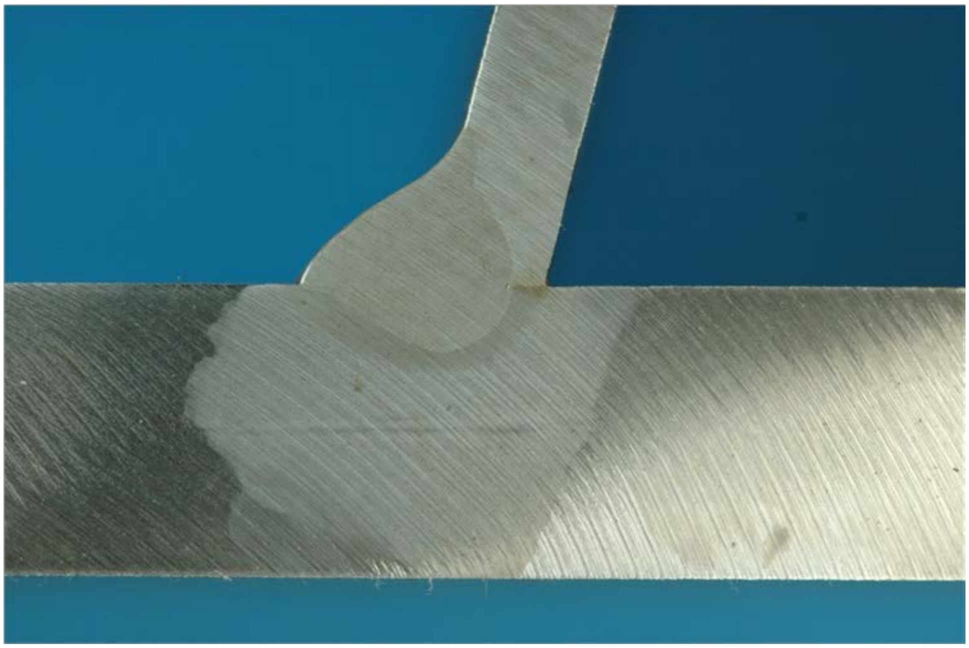

Figure 304. A typical macro-etched section for Rib 2 in MU5

Figure 305. A typical macro-etched section for Rib 3 in MU5

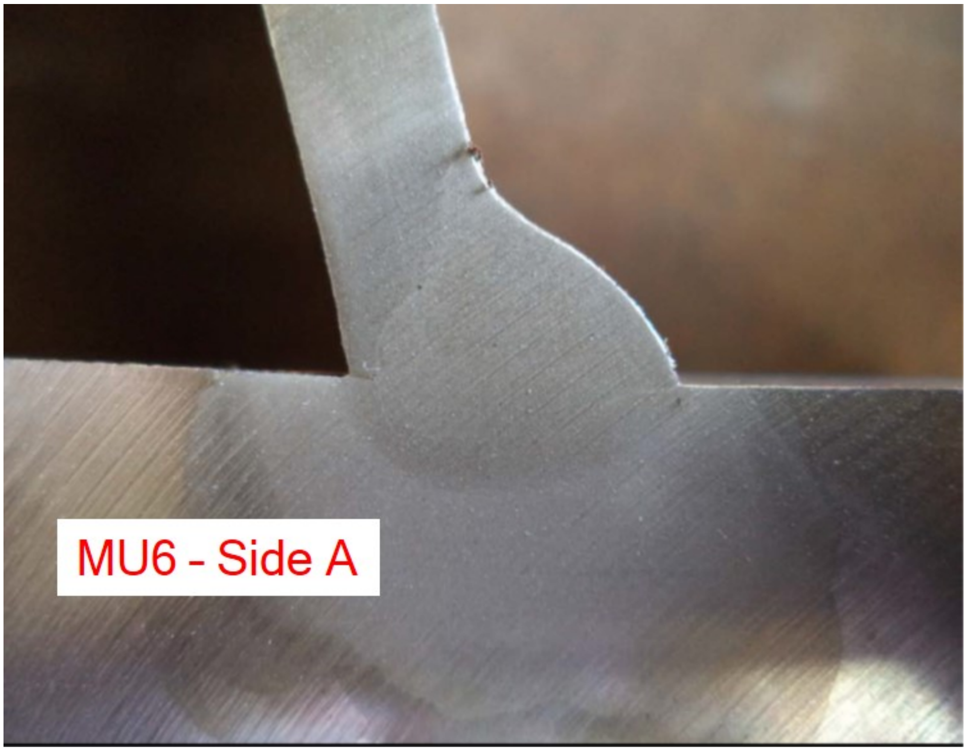

Figure 306. A typical macro-etched section for MU6: Side A

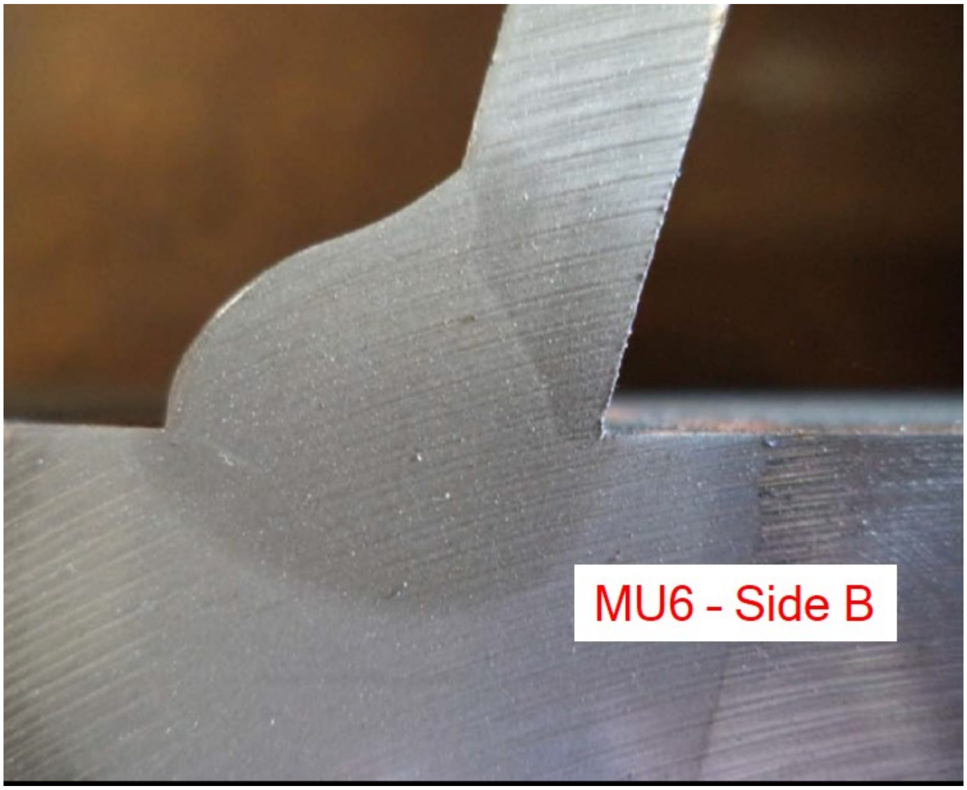

Figure 307. A typical macro-etched section for MU6: Side B

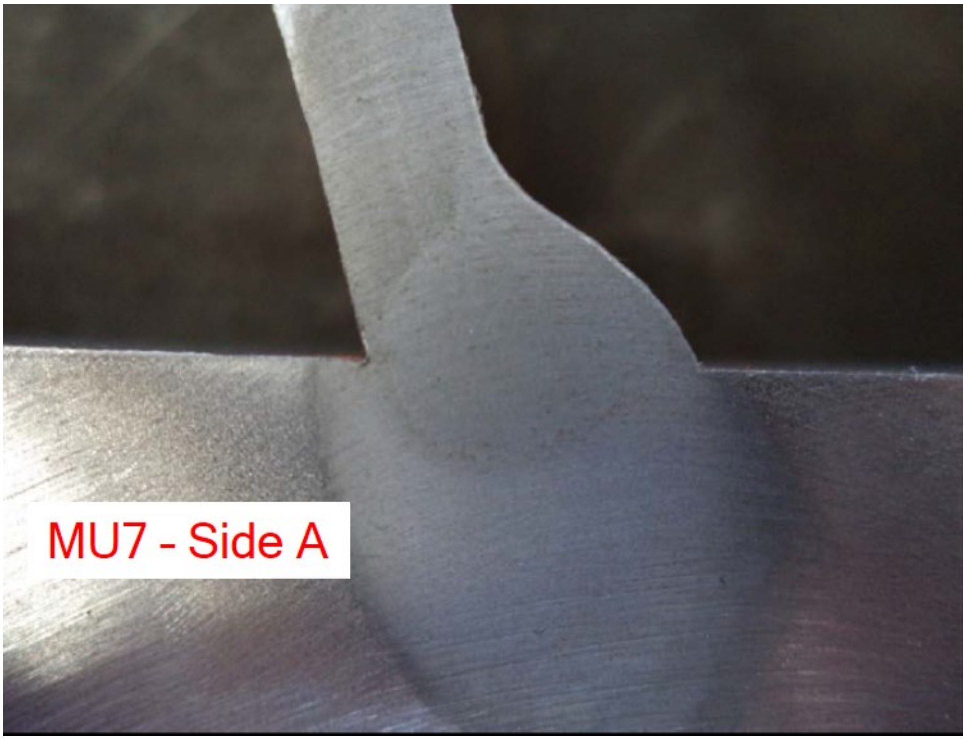

Figure 308. A typical macro-etched section for MU7: Side A

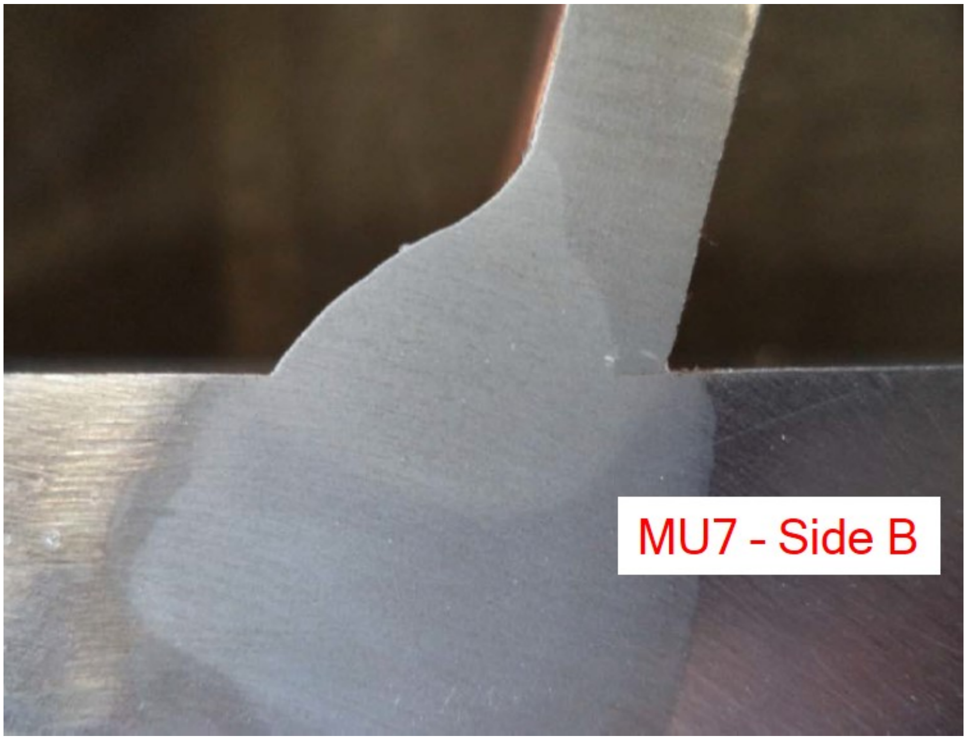

Figure 309. A typical macro-etched section for MU7: Side B

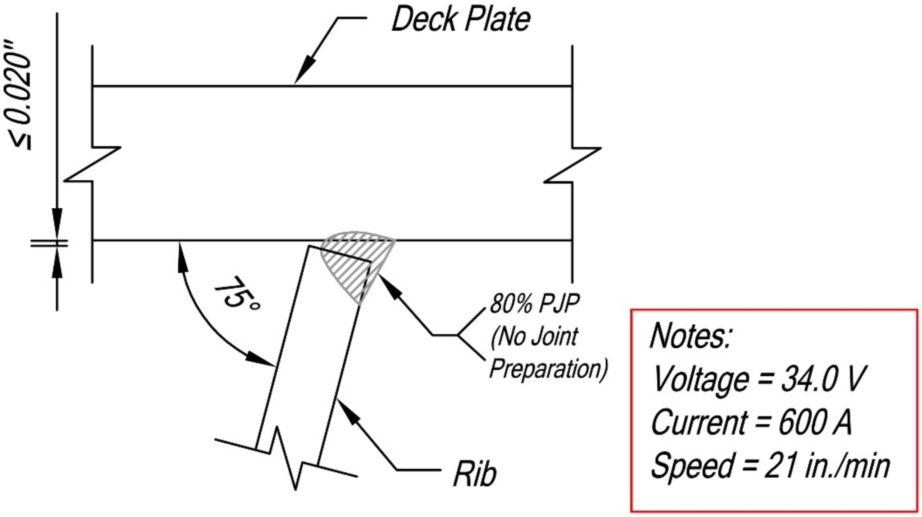

Figure 310. Detail of rib-to-deck plate weld of MU8

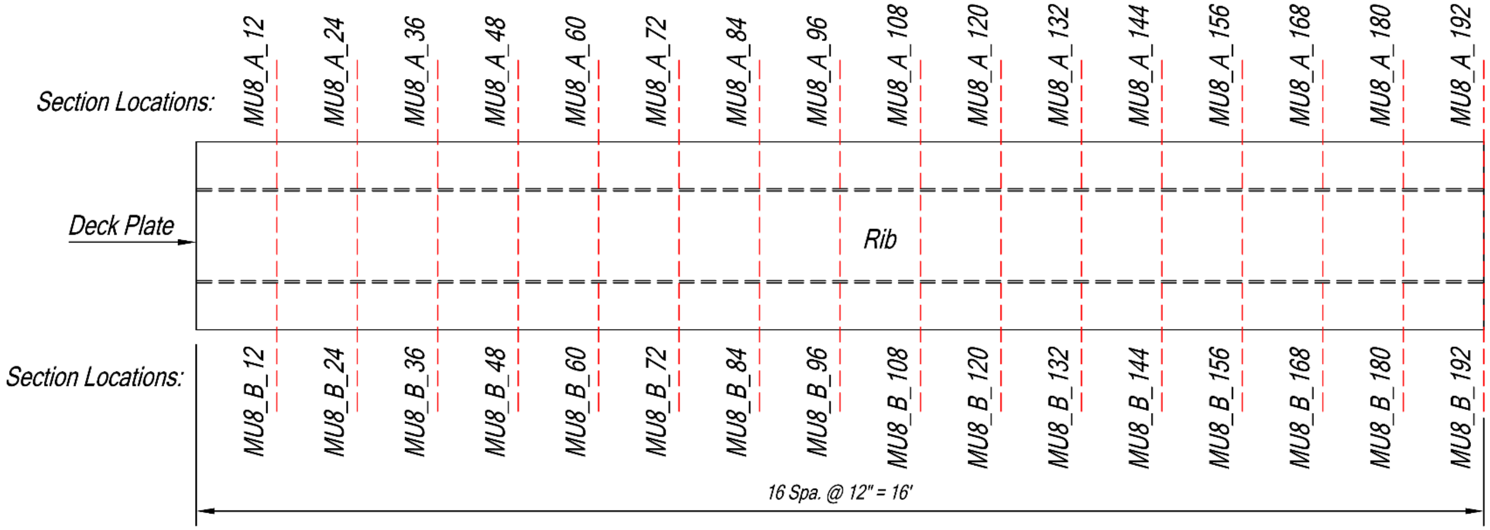

Figure 311. Section identification for MU8

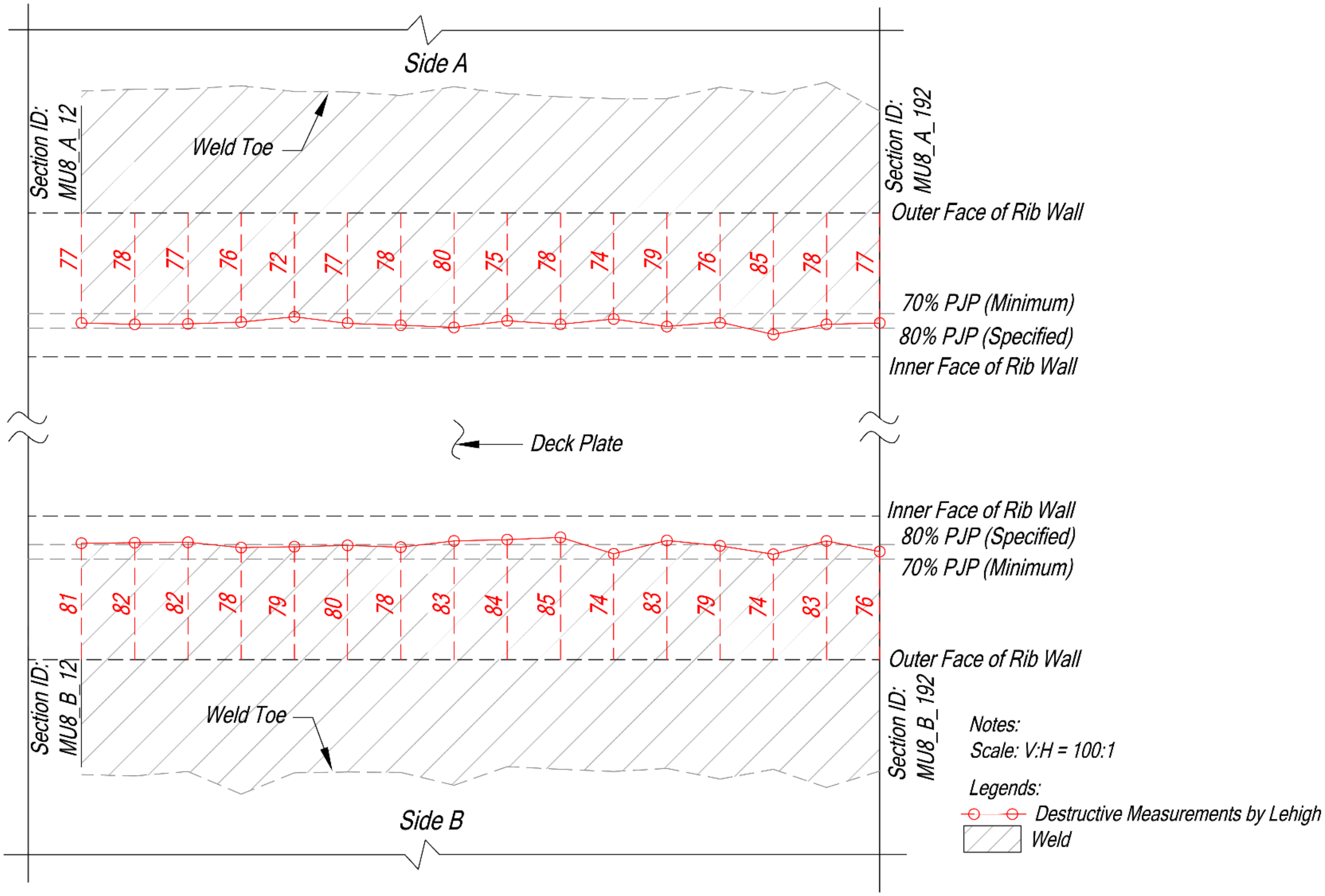

Figure 312. Distribution of weld penetration (%) of rib-to-deck plate weld for MU8

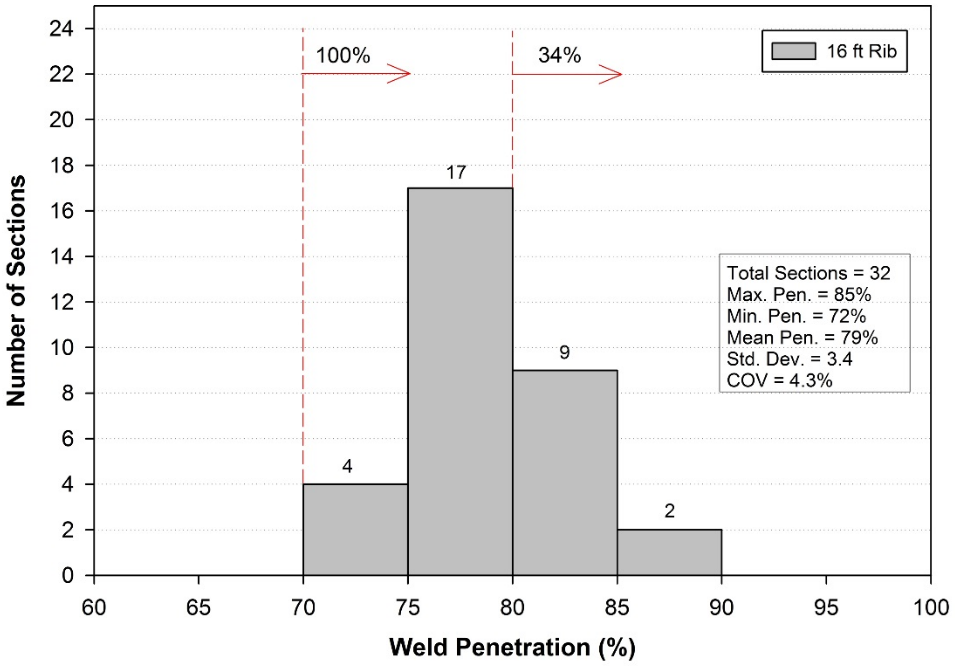

Figure 313. Distribution of weld penetration (%) of rib-to-deck plate weld for MU8

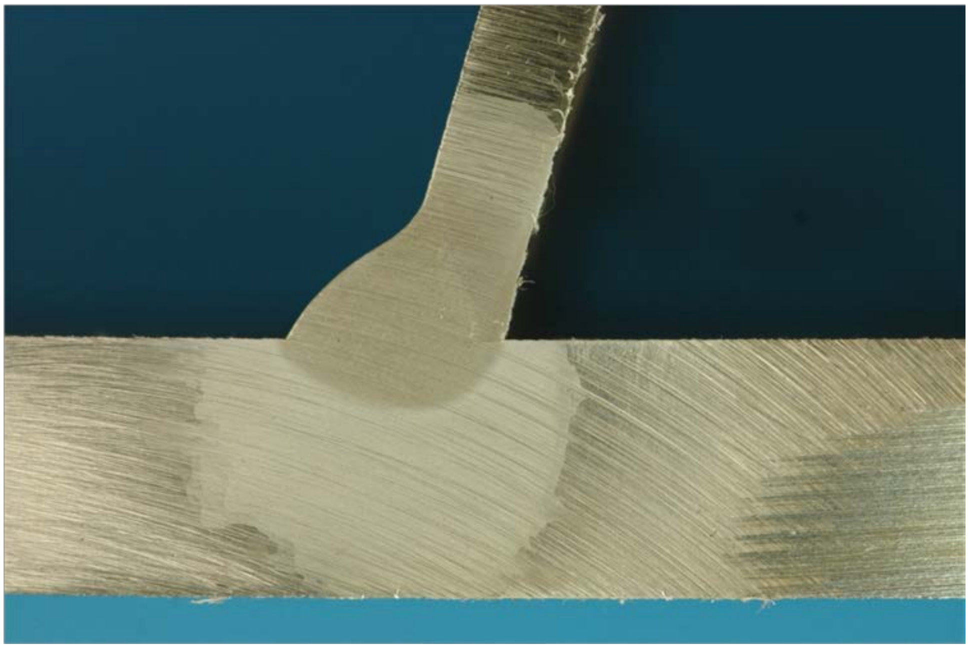

Figure 314. A typical macro-etched section for MU8

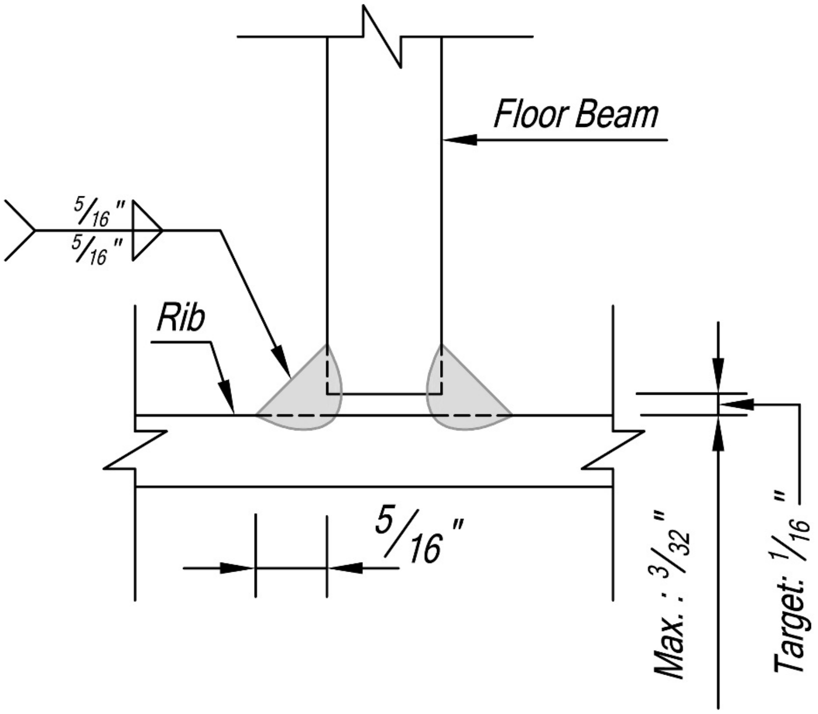

Figure 315. Detail of rib-to-floor beam weld for MU5

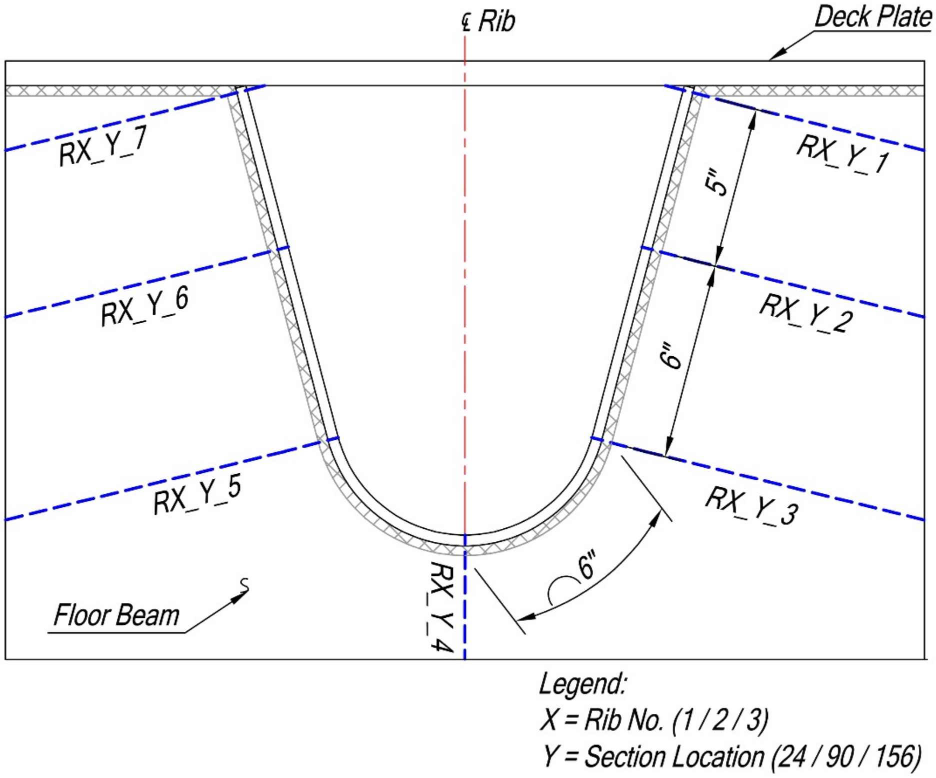

Figure 316. Section identification of rib-to-floor beam weld for MU5

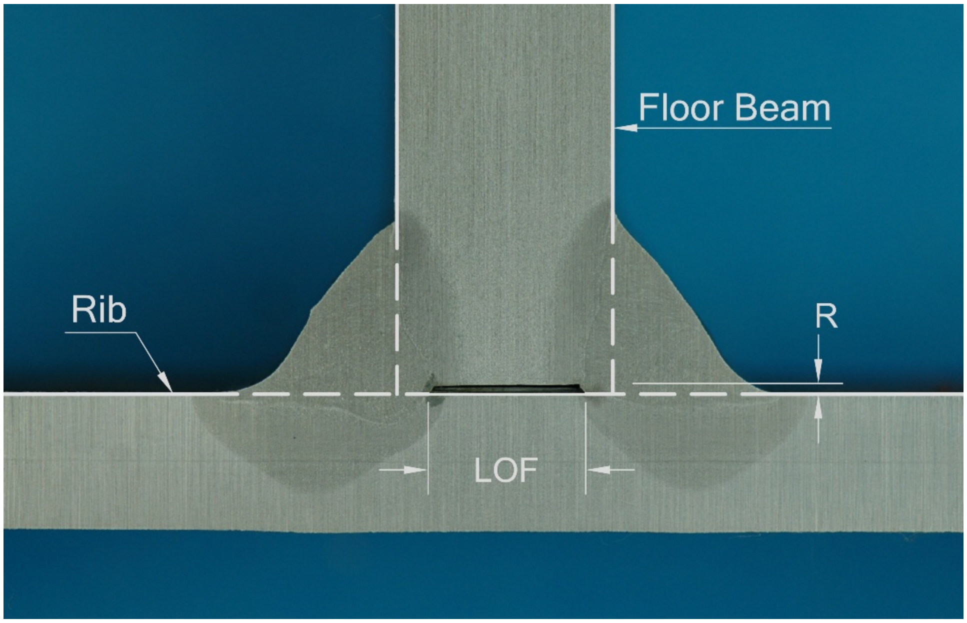

Figure 317. Schematic of rib-to-floor beam weld

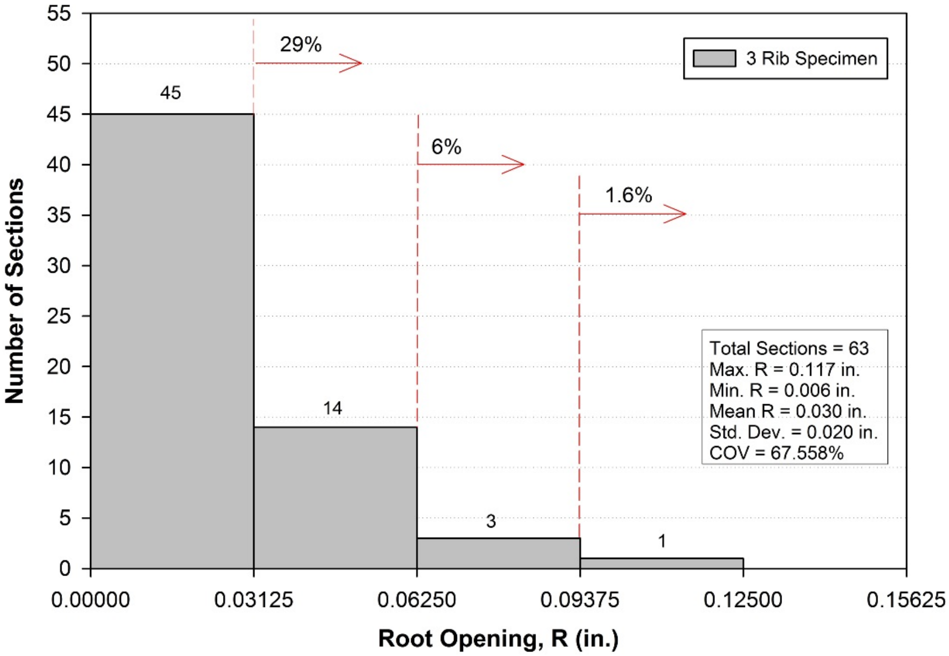

Figure 318. Distribution of R for MU5

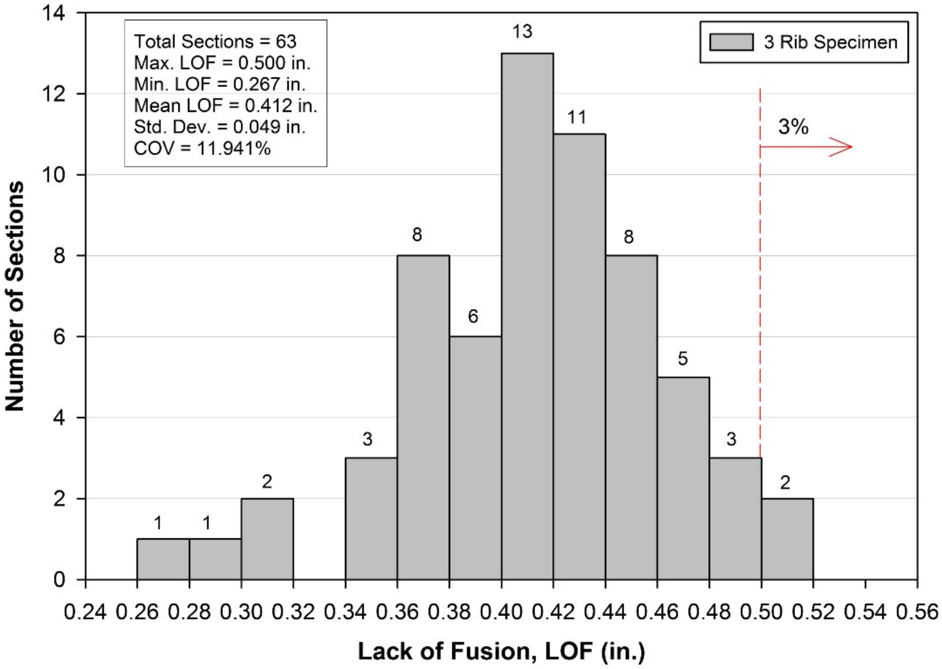

Figure 319. Distribution of LOF for MU5

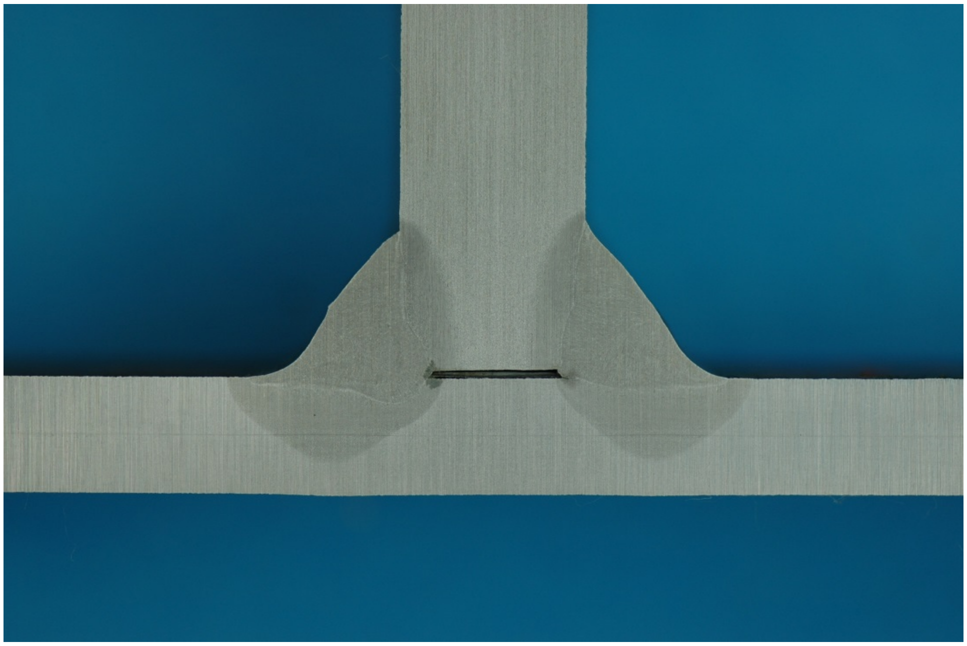

Figure 320. A typical macro-etched section of rib-to-floor beam weld for MU5

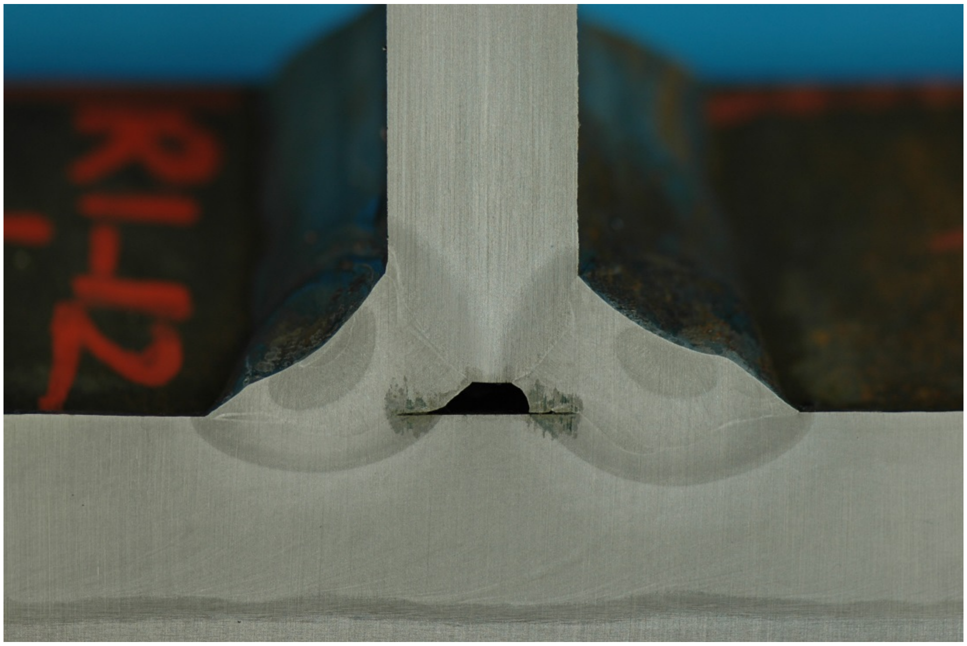

Figure 321. A typical macro-etched section of rib-to-floor beam weld for MU5 at the intersection with rib-to-deck plate weld

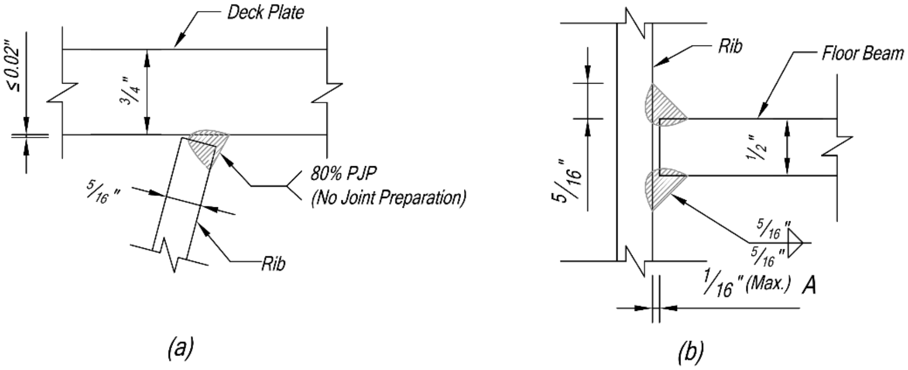

Figure 322. Connection details for full-size specimen: (a) rib-to-deck plate connection; (b) rib-to-floor beam connection

Figure 323. Rib-to-deck plate welding

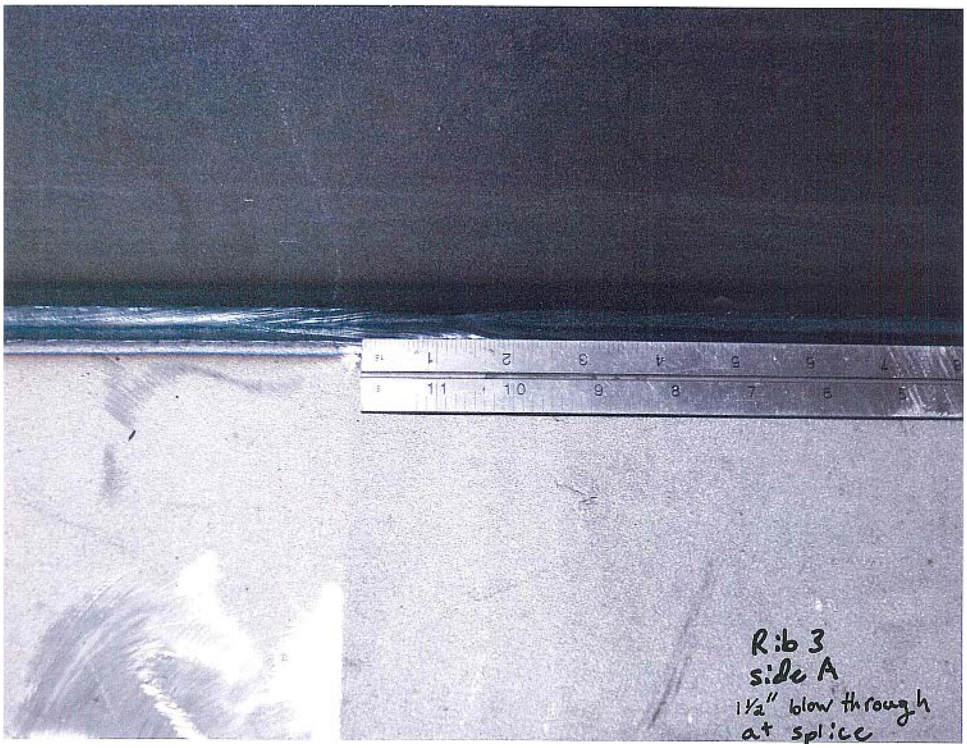

Figure 324. 1½ in. blow through in Rib 3 side A

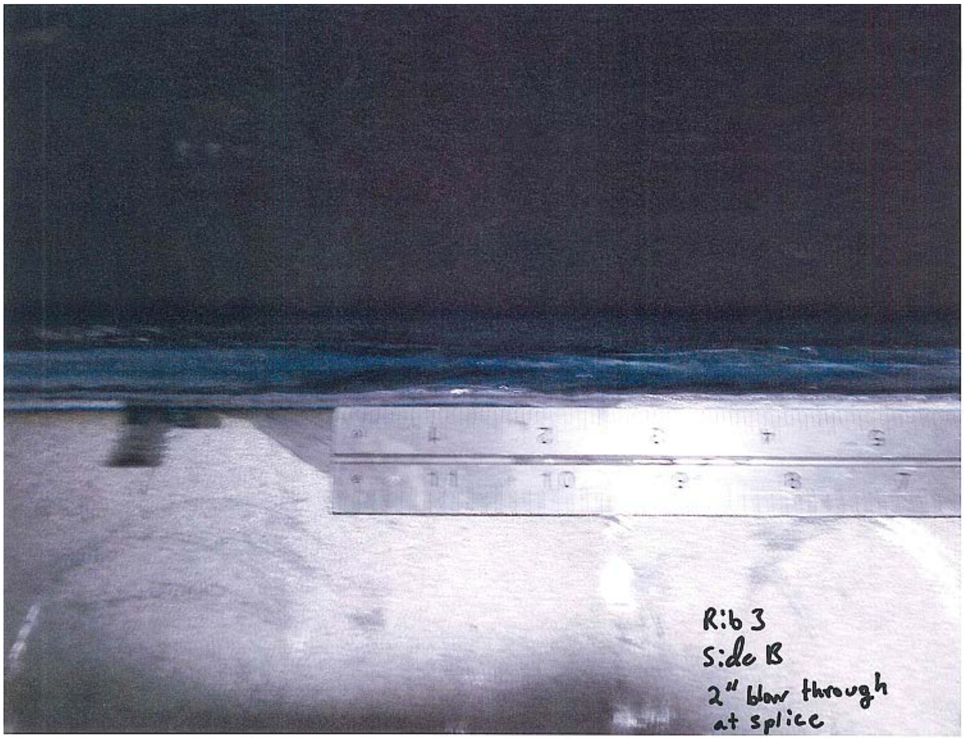

Figure 325. 2 in. blow through in Rib 3 side B

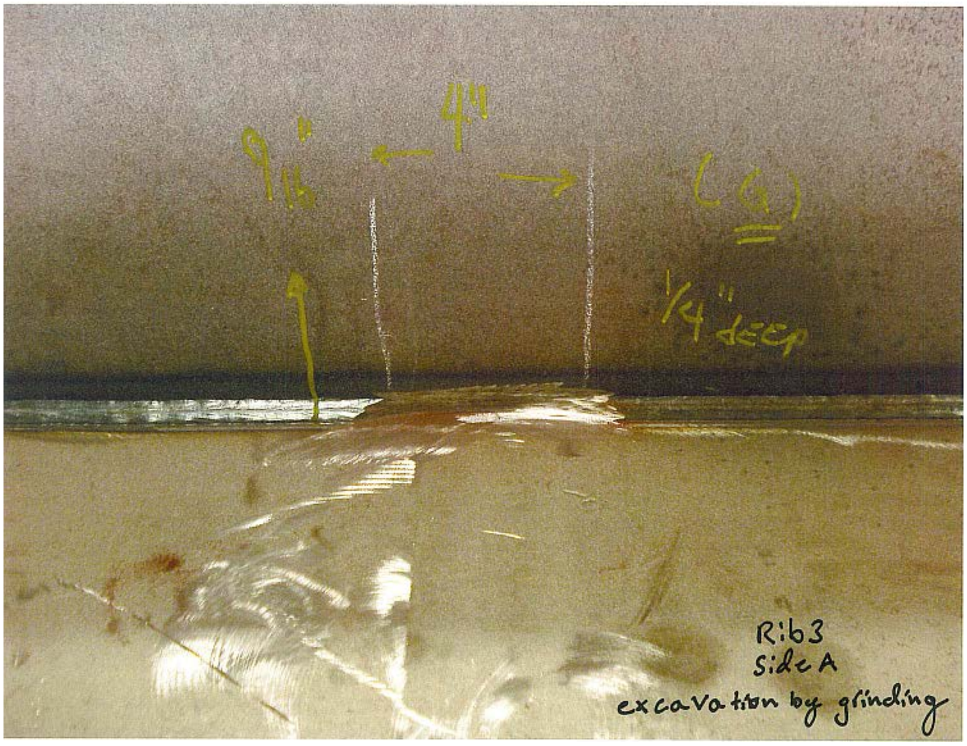

Figure 326. Excavation of blow through portions by grinding in Rib 3

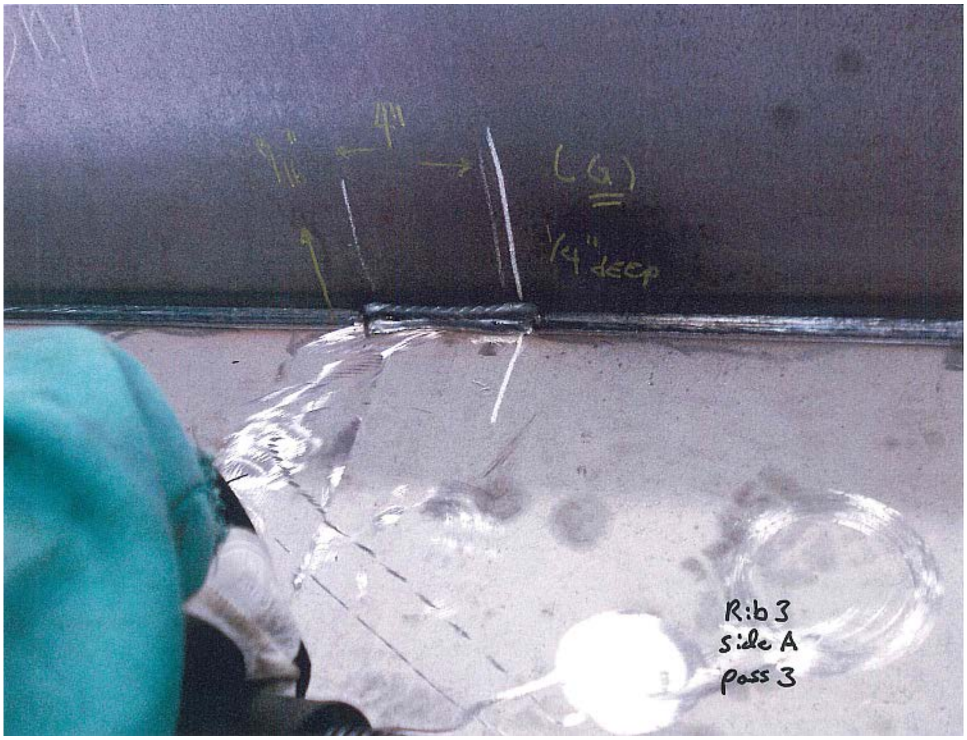

Figure 327. 3 passes of GMAW to fill up the excavated portions in Rib 3

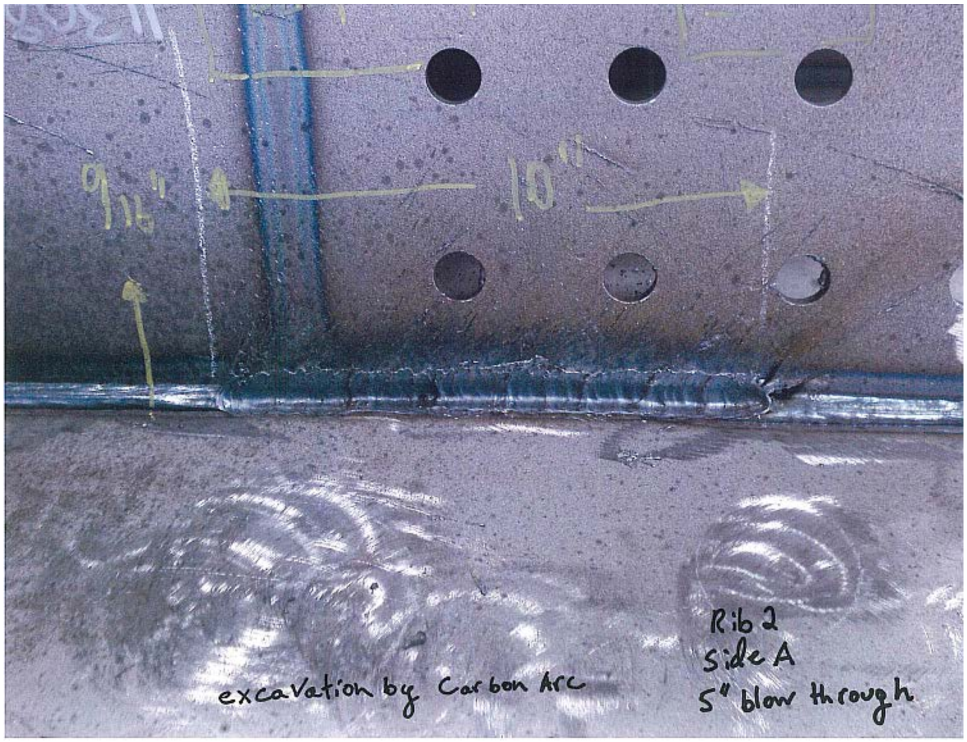

Figure 328. Excavation of 5 in. blow through portions by carbon arc in Rib 2

Figure 329. Excavation of 6 in. blow through portions by carbon arc in Rib 2

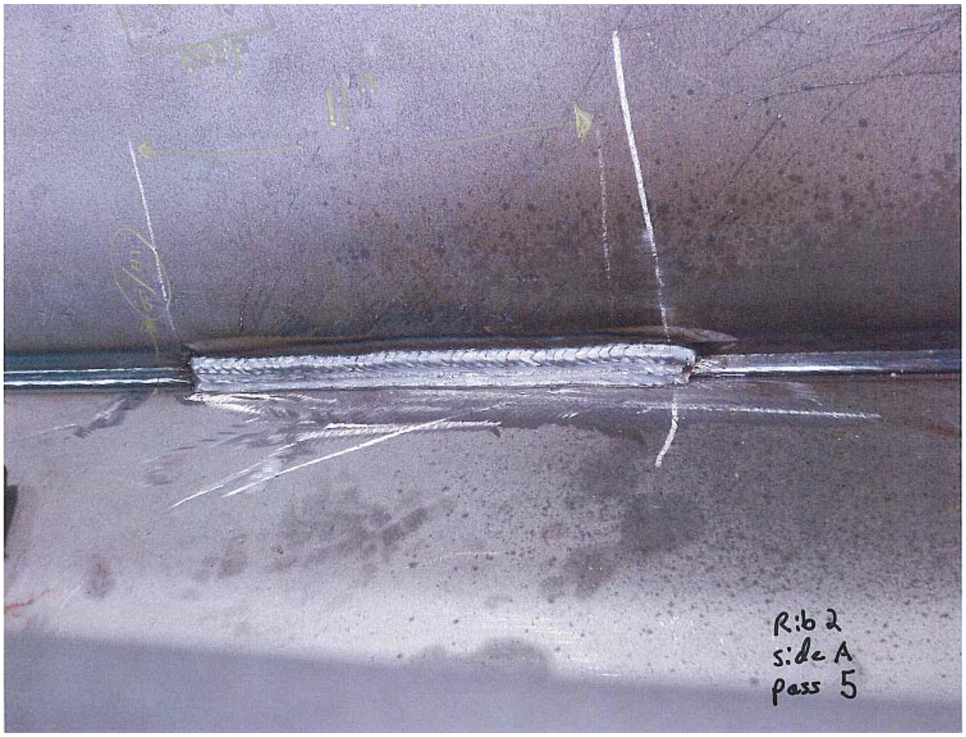

Figure 330. 5 passes of GMAW to fill up the excavated portions in Rib 2

Figure 331. Match-cutting of floor beam for rib-to-floor beam weld

Figure 332. Floor beam-to-deck plate welding

Figure 333. Rib-to-floor beam welding in 2F position

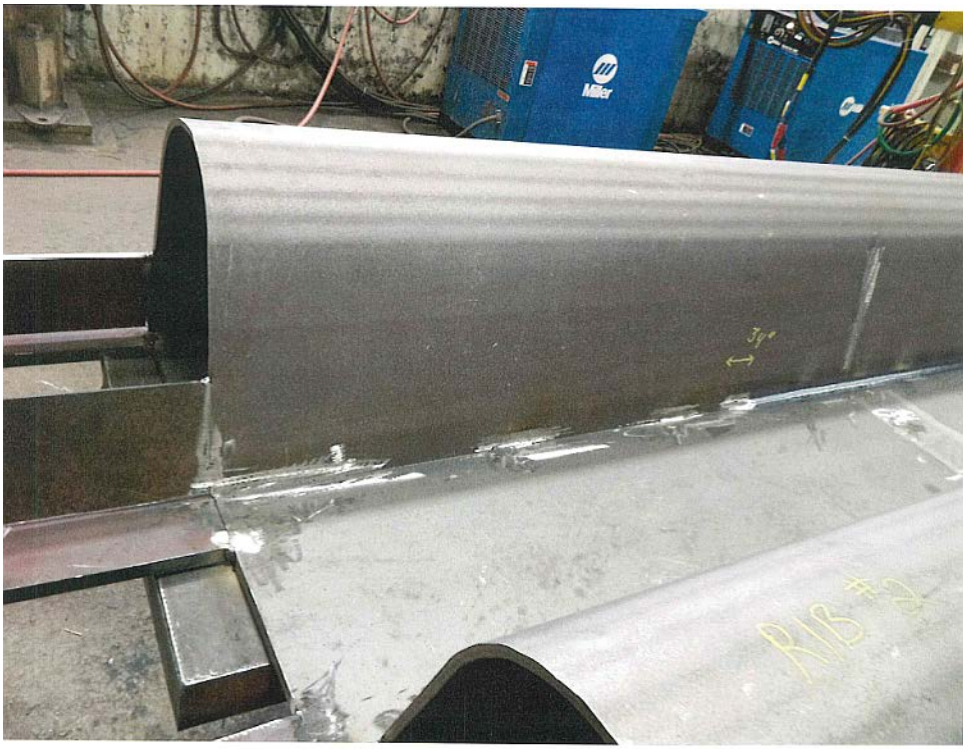

Figure 334. Welding gantry stopped at 34 in. from the end